POLYETHYLENIMINE FILLED MEMBRANES

By

Marcus Young Kim

A Thesis

Submitted to the School of Graduate Studies

in Partial Fulfillment of the Requirements

for the Degree

Doctor of Philosophy in Chemistry

McMaster University

POLYETHYLENIMINE FILLED MEMBRANES

DOCTOR OF PHILOSOPHY (2002) McMaster University

(Chemistry) Hamilton, Ontario

TITLE: POLYETHYLENIMINE FILLED MEMBRANES

AUTHOR: Marcus Young Kim, B.Sc. (York University)

SUPERVISOR: Professor Ronald F. Childs

NUMBER OF PAGES: xxiv, 221

Abstract

The fabrication, properties and performances of polyethylenimine pore filled and pore coated membranes are presented and discussed in this thesis. The membranes were prepared by an *in-situ* cross-linking process that involved filling the pores of a porous polypropylene host substrate with a solution of branched polyethylenimine and a diepoxy cross-linker of known concentration. The filled membrane was sandwiched between two polyethylene terephthalate sheets, to prevent solvent evaporation, and a cross-linked polymer network was formed within the porous microstructure of the host membrane.

Several cross-linkers were chosen based on their size, rigidity and hydrophobicity to cross-link polyethylenimine. A small, hydrophilic cross-linker- ethylene glycol diglycidyl ether- produced clear, space filling gels that had large swelling capacities by absorbing many thousand times its weight in water when immersed in aqueous solutions of varying pH. An oligomeric cross-linker- polypropylene glycol diglycidyl ether- produced colored space filling gels that exhibited moderate swelling abilities in aqueous solutions of varying pH. A rigid, hydrophobic cross-linker- bis-phenol A diglycidyl ether- produced gels that exhibited dimensional contraction (syneresis), scattered light and exhibited low swelling abilities.

Polyethylenimine cross-linked with ethylene glycol diglycidyl ether (PEI-EDGE) is hydrophilic and forms a hydrogel when swollen with water. The physical properties of hydrophobic polypropylene membranes were thus changed to hydrophilic upon the incorporation of the cross-linked polyethylenimine gel. The polyethylenimine gels in the membrane although formally neutral can acquire a charge by deprotonation of water, or

addition of acid, due to the basicity of the aliphatic nitrogens. The membranes were very effective in the nanofiltration of ionic solutes because of the charge in the polyethylenimine gel. The rejection of the ionic feed exhibited Donnan exclusion behavior because the rejections of the ionic solutes were greatly dependent upon the valency of the respective co- and counter-ions and sucrose, a neutral solute, was not rejected. Co-ion rejection increased with an increase in ion valency and conversely, counter-ion rejection decreased with an increase in ion valency. Rejections of NaCl could be observed at high pH's, indicating the gels possessed a significant charge concentration over a large range of pH. The permeabilities of PEI-EDGE filled membranes could be fit to a modeled permeability curve calculated from a hydrodynamic gel permeability model developed by Alicja Mika and Ron Childs of McMaster University.

Membranes filled with polyethylenimine cross-linked with polypropyleneglycol diglycidyl ether (PEI-PODGE) exhibited a morphology distinctly different from the PEI-EDGE filled membranes. Laser fluorescence confocal and environmental scanning electron microscopy showed the presence of PEI-PODGE gel coatings on the outer walls of the host substrate whereas a smooth, space filling gel morphology was seen in PEI-EDGE membranes. The permeability data suggested the existence of a gel plug in the central depths of the host substrate despite the microscopy evidence of coating. The PEI-PODGE membranes, however, exhibited fluxes that were higher than the EDGE cross-linked membranes due to the smaller thickness of the gel plug. The permeabilities of the PODGE cross-linked membranes, therefore, did not fit the modeled permeability curve.

The low salt rejections observed in the PEI-PODGE membranes were attributed to concentration polarization of ionic solutes accumulated in the large cavities on the membrane-feed interface.

Membranes filled with polyethylenimine cross-linked with bis phenol A diglycidyl ether (PEI-BADGE) exhibited unusually high fluxes and low salt rejection. The high fluxes and low salt rejections were consistent with the heterogeneity observed in the morphologies of the bulk PEI-BADGE gels and the effects heterogeneity has on flow through gels. As a result of the effects of heterogeneity, the permeability of PEI-BADGE filled membranes did not fit the modeled permeability curve.

A modification of the pore filling fabrication procedure resulted in the formation of pore-coated ultrafiltration membranes. Motivated by the coated morphology observed in the PEI-PODGE filled membranes, pore coated membranes were fabricated by a controlled evaporation of solvent from a solution of polyethylenimine and cross-linker filled in the pores of a host membrane. The coating imparted a hydrophilic nature to the originally hydrophobic host substrate and the coating could not be removed even when extracted in boiling methanol for a few days. The membranes had very high fluxes typical of ultrafiltration membranes. The fluxes, however, gradually decreased as a function of both the composition and amount of feed passed through the membrane. Drying the membrane restored the flux to a higher value; however, the decrease in flux was observed upon subsequent testing suggesting the coated layer was swelling into the pores.

Acknowledgements

First and foremost, this thesis is dedicated to my mother, **Sonia Kim**. Your constant support, encouragement and love has been my strength and inspiration. This thesis is yours as much as it is mine.

I wish to express my gratitude to my supervisor, **Dr. Ron Childs** and his wife **Grace**. Thank you for your mentorship, encouragement, guidance, hospitality and warm friendship. But most of all, thank you for setting an example of what to strive for professionally and personally.

Much of the work in this thesis was possible because of the brilliant breakthroughs of **Alicja Mika**- a person within whom resides a perfect synthesis of artistry and science.

Thanks also go to my supervisory committee members, Professors **Brian McCarry** and **Harald Stöver** for their expertise and helpful advice.

I am grateful for the expertise of **Marcia West** in cryomicrotoming and Professor **Adam Hitchcock** for the STXM work.

Thanks to my partners in crime: **Dave, Chris, Erica, Sven, Elena**, and **Jinsheng**. The past few years would have been a lot less interesting without you people.

A special thanks go to my friends and family; in particular, my sister **Sherry** and half-sister **Julie** for their constant encouragement and belief in me. Thanks also go to my brother **David** and my dad **John**. Hey **Steve**, *Godspeed* brother.

Finally, words cannot fully express the gratitude I feel for **Carol Dada**. Carol, you are a beautiful person and your influence will live through me to touch countless others. Thank you for being my Virgil.

Table of Contents

List of Figures

List of Tables

List of Schemes

Abbreviations

ACRONYM	
AFM	Atomic force microscopy
ALS	Advanced light source
BADGE	Bis-phenol-A-diglycidyl ether
BPEI	Branched polyethylenimine
BB	Branched polyethylenimine BADGE cross-linked
BE	Branched polyethylenimine EDGE cross-linked
BP	Branched polyethylenimine PODGE cross-linked
CCl_4	Carbon tetrachloride
$CHCl_3$	Chloroform
DABCO	1,4-diazabicyclo[2.2.2]octane
DMF	*N,N'*-dimethyl formamide
DVB	Divinylbenzene
EDGE	Ethyleneglycol diglycidyl ether
ENP	Extended Nernst-Planck
ESEM	Environmental scanning electron microscopy
eV	Electron volts
ICP	Inductively coupled plasma
IEC	Ion exchange capacity
MeOH	Methanol
NDSC	Napthalene-1,5-disulfonyl chloride

NEXAFS	Near edge x-ray absorption fine structure
NMR	Nuclear magnetic resonance
NNI	Nearest neighbor interaction
OD	Optical density
PE	Polyethylene
PEI	Polyethylenimine
PET	Polyethylene terephthalate
PIP	Piperazine
PODGE	Polypropyleneglycol diglycidyl ether
PP	Polypropylene
PVBC	poly(vinylbenzyl chloride)
PVF	Polymer volume fraction
RO	Reverse osmosis
SC	Space charge
STXM	Scanning transmission x-ray microscopy
SVD	Singular value decomposition
TFC	Thin film composite
TIPS	Thermally induced phase separation
TMS	Teorell-Meyer-Sievers model
UF	Ultrafiltration
UV	Ultraviolet
XL	Cross-linking

I dreamed that I floated at will in the great Ether, and I saw the world floating also not far off, but diminished to the size of an apple. Then an angel took it in his hand and brought it to me and said, "this thou must eat". And I ate the world.

-Ralph Waldo Emerson

CHAPTER ONE

Membranes are among the most important and ubiquitous structures in nature, where their functions are critical to developing and sustaining life. Artificial membranes have also established a dominant presence in industrial and biomedical applications with the worldwide membrane market currently estimated at over 19 billion dollars (U.S.) with growth averaging 8-10% per year between 1998 and 2000 [1]. At the most basic and functional definition, membranes are intervening barriers between two phases of different composition which prevent free diffusion while regulating the selective passage of components of one phase into the other. This principle is one of the cornerstones for the awesome diversity and complexity of life on earth and is the basis for membrane science.

1.0 A Brief History

Membrane science is a relatively old discipline with its origins tracing back to Abbé Nollet who, in 1748, discovered the semi-permeability of an animal membrane [2]. Nollet discovered that alcohol, contained in vessels sealed with pig bladder and immersed in water caused an increase in volume of the alcohol and strained the membrane. This phenomenon was termed *osmosis* by Dutrochet in the early 1800's when he conducted similar experiments; however, he misattributed this phenomenon to electricity [3]. In 1855, Fick investigated diffusion by analysis of salt solution transport through porous partitions. The result of this work was the development of the laws of diffusion, which

are named after him and have become one of the fundamental principles in membrane science [4]. In 1911 Donnan discovered a process, named after him, that dealt with distribution of electrolytes across fixed charge surfaces [5]. This Donnan exclusion phenomenon plays a fundamental role in ionic separation processes and will be discussed later in greater detail. The theory of transport across neutral and fixed charge membranes has been evolving for almost a hundred years. One of the milestones in that evolution was the treatment by Teorell [6], Meyer and Sievers [7-9] in the mid 1930's when they used the Nernst-Planck equation and Donnan equilibria to relate the fluxes of permeants with the forces imposed upon them in an ionic membrane.

Membrane science, prior to 1940, was a highly obscure and esoteric discipline that garnered curiosity more than serious research. Curiously enough, however, it was this fledgling discipline of membrane science that, in 1942, introduced two technologies that changed the world forever and ushered in a new era. One was the separation of uranium isotopes ($U^{235}F_6$ and $U^{238}F_6$) by gaseous diffusion in the *Manhattan Project* [10], which gave birth to atomic energy. The other is hemodialysis [11], which has given humanity the means to manipulate life itself.

It wasn't until the late 1950's, however, when Breton and Reid first applied membranes to the desalination of seawater [12,13]. They used symmetric cellulose acetate membranes that had very low water fluxes- approximately a few drops per week. The flux across this membrane was so low, the process was deemed impractical for industrial applications. It was not long after the discovery of Breton *et al.* that Loeb and Sourirajan [14] devised a method for improving water flux performance, while retaining

solute rejection capability by making membranes asymmetric. This opened the proverbial *floodgates* of interest and, since then, the burgeoning number of publications both in the scientific and patent literature serve testimony to the interest in membrane science as both a fertile field of academic research and viable industrial applications.

The growth of membrane science over much of its lifetime has been incremental and slow, with most of the significant advancements and discoveries made in the last 50 years. These advancements have been largely fueled by the ever present need for clean reusable water and more efficient industrial separation processes brought about by increases in industrialization, population and energy costs. The scope and applications of membrane processes today are incredibly complex playing integral roles in fields such as biomedical [15-20], gas separations [21-24], food processing [25-27] and water treatment [28-33]. It is an interdisciplinary discipline that involves the disciplines of polymer, physical, organic and inorganic chemistries, biochemistry, physics, engineering and an increasing number of other disciplines as the boundaries of membrane technologies are continuously advanced. The field of membrane science has flourished to the point where an adequate discussion of more than one subdiscipline is beyond the scope of this thesis. The focus of this thesis, therefore, will be on the fabrication of a new class of membranes based on a pore filling concept and how the chemical properties of the filling affects the physical properties of the membrane; especially with respect to their performance under both dynamic pressure driven applications and static absorption applications.

1.1 Membrane Processes

From a very superficial perspective, a membrane can simply be considered a barrier that rejects solutes that are too large to pass through the pores while smaller molecules can pass through unimpeded. Although pore size does play a major role in performance, this simplistic model- while being true for ultrafiltration and microfiltration membranes- does not fully account for reverse osmosis and nanofiltration processes. **Figure 1.1** illustrates the various pressure driven membrane processes ranging from reverse osmosis to microfiltration as functions of pore size, density and distribution of pore filling and operating pressures.

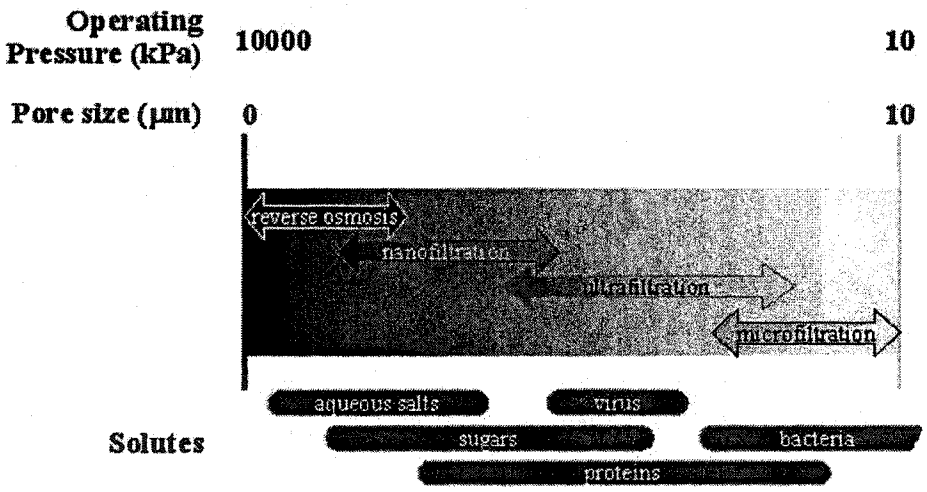

Figure 1.1 Schematic of various membrane processes represented by their operating pressure, pore size and their range of applications

1.1.1 Osmosis and Reverse Osmosis

When two aqueous solutions, with differing concentrations of solutes, are separated by a partition permeable only to the solvent, water will flow from the less concentrated region to the more concentrated one as shown in **Figure 1.2a**. This phenomenon is called *osmosis* and the extent of water flow is determined by the osmotic pressure (π), which is a function of the concentration difference between the two solutions. The osmotic pressure of a concentrated solution (A) is related to the mole fraction (χ_A) and partial molar volume of the solvent (v_A) at a temperature T taking into consideration the gas constant R by the following equation [34].

$$\pi = -\frac{RT}{v_A}\ln \chi_A \qquad (1.1)$$

For dilute solutions, **equation 1.1** simplifies to the van't Hoff equation,

$$\pi = C_A RT \qquad (1.2)$$

where C_A is the concentration of solution A. This flow of water, across the partition, can be reversed if pressure- exceeding the osmotic pressure- is applied to the more concentrated side as depicted in **Figure 1.2c**.

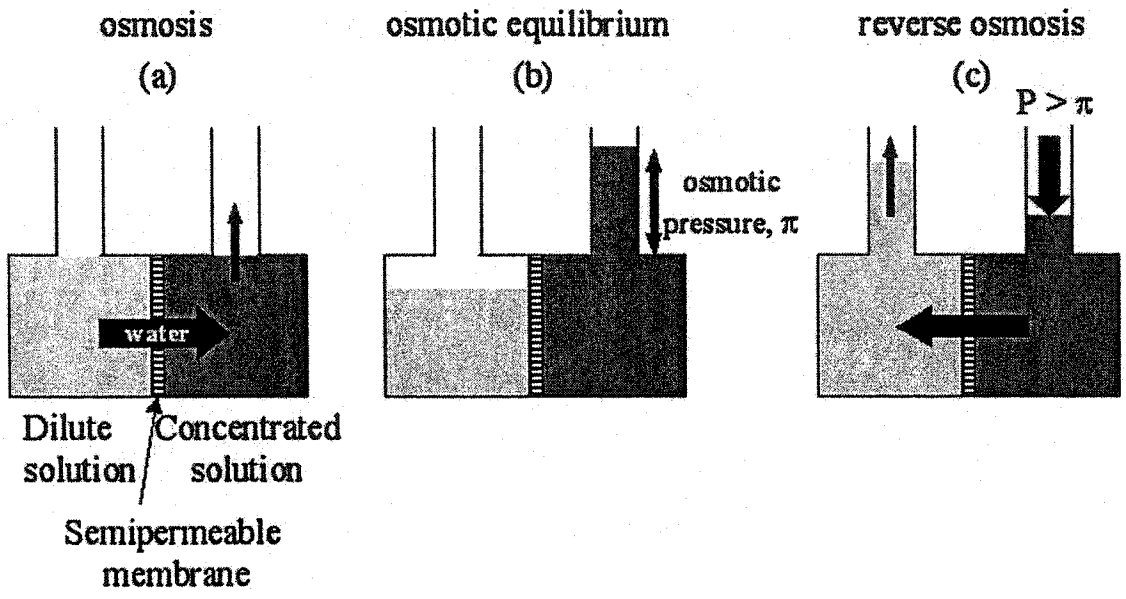

Figure 1.2 The principle of reverse osmosis

Typical structures of membranes are shown in **Figure 1.3**. Membranes can be symmetric- that is, their structure is identical over the entire cross-section of the membrane or they can be asymmetric, in which one side of the membrane is different from the other. As mentioned earlier, the improvements made by Loeb *et al.* on cellulose acetate membranes were to make them asymmetric with a very thin but dense skin layer that rejected solutes. They understood that water flux through the membrane was inversely proportional to the thickness of the separating layer [35]. Indeed, the major advancements in reverse osmosis membrane technology have been variations on this theme with an increased focus on developing and optimizing the chemistry of the barrier layer [28,36-40]. For example, work by Hirose *et al.* [39] and Kwak *et al.* [40] have shown that increasing the surface roughness of the barrier layer of a thin film composite

membrane enhances the water permeability through the membrane. The enhanced permeability was attributed to an increase in surface area [40].

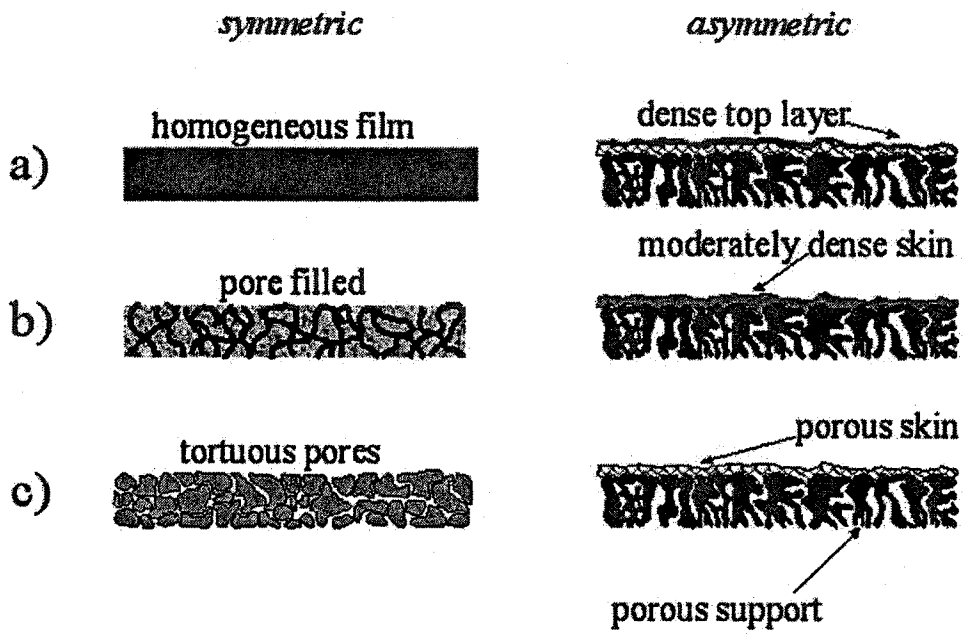

Figure 1.3 Cross-sectional morphologies of reverse osmosis (a), nanofiltration (b) and ultrafiltration (c) membranes

1.1.2 Transport Through Reverse Osmosis Membranes

All of the models put forth to explain transport of solutes and solvent through reverse osmosis membranes can be categorized into either the *pore-flow model* [41-45] or the *solution-diffusion model* [46-50]; although hybrid pore-flow/solution-diffusion models [50] and *black box models* [51,52] based on irreversible thermodynamics have also been proposed. The solution diffusion model, however, has become widely accepted to be correct. This model posits that both solvent and solute dissolve into the membrane

material and diffuse down a chemical potential gradient. Separation is achieved because of differences in solubility and mobility of the permeants in the membrane.

The mechanism of molecular transport for the solution-diffusion process, through polymer films, has been modeled by computer simulation [53]. Thermal motion of the polymer chains cause small statistical fluctuations in free volume to occur such that micro-cavities can randomly form to temporarily house the permeating molecule. Constant thermal motion creates new micro-cavities in the polymer matrix, into which the permeating molecule can jump. Permeation through a reverse osmosis membrane occurs by repeating this process many times. Although the model is crude, it provides a general understanding of the processes involved. A more detailed analysis of water and salt transport can be found in the atomistic simulations by Kotelyanskii *et al.* [54]

Since the solution-diffusion model is based on solubility and diffusion parameters, the molar flux of water (J_w) can be represented by **equation 1.3** if it is assumed that no solute permeates through the membrane:

$$J_w = \frac{D_w K_w c_w \nu_w (\Delta p - \Delta \pi)}{lRT} = A(\Delta p - \Delta \pi) \quad \textbf{(1.3)}$$

where D_w and K_w are the diffusion and partition coefficients for water, c_w is the concentration of water in the feed, ν_w is the molar volume of water, l is the membrane thickness, ΔP is the difference in hydrostatic pressure across the membrane and $\Delta\pi$ is the osmotic pressure difference between the feed and permeate.

In practice, all membranes are *leaky* towards solutes to varying degrees (<100% rejection). This semipermeability towards solutes is measured by the reflection

coefficient σ and represents a membrane's asymptotic rejection limit for that particular solute [55]. A σ =1 is an ideal membrane with 100% rejection, while $\sigma = 0$ is a completely permeable membrane with no solute rejection. The real osmotic pressure difference across the membrane, therefore, is not $\Delta\pi$ but $\sigma\Delta\pi$. The water flux equation modifies to [56]:

$$J_w = A(\Delta P - \sigma\Delta\pi) \quad \textbf{(1.4)}$$

The flux for the solute is also determined by its diffusivity (D_s) and solubility (K_s) in the membrane material; however, unlike water flux, solute flux is unaffected by the applied trans-membrane pressure but is instead, dependent upon the chemical potential established by differences in solute concentrations in the feed (c_{sf}) and the permeate (c_{sp}). **Equation 1.5** represents solute flux in the solution-diffusion model.

$$J_s = \frac{D_s K_s}{l}(c_{sf} - c_{sp}) = B(c_{sf} - c_{sp}) \quad \textbf{(1.5)}$$

Based upon **equations 1.4** and **1.5** the choice of membrane materials must be determined by maximizing A (water flux) and minimizing B (solute flux). This clearly establishes the relationship between membrane material and membrane intrinsic properties. Hydrophilic polymers, therefore, are required because of their high water affinity; which is, in fact, the case with the majority of desalination membranes based on polyamide chemistry [57]. Polymers must also be chosen based on their level of molecular interaction with the permeating solute, which requires a knowledge of the diffusion and partition coefficients between the polymers and solutes.

Although the majority of work in RO technology has been focused on aqueous systems, several groups have studied the performance of polymeric membranes for non-aqueous applications. Sourirajan *et al.* [58-61] were the first to apply RO processes to non-aqueous systems. Working primarily with cellulose acetate membranes, they used a variety of polar/non-polar and aliphatic/aromatic organic solvents for their study. They found that in xylene-ethanol or *n*-heptane-ethanol mixtures, ethanol was preferentially transported through hydrophilic membranes but the order was reversed when the membranes were coated with a hydrophobic layer. They proposed the Preferential Sorption Capillary Flow model for such systems.

Paul *et al.* [62-65], in the mid 1970s, worked on rubbery membrane materials to study their transport characteristics for different organic solvents. They proposed a Solution-Diffusion model [65] as the basis for organic solvent transport. Aminabhavi *et al.* [66,67], using the Solution-Diffusion model, published extensive results of organic solvent transport through rubbery membranes. They studied the importance of cross-linking density and the effects of temperature on the sorption-diffusion of organic solvents.

Raman *et al* [68,69] reported the use of reverse osmosis membranes for solvent recovery and partial deacidification of vegetable oils. Niwa *et al.* [70] reported the use of reverse osmosis for concentration of organic solvents such as methyl ethyl ketone, tetrahydrofuran and ethyl acetate. Koseoglu *et al.* [71] and Schmidt *et al.* [72] have published several results on the stability of some commercially available membranes

towards organic solvents which is one of the key issues in solvent-resistant membrane development.

Solvent resistant membranes for separation of solutes in organic media have been recently reported by several groups [73,74] most notably Bhattacharyya *et al.* [75] where they developed models for transport of an organic solvent based on the Solution-Diffusion model accounting for polymer-solvent interactions with the Flory-Huggins theory. In a more recent report, Bhattacharyya *et al.* [76] investigated solute transport in solvent resistant membranes for non-aqueous systems. The separation behavior of large organic solutes, such as dyes and triglycerides, were investigated in various organic media. They found that solute rejection was dependant strongly on both the type of solvent and membrane; for example, the rejection of an organic dye in hexane was found to be 25% but was –10% in methanol implying preferential sorption and transport of the organic dye over methanol. The coupling of solute and solvent in non-aqueous separations required the applications of alternative models of transport (Spiegler-Kedem model) which gave reasonable approximations of flow.

1.2.1 Nanofiltration

Nanofiltration (NF), as shown in **Figure 1.1**, falls into a transitional region between reverse osmosis (RO)- where membranes essentially have no pores- and ultrafiltration (UF), where the pores are quite large. For this reason, nanofiltration membranes have been termed *loose reverse osmosis* [77] and have performance

characteristics typical of both RO and UF processes. **Table 1.1** summarizes these differences.

Table 1.1 Summary of RO, NF and UF processes. Adapted from Mulder [56]; Ho and Sirkar [78]

Characteristics	Reverse osmosis	Nanofiltration	Ultrafiltration
Ionic rejection	>99%	<99%	0%
Flux range ($l \cdot m^{-2} \cdot h^{-1} \cdot MPa^{-1}$)	0.5-10.4	14-120	100-500
Molecular weight cut off (1000 Da)	<0.5	0.2 - 1	1 -100
Operating pressure (1000 kPa)	1 - 10	0.1 - 2	0.1 - 0.5
Mechanism of separation	Solubility & diffusivity	Solubility & diffusivity and/or ionic interaction	Size exclusion

Nanofiltration membranes have pore sizes that range from 1 to a few nanometers in diameter and are typically fabricated from polyelectrolyte materials. Both sieving and electrical effects play a role in the separation process in nanofiltration. Most of the nanofiltration membranes reported in the literature are charged thin-film composite membranes [36,77,79-81]. However, a new class of pore-filled nanofiltration membranes has been developed by the McMaster Membrane group [82]. These membranes will be discussed in greater detail in chapter two, but their basic construct and details of performance are as follows. The membranes are composite structures composed of a polyelectrolyte hydrogel symmetrically enmeshed in a microporous host. The microporous host simply provides the structural integrity and protects the gel from deformation under pressure and osmotic swelling. All convective and diffusive transport occurs through the hydrogel, thus its properties largely determine the performance characteristics of the membrane. The mechanism of transport through the incorporated

gel has been defined by a hydrodynamic permeability model and will be discussed in the following chapters.

1.2.2 Transport Through Nanofiltration Membranes

Nanofiltration membranes, relative to reverse osmosis membranes, have very open structures. Because of the higher porosities, transport of water typically occurs by convective flow through the pores, although diffusion occurs in dense nanofiltration membranes. The open structure of nanofiltration membranes limits their applications to moderately concentrated feed solutions. Operating pressures, therefore, are much lower than in RO since there is less osmotic pressure to overcome. Most nanofiltration membranes have fixed charges so separation of ionic solutes is achieved by coulombic interactions. This section, therefore, will concentrate on ion transport through charged nanofiltration membranes. Before the ion transport models are discussed, a discussion of ionic solute interactions with fixed charge surfaces (*Donnan equilibrium*) is required.

1.2.2.1 Donnan Exclusion Mechanism for Separation of Dissolved Salts

When a membrane with fixed charges is placed into contact with a dilute electrolyte solution, a dynamic equilibrium is established between the ions in solution and ions within the membrane. Counter-ions- ions with a charge opposite to the membrane charge- diffuse freely and exchange readily between the fixed sites within the

membrane and the contacting solution. Ions in solution with the same charge (co-ions) as the fixed charges are excluded from the membrane because of electrostatic repulsion. This phenomenon is known as Donnan exclusion and is shown in **Figure 1.4.**

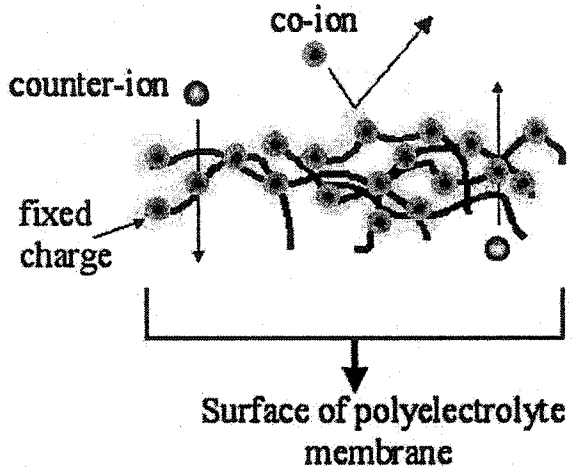

Figure 1.4 Donnan exclusion at the interface of a polyelectrolyte membrane and dilute electrolyte solution. Charge balancing counter-ions within the polyelectrolyte are omitted for clarity

Electroneutrality requires that the fixed charges, in the membrane, be electrically balanced by the counter-ions that are in excess of the co-ions. A consequence of the static nature of the charges within the membrane and the freely diffusive nature of the counter-ions in solution (outflow of counter-ions out of the membrane) is the establishment of a counter-ion concentration gradient between the membrane and the solution. The tendency of counter-ions to balance this concentration difference by diffusing out of the membrane and into the solution is countered by the electrostatic potential, the *Donnan potential* at the membrane-feed interface, created by the charge

imbalance within the membrane. A *Donnan equilibrium* is, thus, established in which the tendency of the ions to level out the concentration differences is balanced by the action of the electric field [83].

1.2.2.2 Transport of Ionic Solutes in the TMS Model

The fixed charge or Teorell [6] and Meyer and Sievers [7-9] (TMS) model has been used to describe rejection of charged reverse osmosis membranes [55]. The model, based on Donnan equilibria and the extended Nernst-Planck equation, predicts that salt rejection by charged membranes is governed by the relative ratio of the membrane effective charge density to the feed salt concentration and not on their absolute values [84,85].

The TMS model assumes a homogeneous distribution of electrical potential and ion concentration throughout the membrane. According to Probstein *et al.* [84] the radial concentration of ions and potential distribution across a pore are uniform when the Debye-Hückel screening length is much longer than the pore radius. Therefore, the TMS model is applicable only to small pores.

Kimura *et al.* successfully showed that rejection of single electrolyte solutions by charged reverse osmosis membranes could be predicted by numerical calculation of the extended-Nernst-Planck equation, accounting for the convective term, combined with the TMS model [85,86].

1.2.2.3 Transport of Ionic Solutes in the Space-Charge Model

The Space-Charge (SC) model developed by Osterle *et al.* [87-89] is operative when the pore size is much larger than the Debye-Hückel screening length and a gradient distribution of electric potential and ions exist in a radial direction across the pores. The pores are treated as straight capillaries and the ions as point charges. Steric effects, therefore, are neglected.

This model is significantly more complicated than the TMS model because of its integration of three equations: the Extended-Nernst-Planck equation, to describe ion transport; the Navier-Stokes equation, to describe volume flow; and the Poisson-Boltzmann equation, to describe the distribution of electric potential and radial ion concentration. Wang *et al.* [90] compared the TMS model with the SC model and found good agreement at small pore radii and low surface charge densities.

.

1.2.3 Ultrafiltration

On the gradient scale of membrane processes shown in **Figure 1.1**, ultrafiltration is also a transitional stage that lies between nanofiltration and microfiltration. The pore sizes of ultrafiltration membranes range from 0.05 μm (on the microfiltration side) to 1 nm (on the nanofiltration side) [91]. Most ultrafiltration membranes have an asymmetric

structure with a finely porous dense top layer responsible for the hydrodynamic resistance.

Separation of microsolutes from macromolecules and colloids in ultrafiltration occurs by a variety of mechanisms that include: exclusion of particles based on shape and size; adsorption of particles onto the internal and external surface of the membrane; *inertial impaction* of relatively large particles, that can enter the pores; and electrostatic interactions between a charged membrane and charged particles [92]. Since ultrafiltration membranes retain large molecules and not salt, the osmotic pressure difference between the feed and permeate solution is typically very low and the filtration can be carried out at relatively low pressures.

1.2.4 Transport Through Ultrafiltration Membranes

Mechanisms for transport through reverse osmosis and nanofiltration membranes are well understood with the establishment of the solution-diffusion and ion transport models. The success of these models was due, in a large part, to their applicability being independent of morphological differences in the membrane structure; that is, both the ion transport and solution-diffusion models are independent of whether the membrane is symmetric or asymmetric. Transport of solutes through ultrafiltration membranes, however, is not well understood because their wide variety of morphologies results in different mechanisms of transport [93].

Baker [93] discusses this point by stating that parameters such as porosity, pore diameter and membrane tortuosity, typically employed to characterize microporous membranes, are imperfect and often misleading. Asymmetric membranes, for example, can have very high overall porosities but such a number is meaningless since the thin top layer responsible for hydrodynamic resistance typically has a much reduced porosity. Ultrafiltration membranes come in a wide range of pore sizes so the quoted pore diameter is usually an average value. Membrane tortuosity (τ), which is a ratio of an average pore length to the membrane thickness, vary significantly unless all the pores are simple cylindrical pores perpendicular to the membrane surface (τ =1).

Hydrodynamic transport through an ultrafiltration membrane is dependent upon the pore geometry and different models have been developed to describe transport through such pores. The simplest model is based on a straight cylindrical pore perpendicular to the membrane surface. Hydrodynamic flow in such a pore is described by the Hagen-Poiseuille equation, assuming all the pores have the same radius, r. Where the volume flux (J) is proportional to the porosity (ε), applied pressure difference (ΔP), and inversely proportional to the membrane thickness (Δx), solution viscosity (η) and tortuosity (τ) which is equal to one in such a pore [94].

$$J = \frac{\varepsilon r^2}{8\eta\tau}\frac{\Delta P}{\Delta x} \quad \textbf{(1.6)}$$

The Hagen-Poiseuille equation is clearly affected by membrane morphology because of its dependence on tortuosity. Ultrafiltration membranes, in practice, rarely have the morphology described above and instead have moderate to high degrees of

tortuosity. In such cases, a modified Hagen-Poiseuille equation can be used which takes into account pore tortuosity through the Carman-Kozeny constant (K):

$$J = \frac{\varepsilon^3}{K\eta S^2 (1-\varepsilon)^2} \frac{\Delta P}{\Delta x} \quad \textbf{(1.7)}$$

where S is the internal surface area and ε is the volume fraction of the pores.

1.3 Pore Filled Membranes

Much of the membrane processes discussed thus far have focused on asymmetric membranes (**Figure 1.3**) since they represent the dominant class of membranes studied academically and used commercially. A new type of membrane construct, mentioned very briefly in **section 1.2.1**, is the pore filled membrane. Pore filled membranes are directly analogous to supported liquid membranes [95]. Supported liquid membranes are made by impregnating a porous hydrophobic host with a hydrophobic organic solvent containing carrier molecules such as crown ethers [96,97] or tertiary amines [98-100]. Since the organic phase is not "locked" into the pores by covalent bonding, the stability of these membranes is based solely on the immiscibility of the organic phase in the surrounding aqueous medium. These membranes, therefore, are not stable to trans-membrane pressures, arising from osmotic pressure differences, and typically lose the incorporated liquid over time [101]. Various attempts of stabilizing the incorporated organic phase have been made ranging from the application of a skin to the two surfaces [102,103] to the incorporation of a small amount of polymer to the organic phase capable

of forming a gel at low solvent concentrations [104]. In the latter case, the liquid film has the properties of a highly swollen cross-linked polymer (gel) rather than that of a liquid.

In the pore filled architecture, a highly solvent swollen gel is enmeshed within the confines of a host matrix by physical entanglement of the cross-linked polymer network [105,106] or by end grafting to the host substrate [107-111]. The term "soft gel in a rigid shell" was first applied by Boschetti [112] to discuss this type of construct; although he used the term in reference to incorporation of gels into packing materials for chromatographic applications. More recently, Kapur and Anderson [113] studied permeability through poly(acrylamide) gels supported in a microporous host. They established that membrane permeability (k_m) can be equated to gel permeability (k) by taking into account the host membrane porosity (ε) and tortuosity (τ), as shown in **equation 1.8.**

$$k = (\tau/\varepsilon)\, k_m \quad \textbf{(1.8)}$$

Kapur and Anderson's work provided a means to determine gel permeability since direct measurements by pressure driven flow through bulk, unsupported, gels result in a non-linear pressure-permeability response due to gel compression. Their work established that gels- despite their highly soft, pliable, nature- can be stabilized against-pressure induced deformations when incorporated in a host substrate. Pore filling, therefore, is not only a viable method for making membranes but also a means to study

gel properties that otherwise could not be possible. This point, and methods of fabricating pore filled membranes, will be discussed in greater detail in the following chapter. **Figure 1.5** shows a schematic representation of a pore filled membrane.

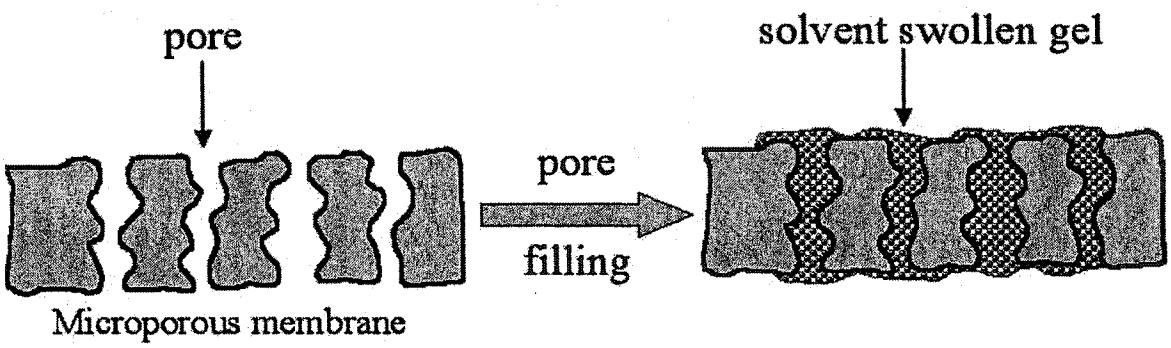

Figure 1.5 Formation of pore filled membrane

1.4 Conclusion

This chapter has provided a general introduction and brief overview of concepts and principles relevant to the discussion of polyethylenimine pore filled membranes. The purpose of this chapter is to provide a general theoretical understanding and perspective of membrane technology. Chapter two will be a detailed, and focused, examination of pore filled membranes with discussions of fabrication, characterization and performance from the perspective of a chronological account of ideas and developments within the McMaster membrane group. Collectively, chapters one and two will establish the context

for the discussion of polyethylenimine pore filled membranes that is the basis of this thesis.

1.5 REFERENCES

1. Strathmann, H. *AIChE J.* **2001**, *47*, 1077
2. Nollet, J.A. *Histoire de l' Académie Royale des Sciences* **1752**, 57 *reprinted in J. Memb. Sci.* **1995**, *100*, 1
3. Dutrochet, R. J. H. *Annales de Chimie et de Physique* **1872**, *35*, 393 *reprinted in J. Memb. Sci.* **1995**, *100*, 5
4. Fick, A. *The London, Edinburgh, and Dublin Philosophical Magazine and Journal of Science* **1855**, *X*, 59 *reprinted in J. Memb. Sci.* **1995**, *100*, 33
5. Donnan, F. G. *Zeitschrift für Elektrochemie und angewandte physikalische Chemie* **1911**, *17*, 572 *reprinted in J. Memb. Sci.* **1995**, *100*, 45
6. Teorell, T. *Prog. Biophys. Biophys. Chem.* **1953**, *3*, 305
7. Meyer, K.H. & Sievers, J.F. *Helv. Chim. Acta.* **1936**, *19*, 649
8. Meyer, K.H. & Sievers, J.F. *Helv. Chim. Acta.* **1936**, *19*, 665
9. Meyer, K.H. & Sievers, J.F. *Helv. Chim. Acta.* **1936**, *19*, 987
10. Baker, R.W. Membrane Technology and Applications. New York, McGraw-Hill, 2000
11. Merill, J.P. *Scientific American* **1961**, *205*, 56
12. Reid, C. E.; Breton, E. J. *J. App. Polym. Sci.* **1959**, *1*, 133

13. Breton, E.J. *Office of Saline Water, U.S. Dept. of the Interior, Res. & Dev. Prog. Rept.* **1957**, *April*, 16

14. Loeb, S.; Sourirajan, S. *Adv. Chem. Sep.* **1962**, *38*, 117

15. Jonsson, G. *Kidney Dialysis* In: Membrane Handbook, Ho, W.S & Sirkar, K.K. (ed.), New York, Van Nostrand Reinhold, 1992, 625

16. Kessler, S.H. & Klein, E. *Applications* In: Microfiltration and Ultrafiltration-Principles and Applications, Marcel Dekker, 1996, 206

17. Lysaght, M.J.; Boggs, D.R.; Taimisto, M.H. *Membranes in Artificial Organs.* In: Synthetic Membranes, Chenoweth, M.B. (ed.), Chur, Switzerland, Hardwood Academic Publishers, 1986

18. Kolf, W.J. & Berk, H.T. *Aeta Med. Scan.* **1944**, *117*, 121

19. Stowe, J.C. *Hemodialysis Apparatus* In: Handbook of Dialysis, 2nd ed. Daugirdas, J.T. & Ing, T.S. (eds.), New York, NY, Lippincott-Raven Publishers, 1994

20. Santus, G. & Baker, R.W. *J. Cont. Rel.* **1995**, *35*, 1

21. Toschima, N. (ed.) Polymers for Gas Separation, Wenheim, VCH, 1991

22. Paul, D.R. & Yampolskii, Y. (ed.) Polymeric Gas Separation Membranes, London, CRC Press, 1994

23. Koros, W.J. & Fleming, G.K. *J. Memb. Sci.* **1993**, *83*, 1

24. Spillman, R.W. *Chem. Eng. Prog.* **1989**, *85*, 41

25. Eykamp, W. *Microfiltration and Ultrafiltration.* In: Membrane Separation Technology. Principles and Applications., Noble, R.D. & Stern, S.A. (eds), Amsterdam, Elsevier, 1995

26. Kosikowski, F.V. *Membrane Separations in Food Processing.* In: Membrane Separations in Biotechnology, McGregor, W.C. (ed), New York, Marcel Dekker, 1986

27. Blanck, R.G. & Eykamp, W. *Fruit Juice Ultrafiltration.* In: Recent Advances in Separation Techniques-III, Li, N.N. (ed.), AIChE Symposium Series no. 250, 1986, p.82

28. Sourirajan, S., Reverse Osmosis, New York, Academic Press, 1970

29. Ko, A. & Guy, D.B. *Brackish and Sea Water Desalting.* In: Reverse Osmosis Technology, Parekh, B. (ed.), New York, Marcel Dekker, 1988

30. Firth, C.F., *Electronic Grade Water Production Using Reverse Osmosis Technology.* In: Reverse Osmosis Technology, Parekh, B. (ed.), New York, Marcel Dekker, 1988

31. Lonsdale, H.K. *Desalination* **1973**, *13*, 317

32. Glimenius, R. *Desalination* **1980**, *35*, 259

33. Cruver, J.E. & Nusbaum, I. *J. Water. Poll. Cont. Fed.* **1974**, *46*, 301

34. Daniels, F. & Alberty, R.A., Physical Chemistry 3rd. ed., New York, John Wiley and Sons Inc., 1972

35. Dutta, B. K.; Randolph, D.; Sikdar, S. K. *J. Memb. Sci.* **1990**, *54*, 51

36. Petersen, R. J. *J. Memb. Sci.* **1993**, *83*, 81

37. Petersen, R. J. & Cadotte, J. E., *Thin film composite membranes.* In: Handbook of Industrial Membrane Technology, Porter, M.E. (ed.), Park Ridge, N.J., Noyes Publications, 1990

38. Ji, J.; Trushinski, B.J.; Childs, R.F.; Dickson, J.M.; McCarry, B.E. *J. Appl. Polym. Sci.* **1997**, *64*, 2381

39. Hirose, M.; Ito, H.; Kamikaya, Y. *J. Memb. Sci.* **1996**, *121*, 209

40. Kwak, S.Y.; Jung, S.G.; Yoon, Y.S.; Ihm, D.W. *J. Polym. Sci.: Part B: Polym. Phys.* **1999**, *37*, 1429

41. Kimura, S. & Sourirajan, S. *AIChE J.* **1967**, *13*, 497

42. Matsuura, T.; Sourirajan, S. *Ind. Eng. Chem. Process Des. Dev.* **1981**, *20*, 273

43. Jacazio, G.R.; Probstein, R.F.; Sonin, A.A.; Yung, D. *J. Phys. Chem.* **1972**, *76*, 4015

44. Neogi, P. & Ruckenstein, E. *J. Coll. Int. Sci.* **1981**, *79*, 159

45. Merten, U. (ed.) In: Desalination by Reverse Osmosis, Cambridge, M.I.T. Press, 1966

46. Wijmans, J.G. & Baker, R.W. *J. Memb. Sci.* **1995**, *107*, 1

47. Lonsdale, H.K.; Merten, U.; Riley, R.L. *J. Appl. Polym. Sci.* **1965**, *9*, 1341

48. Burghoff, H.G.; Lee, K.L.; Pusch, W. *J. Appl. Polym. Sci.* **1980**, *25*, 323

49. Jonsson, G. *Desalination* **1980**, *35*, 21

50. Sherwood, T.K.; Brian, P.L.; Fisher, R.E. *Ind. Eng. Chem. Fundamentals* **1967**, *6*, 2

51. Kedem, O. & Katchalsky, A. *Biochem. Biopys. Acta.* **1958**, *27*, 229

52. Spiegler, K.S. & Kedem, O. *Desalination* **1966**, *1*, 311

53. Smit, E.; Mulder, M.H.; Smolders, C.A.; Karrenbeld, H.; van Eerden, J.; Feil, D. *J. Memb. Sci.* **1992**, *73*, 247

54. Kotelyanskill, M.J.; Wagner, N.J.; Paulaitis, M.E. *J. Memb. Sci.* **1998**, *139*, 1

55. Hoffer, E. & Kedem, O. *Desalination* **1967**, *2*, 25

56. Mulder, M. Basic Principles of Membrane Technology, 2nd ed. Dordrecht, Kluwer Academic Publishers, 1996, p. 17

57. Cadotte, J.E. & Petersen, R.J. *Thin film reverse osmosis membranes: origin, development and recent advances.* In: Synthetic Membranes. Vol.I, Desalination, Turbak, A.F. (ed.), Washington, D.C., American Chemical Society, 1981

58. Kopecek, J. & Sourirajan, S. *Ind. Eng. Chem. Process Design Dev.* **1970**, *9*, 5

59. Farnand, B.; Talbot, F.; Matsuura, T.; Sourirajan, S. *Ind. Eng. Chem. Process Design Dev.* **1983**, *22*, 179

60. Sourirajan, S. *Nature* **1964**, *203*, 1348

61. Sourirajan, S. & Matsuura, T. Reverse Osmosis/Ultrafiltration Principles. Ottawa, National Research Council of Canada, 1985

62. Paul, D.R. & Ebra-Lima, O.M. *J. Appl. Polym. Sci.* **1970**, *15*, 2199

63. Paul, D.R.; Paciotti, J.D.; Ebra-Lima, O.M. *J. Appl. Polym. Sci.* **1975**, *19*, 1837

64. Paul, D.R.; Paciotti, J.D. *J. Polym. Sci.* **1975**, *13*, 1201

65. Paul, D.R. *Sep. Purif. Meth.* **1976**, *5*, 33

66. Aminabhavi, T.M.; Khinnavar, R.S. *Polymer* **1993**, *34*, 1006

67. Aminabhavi, T.M.; Payde, H.T. *J. Appl. Polym. Sci.* **1995**, *55*, 17

68. Raman, L.P.; Cheryan, M.; Rajagopalan, N. *Lipid* **1996**, *98*, 10

69. Raman, L.P.; Cheryan, M.; Rajagopalan, N. *J. Am. Oil Chemists' Soc.* **1996**, *73*, 219

70. Niwa, M.; Ohya, H.; Kuwahara, E.; Negishi, Y. *J. Chem. Eng. Jpn.* **1998**, *21*, 164

71. Koseoglu, S.S.; Lawhorn, J.T.; Lusas, E.W. *J. Am. Oil Chemists' Soc.* **1990**, *67*, 315

72. Schmidt, M.; Mizra, S.; Schunert, R.; Rodicker, H. *Chemie Ingeniuer Technik.* **1998**, *71*, 199

73. Tsuru, T.; Sudoh, T.; Yoshioka, T.; Asaeda, M. *J. Memb. Sci.* **2001**, *185*, 253

74. Gibbins, E.; Antonio, M.; Nair, D.; White, L.; Freitas, L.; Livingston, A.; *Desalination* **2002**, *147*, 307

75. Bhanashuali, D.; Kloos, S.; Kurth, C.; Bhattacharyya, D. *J. Memb. Sci.* **2001**, *189*, 1

76. Bhanashuali, D.; Kloos, S.; Bhattacharyya, D. *J. Memb. Sci.* **2002**, *208*, 343

77. Tsuru, T.; Urairi, M.; Nakao, S.; Kimura, S. *Desalination* **1991**, *81*, 219

78. Ho, W. & Sirkar, K. Membrane Handbook, New York, Van Norstrand Reinhold, 1992

79. Cadotte, J.; Forester, R.; Kim, M.; Petersen, R.; Stocker, T. *Desalination* **1988**, *70*, 77

80. Rautenbach, R. & Groschl, A. *Desalination* **1990**, *77*, 73

81. Ikeda, K.; Nakano, T.; Ito, H.; Kubota, T.; Yamamoto, S. *Desalination* **1988**, *68*, 109

82. Childs, R.F.; Mika, A.M.; Pandey, A.K.; McCrory, C.; Mouton, S.; Dickson, J. *Sep. Pur. Tech.* **2001**, *22-23*, 507

83. Hefferich, F. Ion Exchange, McGraw Hill Book Co. Inc., Toronto, 1962

84. Probstein, R.F.; Sonin, A.A.; Yung, D. *Desalination* **1973**, *13*, 303

85. Tsuru, T.; Nakao, S.; Kimura, S. *J. Chem. Eng. Jpn.* **1991**, *24*, 511

86. Tsuru, T.; Urari, M.; Nakao, S.; Kimura, S. *J. Chem. Eng. Jpn.* **1991**, *24*, 518

87. Morrison, F.A. & Osterle, J.F. *J. Chem. Phys.* **1965**, *43*, 2111

88. Gross, R.J. & Osterle, J.F. *J. Chem. Phys.* **1968**, *49*, 228

89. Fair, J.C. & Osterle, J.F. *J. Chem. Phys.* **1971**, *54*, 3307

90. Wang, X.L.; Tsuru, T.; Nakao, S.I.; Kimura, S. *J. Memb. Sci.* **1995**, *103*, 117

91. ibid 56, p. 293

92. Porter, M.C. Synthetic Membranes. Science, Engineering & Application, Bungay, P.M. (ed.) Reidel Publishing, 1986, 234

93. ibid 10, p.66

94. ibid 56, p224

95. Schulz, G. *Desalination* **1988**, *68*, 191

96. Lamb, J.D.; Brown, P.R.; Christensen, J.J.; Bradshaw, J.S.; Garrick, D.G.; Izatt, R.M. *J. Memb. Sci.* **1983**, *13*, 89

97. Izatt, R.M.; Haws, R.M.; Lamb, J.D.; Dearden, D.V.; Brown, P.R.; Christensen, J.J. *J. Memb. Sci.* **1984**, *20*, 273

98. Babcock, W.C.; Baker, R.W.; Conrod, M.G.; Smith, K. *J. Memb. Sci.* **1980**, *7*, 17

99. Babcock, W.C.; Baker, R.W.; Chapelle, E.; Smith, K. *J. Memb. Sci.* **1980**, *7*, 89

100. Imato, T.; Yabu, S.; Morooka, A. *J. Memb. Sci.* **1982**, *10*, 21

101. Kemperman, A.J.; Bargeman, D.; van den Boomgaard, T.; Strathmann, H. *Sep. Sci. Technol.* **1996**, *31*, 2733

102. Wijers, M.C.; Jin, M.; Wessling, M. Strathmann, H. *J. Memb. Sci.* **1998**, *147*, 117

103. Wang, Y. & Doyle, F.M. *J. Memb. Sci.* **1999**, *159*, 167

104. ibid 56, p. 355

105. Makino, Y.; Hamada, K.; Iijima, T. *Polymer Journal* **1987**, *19*, 737

106. Nakanishi, T.; Usuda, Y.; Tak, T. *Polymer Commun.* **1986**, *26*, 300

107. Jayachandran, K.N. & Chatterji, P.R. *J.M.S. Pure Appl. Chem.* **1998**, *A35*, 1971

108. Thom, V.; Jankova, K.; Ulbricht, M. *Macromol. Chem. Phys.* **1998**, *199*, 2723

109. Larsson, C. & Wesslen, B. *J. Appl. Polym. Sci.* **1993**, *50*, 345

110. Bellobono, I.; Selli, E.; Marcandelli, B. *J. Photochem.* **1986**, *35*, 231

111. Imaizumi, M.; Kubota, H.; Hata, Y. *Eur. Polym. J.* **1994**, *30*, 979

112. Boschetti, E. *J. Chromatogr. A.* **1994**, *658*, 207

113. Kapur, V.; Charkoudian, J.; Kessler, S.; Anderson, J.L. *Ind. Eng. Chem. Res.* **1996**, *35*, 3179

CHAPTER TWO

FROM COATING TO PORE FILLING: THE DEVELOPMENT OF THE GEL FILLED MEMBRANE TECHNOLOGY AT McMASTER UNIVERSITY

Abstract

This chapter discusses the major achievements of the membrane group at McMaster University. Although many people have collectively contributed to the understanding of membrane processes, the majority of the work reported here have been developed and done by Drs. Alicja Mika and Ron Childs. The writing of this chapter was motivated by a desire to chronicle the details and evolution of ideas that are both sublime in their logic and profound in their contributions to membrane science. This chapter integrates the contents of many published papers and provides a contextual framework for the chapters to follow.

2.1 Surface Modification of Thin Film Composites

Early research in the McMaster Membrane group focused on thin film composite reverse osmosis membranes [1] with particular focus on developing methods of modifying and optimizing the surface layer [2-4]. A variety of methods of optimization of the chemical nature and physical structure of the surface layer of a thin film composite had been known [5-11]; however, such methods typically had poor reproducibility and were relatively inefficient in achieving the desired chemical transformations. Methods that produced high degrees of modification typically lead to degradation of the initial membrane materials. A post fabrication, photochemical route was therefore developed to meet the needs of surface optimization while not compromising the structural integrity of the membrane itself.

A diazoketone functionality was chosen as a moiety for derivatization of a monomer because of their well established use in photoresist chemistry [12-18]. Interfacial polymerization of ethanediamine with a disulfonyl chloride diazoketone was performed on the surface of a proprietary ultrafiltration polysulfone support as shown in **Scheme 2.1**.

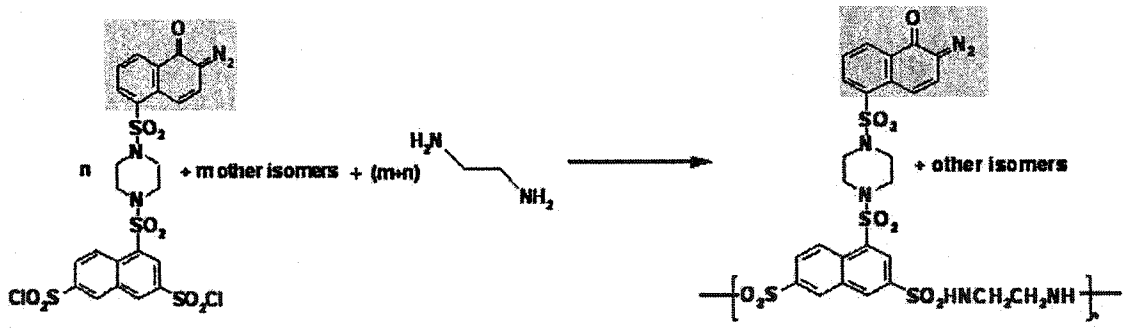

Scheme 2.1 Polymerization of a disulfonyl chloride diazoketone with ethanediamine on the surface of the polysulfone ultrafiltration membrane. Diazoketone moiety shaded in gray

The diazoketone chromophore absorbs at long wavelengths (350 nm) where degradation of the polymer support is not expected to occur. Absorption of ultraviolet light results in a photochemical reaction where nitrogen is expelled and a ketene intermediate is formed [3]. This ketene intermediate is highly reactive towards any ambient nucleophiles in its vicinity to generate a new functional group as shown in **Scheme 2.2**.

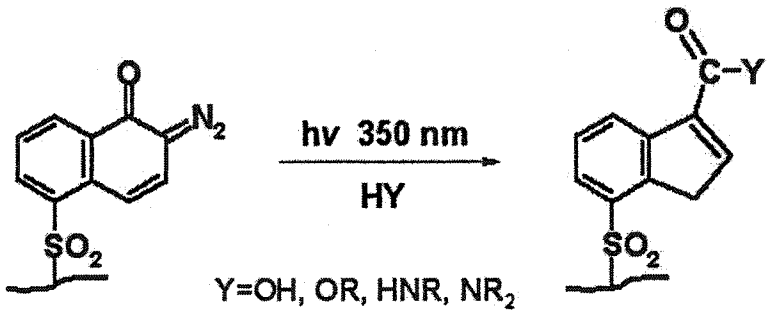

Scheme 2.2 Ultraviolet light induced transformation of diazoketone moiety

The membranes performed poorly as reverse osmosis membranes with low rejections of 0.17 M NaCl (< 34%). Their poor performance, combined with long

reaction times for fabrication made them impractical for industrial applications; however, the incorporation of a photochemically modifiable surface agent was a novel idea with great potential.

2.2 Pore Coating and Pore Filling: New Paradigms in Membrane Construction

At about this time, 3M corporation became aware of the surface activation technology and were interested in applying it to modifying the surface properties of their hydrophobic thermally induced phase separated (TIPS) microporous membranes. They found previous attempts at changing the surface properties by coating with a hydrophilic polymer (poly(vinyl alcohol)) to be difficult and thus initiated a joint collaboration with the McMaster membrane group. These TIPS membranes also represented a significant turning point in the research conducted by the Membrane group at McMaster because they represented a highly versatile platform for exploring many different membrane constructs.

2.2.1 The TIPS Host Substrate

3M manufactured the poly(propylene) TIPS host membrane by a thermally induced phase separation method [19]. The membranes were prepared by melt-blending the polypropylene and mineral oil and extruding it into a film. The mineral oil acts as a solvent for polypropylene at high temperatures and a nonsolvent at lower temperatures. Therefore, as the extruded film is cooled rapidly, phase separation of the polypropylene

from the mineral oil occurs and the polymer solidifies. The mineral oil is removed from the polypropylene by solvent extraction and the formed membrane is stretched axially to yield the desired pore size and thickness [20].

The polypropylene membranes met the requirements of a good host substrate in that they are chemically inert, highly porous and possess good tensile strength. The latter two properties are of extreme importance because the properties of the pore filled membrane are determined largely by the nature of the incorporated gel. All convective and diffusive transport occurs through the gel phase therefore the porosity of the host determines the amount of gel that can be incorporated. Polyelectrolyte gels, however, are structurally weak and susceptible to large osmotic swelling and deformation under applied pressures [21]. A strong skeletal host, therefore, is required for containment of the gels for any practical pressure driven applications. An electron micrograph of a TIPS membrane is shown below.

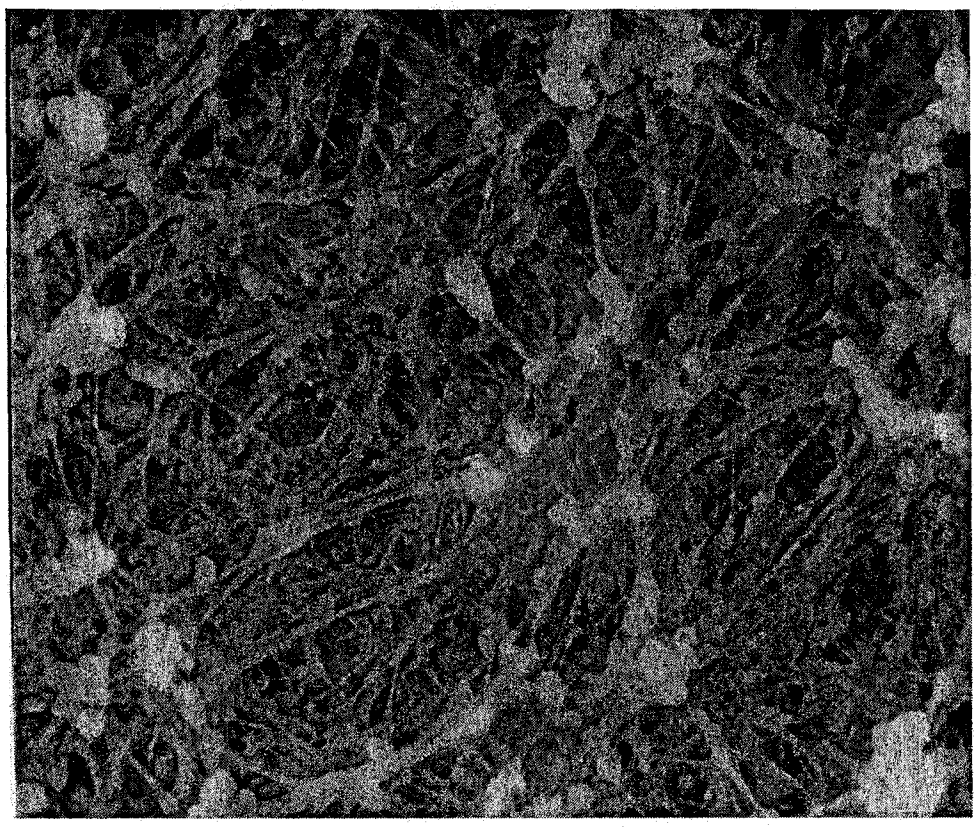

Figure 2.1 Environmental Scanning Electron Micrograph of a polypropylene TIPS membrane (PP3) obtained by the author

2.2.2 Development of a Coating Technique

The coating of the internal structure of a polypropylene membrane was accomplished by use of a novel interfacial polymerization technique. Sulfonamide chemistry similar to the surface modification of thin film composites mentioned earlier was used. [22]. A polysulfonamide layer was coated onto the base membrane structure by a sequential process that first involved evaporative deposition of an α,ω-diamine (ranging from ethyl to dodecyl). The diamine coating was then polymerized by

contacting the coated membrane with a solution of 1,5-napthalene disulfonyl chloride (NDSC) (**Figure 2.2a**) and cross-linked with 1,3,6-napthalene trisulfonyl chloride (NTSC) (**Figure 2.2b**).

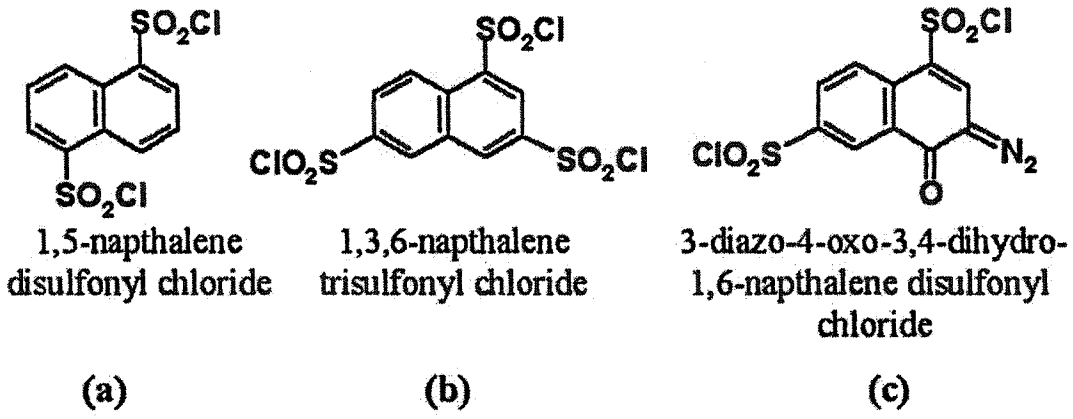

Figure 2.2 Sulfonyl chloride comonomers used for polysulfonamide coating reactions

A diazoketone comonomer (**Figure 2.2c**) was also used as a means of functionalizing the internal microstructure of a microporous membrane and this process was granted US patent protection in 1997 [23]. Because the coating process is a two-step procedure, in the interfacial polycondensation reaction of the deposited diamine, the solvent strength of the NDSC/NTSC solution was found to be a crucial parameter in the efficacy of this process. Solvents that dissolved the diamine, and growing oligomeric chains, displaced the polysulfonamide coating by allowing diffusion away from the pore walls; however, the use of a solvent that could not dissolve the diamine or growing oligomeric chain ensured the reaction could only proceed at the pore surface/solvent interface.

The coated membranes resembled the dendritic nascent membrane structure, under scanning electron microscopy; however, most of the membranes exhibited uneven and non-homogeneous coatings due to granular formations dispersed throughout the microstructure. Only membranes fabricated with 1,8-octanediamine yielded smooth, homogeneous coatings. Regardless of the morphology, the coated layer changed the surface property of the polypropylene membranes from hydrophobic to hydrophilic, determined by reduced fouling tendencies in permeation studies with polystyrene and carboxylate modified polystyrene latex spheres.

2.2.3 Further Coating Attempts by Photochemical *in situ* Polymerization

At about the same time, a technique to incorporate a polyelectrolyte was being explored by an *in situ* polymerization process [24]. Examples of graft polymerization were well known and the technique had been extensively reviewed in numerous articles and books [25-31]. The intent with the *in situ* polymerization process was to coat the internal surface of the membrane by photografting a hydrophilic polymer, or one that could be made hydrophilic in a simple post-fabrication step. To this end, the microporous host membranes were impregnated with a solution 4-vinylpyridine and photoinitiator (benzoin ethyl ether) and polymerized by UV light (300nm) activation. Membranes made by this route were extremely robust and the incorporated polymer could not be extracted.

The technique was successful in grafting large amounts of poly(4-vinyl pyridine) with mass gains of up to 126% achieved. But the most startling finding was a spectacular pH valve observed upon addition of acid. Pressure driven solvent flux through the membrane could be reduced by three orders of magnitude- effectively transforming a microfiltration membrane to a nanofiltration membrane- by lowering the pH to below 4 as illustrated in **Figure 2.3**. This clearly indicated the grafted poly(4-vinyl pyridine) existed in a collapsed state, on the pore walls, but extended to fill the pores when protonated due to electrostatic repulsions between the fixed charge centers.

The membranes, in the acidic pH regime, could separate salts whereas no rejection of solutes was observed at pH ranges above 4 when the valve was open. However, flux and salt separation varied greatly upon the concentration of the salt in the feed. This indicated that convective flow of solvent through the protonated polymer matrix was a very dynamic process due to the mobility of the polymer chains. This suggested that immobilization of the grafted polymers by cross-linking should increase the stability of these membranes.

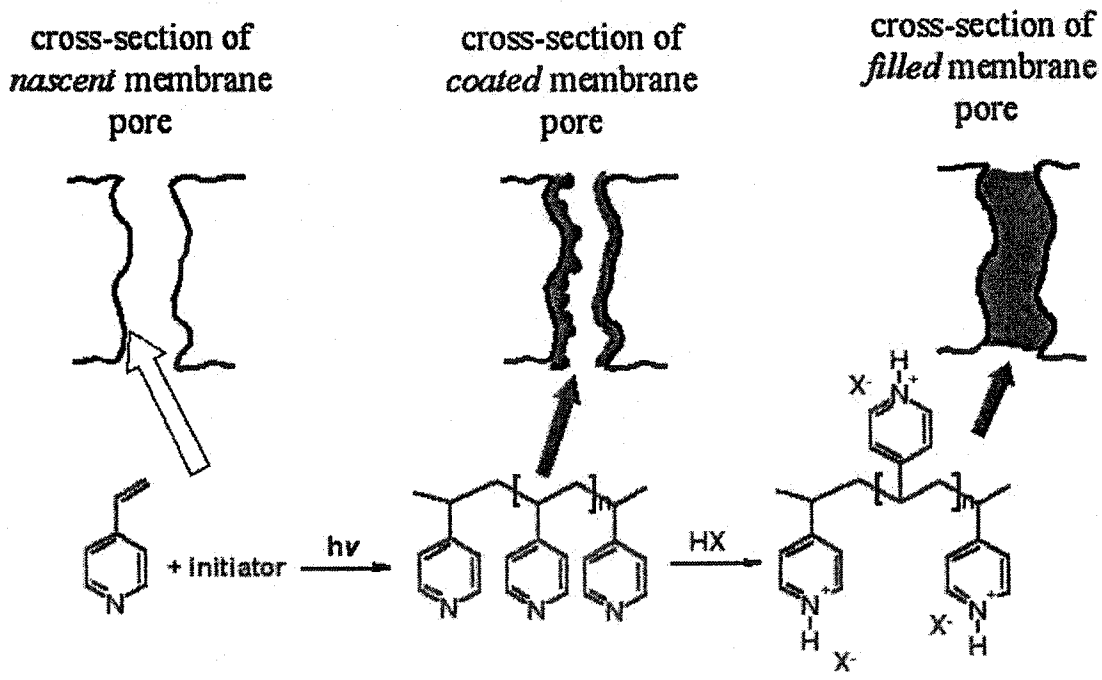

Figure 2.3 Coated membrane formed by in situ polymerization of 4-vinylpyridine in the pores of a polyolefinic microfiltration membrane. Coated polymer expands when protonated to give pore filled membrane [24]

2.2.4 Development of a Pore Filling Technique

The environmental sensitivity and adjustable properties of the poly(4-vinyl pyridine) grafted membranes created much interest in this new membrane construct. The focus was again directed at reverse osmosis; however, unlike the thin-film composite membranes previously discussed, these new pore filled membranes were symmetric in their morphology, easy to manufacture defect free and could be made with good control over parameters such as cross-linking and mass gains.

As discussed previously, the poly(4-vinylpyridine) photografted membranes exhibited reverse osmosis behavior when protonated, but their flux and salt separation performances were highly variable depending on the feed ionic strength. To improve their stability, 4-vinylpyridine was photografted with small amounts (up to 2.2% w/w) of divinylbenzene (DVB) as a cross-linker [32]. Mass gains increased with DVB content and substantial graft yields of up to 200% were attained. Furthermore, cross-linking immobilized the grafted polymers in the pore such that it could not collapse back onto the pore wall.

The effect of cross-linking was observed in the improved membrane stability with respect to feed composition and ionic strength; furthermore, an increase in cross-linking resulted in a decrease in flux with an increase in rejection of ionic solutes. These findings generated a great deal of excitement in this new class of reverse osmosis membranes. Solute rejections exceeded what was previously observed with the thin film composite membranes, mentioned earlier [1], and the fluxes were comparable even though the thickness of the pore filled membranes were several hundred times greater than the separating layer of the thin film composites! These membranes represented great potential in reverse osmosis/nanofiltration applications and effort was directed at optimizing their performance.

2.2.5 *In situ* Polymerization of Vinyl Monomers Initiated by an Incorporated *Azo* Initiator

New methods of membrane construction and morphologies were actively being explored with the flexibility offered by the TIPS substrates. With the establishment of the *in situ* polymerized pore-coating and pore-filling technique with poly(4-vinyl pyridine), incorporation of other monomers such as acrylic acid, vinylbenzyl chloride, styrene and styrene sulfonic acid was considered. Attempts at photografting these monomers, in the absence of cross-linkers, were unsuccessful and a new method of incorporation was developed which involved incorporation of a radical initiator into a surface coated polymer layer [33]. This new method was a tandem two step process that first involved coating the pores of a microfiltration membrane with polyethylenimine (PEI) cross-linked with NDSC with a post-fabrication attachment of the radical initiator 4,4'-azobis(4-cyanovaleryl chloride) as illustrated in **Figure 2.4**. This idea was a variation of the surface activation with diazoketone coating concept reported earlier [22].

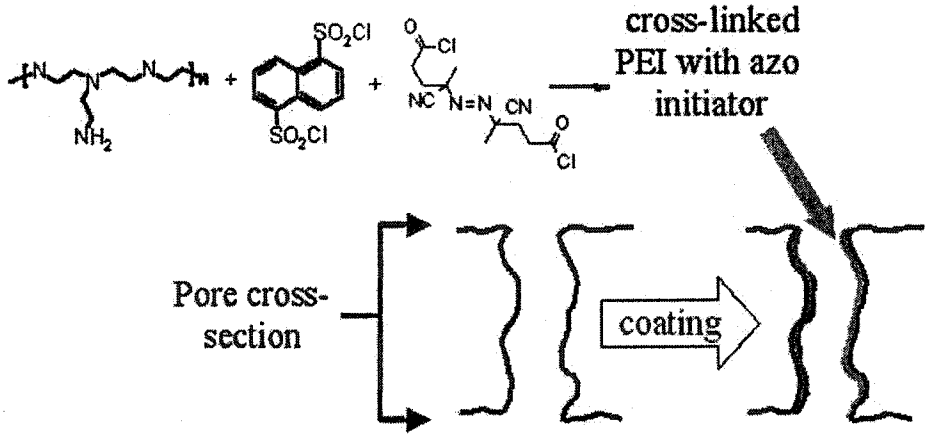

Figure 2.4 Coating the pores of a microporous membrane with polyethylenimine and incorporating a thermally degradable azo initiator [33]

Vinyl monomers were then introduced in a subsequent step and polymerized by thermal initiation at 70° C as depicted in **Figure 2.5**. A wide variety of polymers, such as polystyrene, poly(4-vinylpyridine), and poly(acrylic acid) were successfully *in situ* polymerized by this method. Membranes grafted with poly(acrylic acid) also exhibited the pH valve effect, but in the opposite direction of poly(4-vinylpyridine) since poly(acrylic acid) is charged at high pH values.

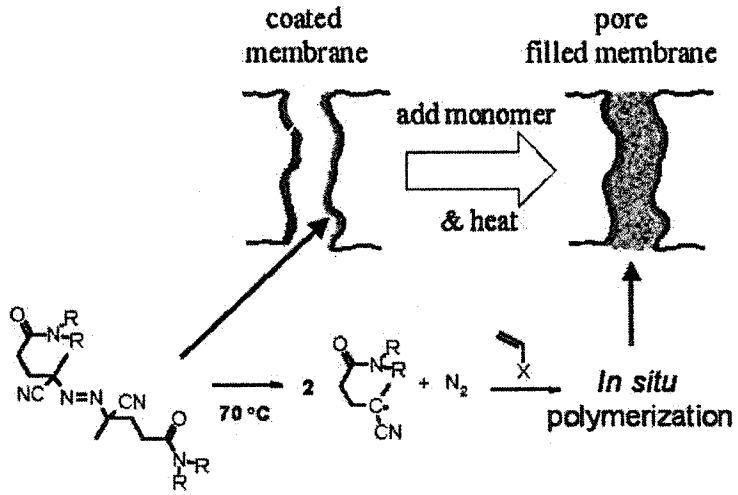

Figure 2.5 Thermal degradation of the incorporated azo compound in the presence of vinyl monomers [33]

2.2.6 Development of the Pore Filling Technique by *in situ* Cross-linking of Preformed Polymers

The coating/grafting method established two very important routes for modifying the properties of the TIPS substrate. First, the internal microstructure of the TIPS membrane could be coated with a prefabricated polymer and secondly, *in situ*

polymerization could occur via thermal initiation from an activated coated surface to incorporate a large variety of vinyl monomers. The PEI coat changed the surface properties of the base polyolefin membrane from hydrophobic to moderately hydrophilic with measurable ion-exchange capacities (IEC). **Table 2.1** shows some physical properties of PEI coated membranes.

Table 2.1 Physical Properties and Pure Water Flux Measured at 100 kPa and 25 °C of Nascent and PEI Coated Membranes from [33]

Membrane	Mass Gain of PEI (%)	IEC (meq/g)	Pure Water Flux (kg/m^2h)
Nascent	0	0	10728
Coated 1	28	0.69	-
Coated 2	18	0.05	7704

As can be seen from the pure water flux data in **Table 2.1**, the coated membrane 2 still retains the microfiltration characteristics of the base substrate with only a minor decrease in flux.

When the coating experiment was repeated with a higher concentrated solution of PEI, large amounts of the polymer could be deposited. Cross-linking of this PEI layer resulted in membranes exhibiting remarkable fluxes and separations characteristic of nanofiltration membranes at *ultra-low* pressures. Details of this finding will be discussed later in chapter three.

The membranes produced by this route, however, were often inconsistent in their performance with long times required for equilibration. A better method of fabrication was thus required since the membranes made by this route were often difficult to

reproduce. This method, despite its shortcomings, provided an intriguing route for pore filling by *in situ* cross-linking of a preformed polymer.

A modified, and superior, method of *in situ* cross-linking preformed polymers was developed by Pandey *et al.* [34-36] where poly(vinylbenzyl chloride) (PVBCl) polymers were *in situ* cross-linked with piperazine (PIP) or 1,4-diazabicyclo[2.2.2]octane (DABCO) as shown in **Scheme 2.3**. This method has also been used to fabricate membranes containing poly(4-vinyl pyridine) as depicted in **Scheme 2.4** and polyethylenimine as will be shown in the following chapters.

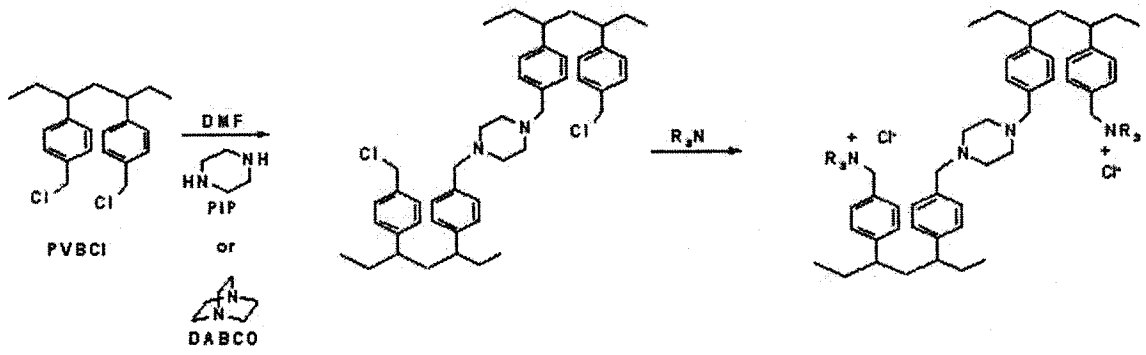

Scheme 2.3 In situ cross-linking of polyvinyl benzyl chloride [35]

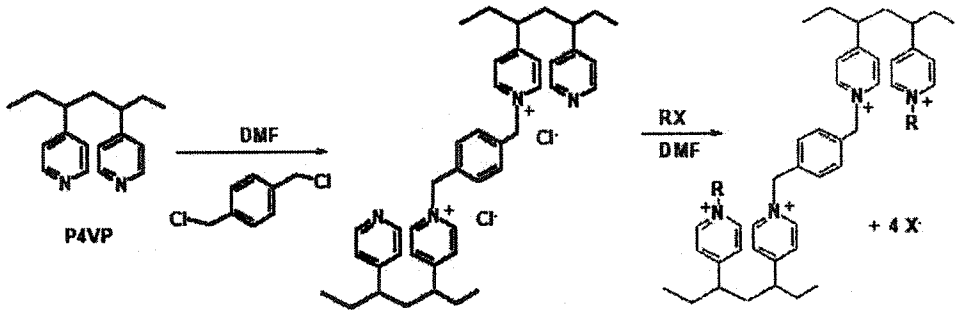

Scheme 2.4 In situ cross-linking of poly(4-vinyl pyridine) [34]

This *in situ* cross-linking method of making pore filled membranes provides good control over parameters such as gel polymer concentration and degrees of cross-linking [35]. This method is not suitable for making membranes requiring high mass loadings because a solvent must be used to insert the preformed polymer and cross-linker into the porous host. The amount of material that can be incorporated is, therefore, limited by the solubility of the polymer in the solvent and the solution viscosity. The *in situ* polymerization method does not impose such restrictions and is the method of choice to make membranes requiring very high mass loadings [37,38].

2.3 Performance of Pore Filled Membranes Under Pressure Driven Conditions

Much of the work and understanding of the pore filled membrane technology have been accomplished on poly(4-vinyl pyridine) filled membranes, although poly(acrylic acid), poly(vinylbenzyl ammonium), poly(styrene sulfonic acid) and polyethylenimine (as will be discussed later) have all been studied extensively as pore fillers. Throughout the development of this technology, it has become clear that the study of pore filled membranes is really a fundamental study of the properties of the polyelectrolyte gel filling itself. The host membrane, provided it possesses the requisite mechanical strength, serves merely as a convenient containment device to study the polyelectrolyte gel without the constraints imposed by their inherent fragility. Anderson *et al.* understood this principle and were the first to apply it to the hydrodynamic study of polyacrylamide pore filled membranes [39].

This *gel in a shell* construct allows for a fundamental investigation of the hydrogel physical properties which, in turn, would provide the means to custom tailor and optimize performance for any membrane application. With methods of fabrication firmly established in the previous sections, the following sections will report on the evolution of the pore filled technology from a largely empirical and phenomenological understanding to the current and powerful models of permeability and charged solute separations.

2.3.1 Gels, Brushes and pH Valves

As mentioned before, the physicochemical behavior of poly(4-vinyl pyridine) is governed by a balance between the attractive interactions among the fixed charges and counter-ions versus electrostatic repulsive interactions among the fixed charges on the macromolecular chain [40]. This conformational sensitivity of poly(4-vinyl pyridine) to pH was observed in the remarkable valve effect where membranes exhibited three orders of magnitude change in flux within the pH range of 2 to 5 [24,41]. An explanation of this phenomenon required a more fundamental understanding of the physical/chemical processes involved with flow through a polyelectrolyte filled pore. This was approached by examination of two models of hydrodynamic permeability- pressure driven flow through a cylinder pore partly obscured by a graft layer [42-46] (brush model) and the hydrodynamic flow through an interpenetrating polymer network [39] (pore-filled model) as illustrated in **Figure 2.6**.

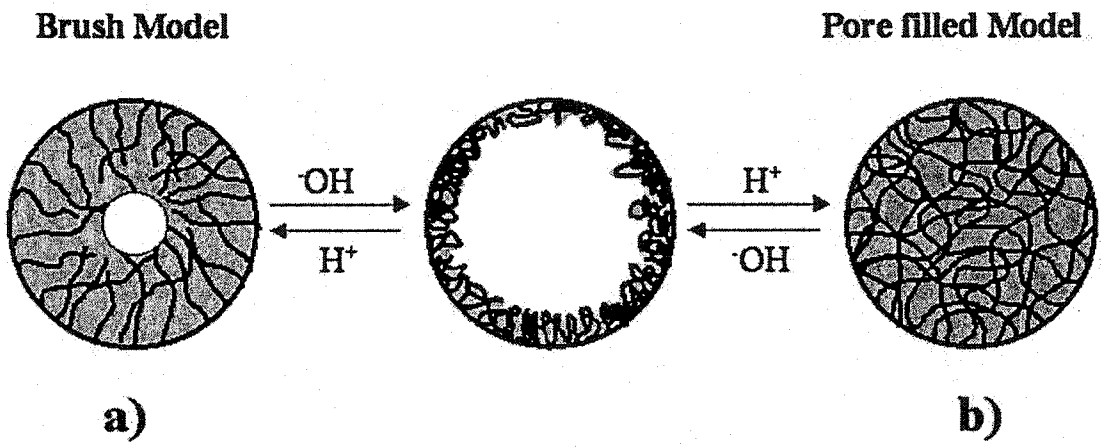

Figure 2.6 Schematic representation of a brush filled a) and an interpenetrating polymer network b) pore

The brush model (**Figure 2.6a**) describes hydrodynamic flow through pores obstructed with grafted polymer layers. In this model, the poly(4-vinyl pyridinium) chains were assumed to extend into the pores forming an open, small center channel that served as the main conduit for hydrodynamic flow with a negligible amount of permeation through the grafted polymer segments (shaded in gray). Pressure driven flow, Q, through such a membrane of thickness d containing N_p right cylindrical pores of radius R obstructed with grafted polymer layer of thickness L_H is described by the Hagen-Poiseuille equation with a slip-velocity boundary condition imposed at the pore wall:

$$Q = N_p \frac{\pi R^4}{8\eta d} \Delta P \left[1 - 4\frac{L_H}{R} \right] \quad \textbf{(2.1)}$$

where η is the solution viscosity and ΔP is the pressure difference across the membrane.

The pore filled model (**Figure 2.6b**), on the other hand, describes hydrodynamic flow through an interpenetrating homogeneous polymer network. In this treatment, the

extended poly(4-vinyl pyridinium) chains overlapped and the large pore is effectively replaced with a large number of much smaller pores of radius r_h created by flow around the interpenetrating polymer segments (gray area, **Figure 2.6b**). Under these conditions, the permeability P is proportional to the porosity ε and the square of the hydraulic pore radius r_h and inversely proportional to the solution viscosity and Kozeny's constant which is 5 for $\varepsilon \approx 2/3$

$$P = \frac{\varepsilon r_h^2}{\eta K^*} \quad (2.2)$$

To determine which model is applicable for a given pore size, the effects of chain parameters such as the radius of gyration [47] and total persistence length as a function of the molecular weight of the incorporated polyelectrolyte [48-49] were analyzed. This quantitative treatment established the molecular weights of the polyelectrolyte necessary to form a brush or an interpenetrating network as a function of pore size. At the time, permeability data alone could not determine which model was operational, to a given situation; however, examination of permeability in the context of polymer physical properties started to establish a more quantitative and fundamental approach for understanding hydrodynamic flow through these membranes.

2.3.2 Permeability as a Function of Polymer Volume Fraction

With the establishment of the pore filling technique, many different pore fillings were investigated with respect to their permeability and salt separating abilities.

Fundamental questions regarding the influence of the chemical nature and concentration of the pore filled gel on permeability and ionic solute separation had to be addressed. Kapur and Anderson [39], investigated hydraulic permeability of poly(acrylamide) and derivatized charged poly(acrylamide) gel filled membranes. They reported that the permeability of the membranes was essentially independent of the physical properties of the gel; although the degree of ionization in the derivatized gel was nominal and as such the results weren't unexpected.

The McMaster group studied permeabilities of membranes with various pore filled agents to determine the effects of the chemical nature of the pore filler on permeability (**Figure 2.7**) [34].

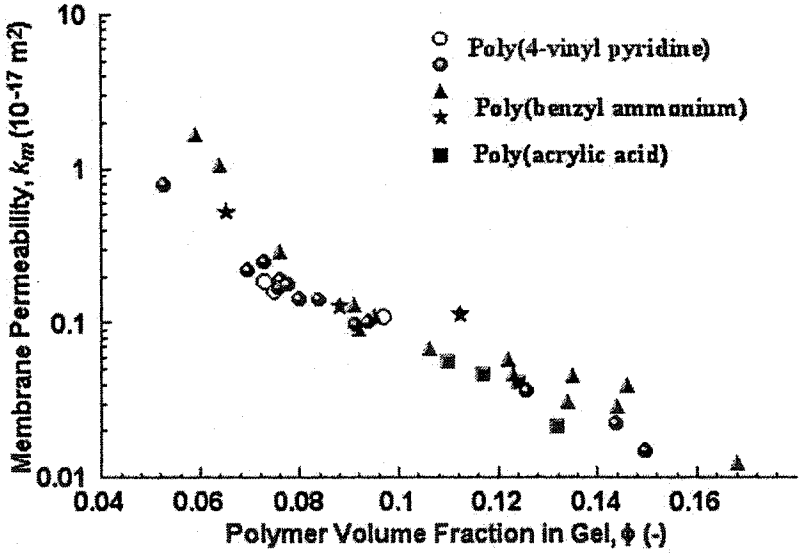

Figure 2.7 Membrane permeability as a function of gel polymer volume fraction for various pore fillings [34]

The empirical plot shown in **Figure 2.7** shows a good correlation between the different pore fillings, except for some scatter at the extreme values of polymer volume fractions. Lack of resolution in the data could not establish any significant differences in permeability arising from differences in chemical properties of the gel; however, a *general* relationship between gel polymer volume fraction and membrane permeability was determined.

$$k_m = f(\phi) \quad \textbf{(2.3)}$$

2.3.3 Towards a Permeability Model

The approach to membrane construction thus far had been mostly empirical, motivated in a large part by the desire to make membranes that could out-perform commercial nanofiltration membranes at ultra-low pressures. Tremendous strides had been made in that direction with development of membranes that were equal to, and eventually better than, the *state of the art* commercial membrane made by Osmonics Corporation, Desal-51 [36, 50]. However, with the accomplishment of each milestone, the need to fundamentally describe the processes that occurred within the gel to account for membrane performance became increasingly apparent and important.

Focus was, therefore, shifted to analyzing existing models that described permeation through gels. Darcy's law states that fluid velocity though a porous medium, like an isotropic gel, is directly proportional to the applied pressure and the

hydrodynamic permeability of the gel (k, **equation 2.4**) and inversely proportional to the solution viscosity. The hydrodynamic permeability, k, is a fundamental property of gels and is closely related to the microstructure of the gel network, with the square root of hydrodynamic permeability, $\sqrt{k}$, being regarded as a measure of the average gel mesh size- the conduit for flow. Furthermore, knowledge of k along with solute diffusion coefficients must be known to model transport within gels [51,52].

$$v = -\frac{k}{\eta}\nabla P \quad \textbf{(2.4)}$$

There are intractable difficulties with direct measurement of the hydrodynamic permeability of gels because of their intrinsic compressibility and fragility under applied pressures. Plots of superficial velocity versus applied pressure across a gel are nonlinear because pressure induced compression results in a decrease in k [39]. Because polymeric gels have a chain-like structure, they are often modeled as a network of straight cylinders of radius a_f. Several attempts have been made to calculate k from first principles by modeling transport through such a network. Some examples of these attempts include the work of Sangani and Acrivos [53], later modified by Tsay and Weinbaum [54], where flow through an array of cylinders at 45° with respect to the alignment of the array (**Figure 2.8a**) was numerically solved using the Stokes equations. Other attempts include flow through random arrays of cylinders [55] (**Figure 2.8b**) and semi-empirical fits from experimental data [56].

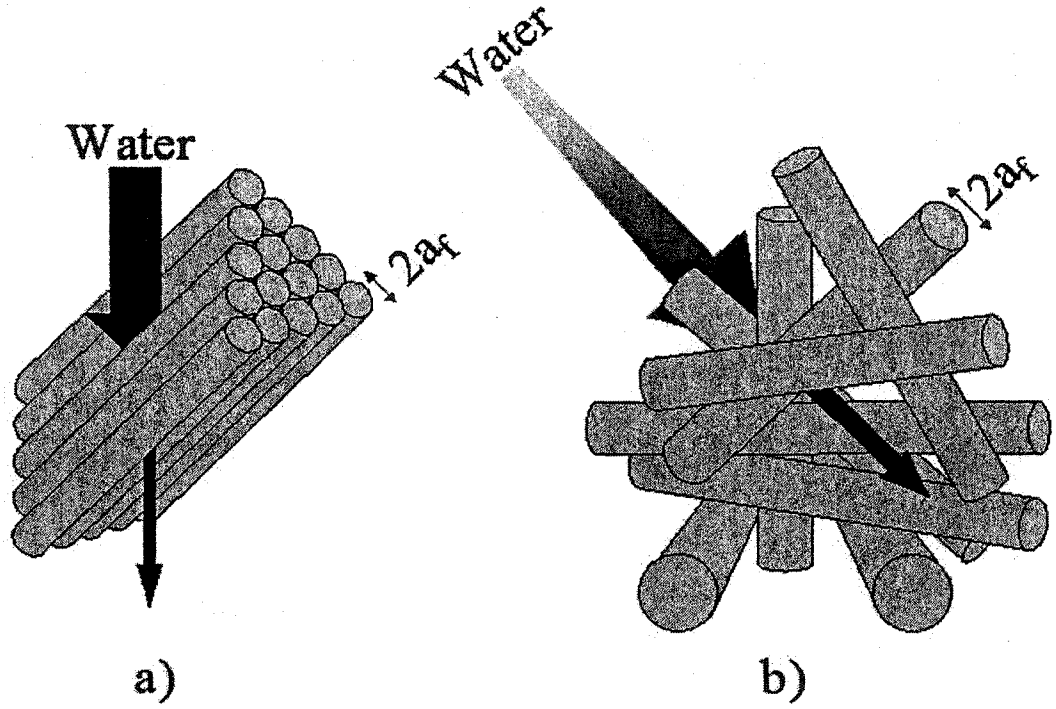

Figure 2.8 Schematic representation of some early models used to calculate hydrodynamic permeability

In these models, the gel hydrodynamic permeability was expressed as a function of the volume fraction of chains (ϕ), where $f(\phi)$ depends on the spatial arrangement of the chains [39]:

$$k = a_f^2 f(\phi) \quad \textbf{(2.5)}$$

2.3.4 Spheres and Wormlike Chains

Mika and Childs noted that none of the hydrodynamic permeability models accounted for changes in a_f as a function of gel polymer concentration (ϕ). They found

that when a_f is kept constant, none of the expressions for $f(\phi)$ fit the experimental data over a wide range of gel concentrations [57]. Furthermore, they noted that when a_f is allowed to become a function of gel concentration, a much better fit to the data was observed. Since polymer chains tend to swell with dilution, they questioned whether modeling with arrays of straight cylinders of fixed radius was appropriate.

For this reason, a more robust method for calculating permeability of gels from first principles was sought by first establishing the physical parameters of the gel, using scaling methods for semidilute polymer solutions coupled with physical properties of polyelectrolytes, and then applying existing hydrodynamic flow models to the calculated physical parameters [57].

In this treatment, the confined gel was treated as a semidilute polymer solution of the same polymer concentration (volume fraction). In the semidilute regime, the dominant factor influencing static and dynamic properties of the polymer solution is the short range correlation length, ξ_p, which is proportional to the average distance between interchain contacts [58]. The approach used to estimate the correlation length was to modify Schaefer's model for neutral polymers in semidilute solution with Odijk's model for electrostatic persistence length.

Schaefer [58] developed a method for estimating the correlation length of neutral polymers by relating the Flory-Huggins interaction parameter (χ), a thermodynamic property of polymer-solvent interaction, to the so-called *blob* model of chain statistics developed by de Gennes [59]. In semi-dilute solutions, the polymer chain is viewed as a

sequence of blobs of diameter equal to the correlation length, ξ_p, in which short monomer-monomer sequences are presumed to be ideal but long sequences are fully swollen due to excluded volume effects (**Figure 2.9**) [60].

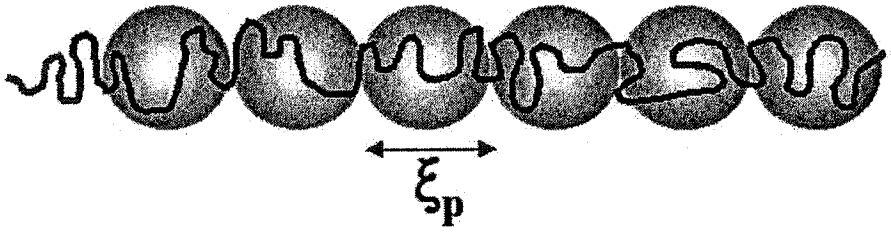

Figure 2.9 De Gennes' blob representation of a polymer chain and the associated correlation length in semidilute polymer solution

According to Schaefer, the correlation length, as expressed in **equation 2.6**, is dependent upon several factors that influence interchain monomer-monomer interactions. These factors include, polymer concentration (ϕ), the number of bonds in the persistence length obtained from the characteristic ratio ($n = C_\infty/6$) and the long range three body excluded volume parameter (a).

$$\xi_p = \frac{n^2 a}{[n(1-2\chi)\phi + wa^{-6}\phi^2]^{1/2}} \quad (2.6)$$

Schaefer's model for calculation of the correlation length does not take into consideration the effects of electrostatic interactions along the polymer backbone on the persistence length. **Equation 2.6**, as written, is not applicable to polyelectrolyte systems; therefore, estimation of the correlation length, ξ_p, in semidilute polyelectrolyte solutions had to be modified to take conformational effects of charge into account.

2.3.5 Charged Rods and Neutral Coils

Polyelectrolytes, at infinite dilution and in the absence of salt, exist in a fully extended rod-like conformation. As illustrated in **Figure 2.10**, electrostatic repulsions along the polyelectrolyte (shown as small spheres on the chain) results in periodic local stiffening of the polymer backbone and is affected by the dielectric constant of the solvent, temperature, salt concentration and contour distance between the fixed charges on the polyelectrolyte. Small molecule electrolytes mitigate the repulsive electrostatic forces on the chain by shielding the fixed charges. As salt concentration is increased, intramolecular associative forces such as van der Waals and hydrophobic interactions become increasingly important and the polyelectrolyte adopts a more compact, flexible coil-like conformation. Regional changes due to increased flexibility affects the chain at the macroscopic level as exhibited in changes in correlation length.

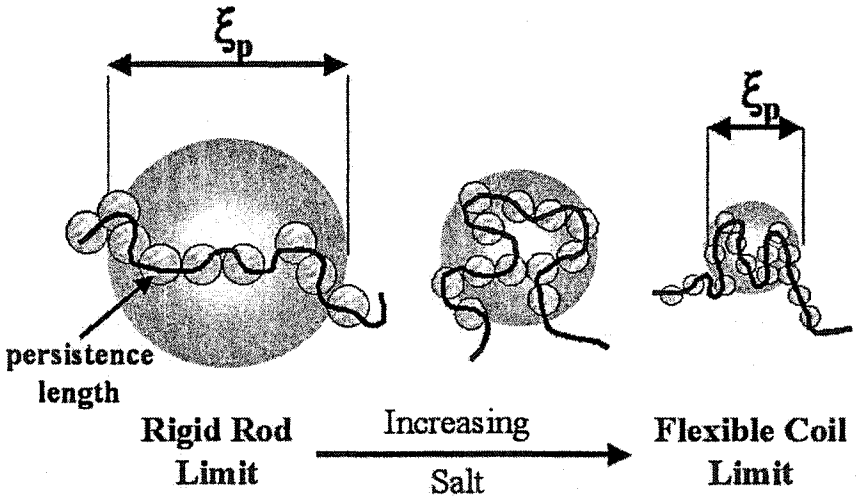

Figure 2.10 Conformational sensitivity of a wormlike polyelectrolyte to salt concentration

The electrostatic persistence length L_e for a wormlike polyelectrolyte chain of contour length l bearing P elementary charges that are separated by a contour distance $A = l/P$ is given by **equation 2.7**, provided the separation of charges A is greater than the Bjerrum length $l_B = q_e^2/Dk_BT$ (D is the dielectric constant of the solvent, and k_BT is the Boltzmann factor) [61,62].

$$L_e = \frac{l_B}{4\kappa^2 A^2} \quad \textbf{(2.7)}$$

Equation 2.7 applies only to the rigid rod conformation, which exist under salt free conditions (*vide supra*) where no interchain stiffening occurs; that is, only charges on one chain increase the persistence length and that only the uncondensed counter-ions screen the polyion [63]. The Debye-Hückel parameter, κ, under these conditions is given by

$$\kappa^2 = 4\pi Ac \quad \textbf{(2.8)}$$

where c is the concentration of charge bearing chain segments per unit volume of solution. The number of bonds in the persistence length (n) in Schaeffer's **equation 2.6** must therefore take into account the electrostatic persistence length to be applicable to polyelectrolyte systems. The number of bonds in the total persistence length is an additive function

$$T = n_p + n_e \quad \textbf{(2.9)}$$

of the number of bonds in the bare persistence length where $n_p = C_\infty/6$ and the number of bonds in the electrostatic persistence length $n_e = 0.83^2 L_e/3a$. As salt concentration is increased, the number of bonds in the persistence length reduces to the number of bonds

in the bare persistence length since the electrostatic persistence length approaches zero. Schaeffer's modified equation, taking into account the effect of electrostatic persistence length, can thus be written as:

$$\xi_p = \frac{T^2 a}{[n(1-2\chi)\phi + wa^{-6}\phi^2]^{1/2}} \quad \textbf{(2.10)}$$

2.3.6 Hydrodynamic Flow Through an Assemblage of Spheres

Solution properties such as the collective diffusion constant, the chain friction constant and the sedimentation constant of a polymer can be obtained if ξ_p is known [58]. At high polymer concentrations, in the semidilute regime, the sedimentation of polymer chains in a solvent and the permeation of solvent through a porous plug of polymeric material is analogous. The scaling theory applied to sedimentation treats a semidilute polymer solution as a continuum formed by entangled chains that can be divided into spheres of diameter equal to the correlation length ξ_p [57]. There is some evidence to suggest that solvent penetration into the sphere does not occur and is instead forced into an orderly fashion around the blobs [64]. Using this as a model for viscous flow of solvent through a gel (semidilute polymer solution), Mika and Childs calculated the hydrodynamic permeability by treating the gel as a porous plug made of an assemblage of impenetrable spheres of diameter equal to the correlation length as depicted in **Figure 2.11**.

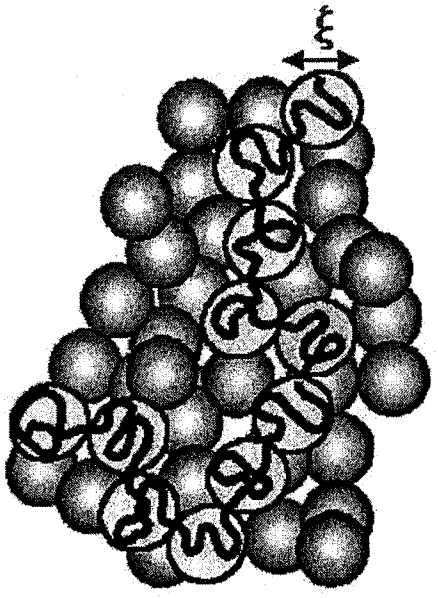

Figure 2.11 The structure of polymer chains under semidilute conditions treated as an assemblage of spheres with diameter equal to the correlation length

Using Happel's model of flow through an assemblage of hard spheres of radius R, equal to ½ of the correlation length ξ_p, occupying a volume fraction ϕ, the gel hydrodynamic permeability was calculated according to **equation 2.11** [65,66].

$$k = \frac{2R^2}{9\phi}\left[\frac{3-(9/2)\phi^{1/3}+(9/2)\phi^{5/3}-3\phi^2}{3+2\phi^{5/3}}\right] \quad \textbf{(2.11)}$$

In this model, flow of solvent and solutes was restricted to the interstices between the spheres and no penetration of the spheres was assumed. The predictions of this model were then compared to experimental gel permeability data calculated from the membrane permeability data using the empirical relationship derived by Kapur and Anderson [39] **(equation 2.12)**

$$k_m = k_p \frac{\varepsilon}{\tau} \quad \textbf{(2.12)}$$

where k_m is membrane permeability, k_p is gel permeability, ε is substrate porosity and τ, substrate tortuosity. The fit of the experimental permeability data to the permeability predicted by the model, as shown in **Figure 2.12** is astounding.

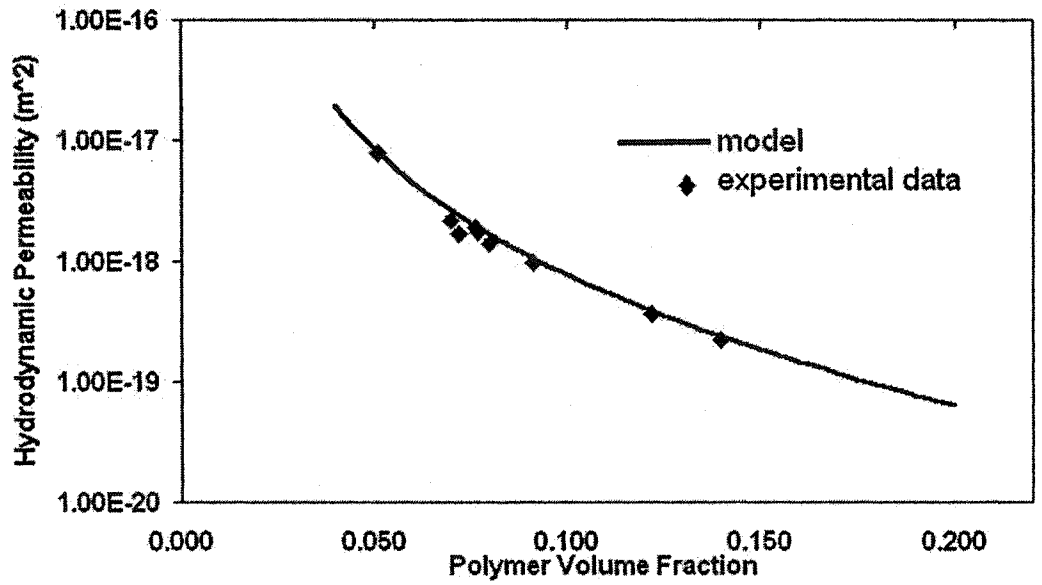

Figure 2.12 Correlation of the predicted hydrodynamic permeability to experimental permeability of poly(4-vinyl pyridine) membranes [57]

The development of the model was an extraordinary achievement because it provided a means for predicting the hydrodynamic permeability, of any gel, with incredible accuracy from first principles. The model, despite its predictive capability is valid only for isotropic gels; that is, gels that are homogeneous in its morphological structure because micro and macro heterogeneities will cause substantial deviations from the predicted permeabilites [67]. With the firm establishment of the permeability model

and understanding of the factors that affect hydrodynamic flow through a gel, the final step to designing and optimizing nanofiltration membranes was determination of factors that influence solute rejection.

2.4 Salt Separation of Pore Filled Membranes

Solute separation in reverse osmosis, as discussed in **Chapter 1**, occurs through a differential sorption/diffusion of solutes into the membrane. This mechanism, however, is not applicable to polyelectrolyte gel-filled membranes because the gel-mesh sizes are typically much larger than the ionic radii of small molecule electrolytes. Sieving, therefore, does not play a role in salt separations. Instead, as also discussed in **Chapter 1**, the fixed charges establish a Donnan potential in the membrane and reject ionic solutes based on Donnan exclusion. The salt rejection and flux performances of some polyelectrolyte gel filled membranes were compared to a commercial nanofiltration membrane in **Table 2.2**.

Table 2.2 Comparison of tap water separation performance among pore filled and a commercial membranes at 100 kPa and pH 5.5. Feed composition: Na^+ = 17 ppm; Mg^{2+} = 15 ppm; Ca^{2+} = 55 ppm. Adapted from Mika *et al.* [36]

Membrane	Gel-Polymer volume fraction	Flux (kg/m^2h)	Rejection (%)		
			Na^+	Mg^{2+}	Ca^{2+}
PVBA-PIP	0.075	13	34	79	80
PVBA-DABCO	0.082	8	31	83	68
PVP-DCX	0.054	20	21	51	40
Desal-51	-	7	24	72	54

Poly(vinylbenzyl ammonium) cross-linked with piperazine (PVBA-PIP) and poly(vinylbenzyl ammonium) cross-linked with DABCO (PVBA-DABCO) both out performed the thin film composite Desal-51 in flux and solute rejection. The poly(4-vinylpyridine) cross-linked with dichloroxylene (PVP-DCX), although not as efficient in separating salts compared to the commercial membrane, had approximately three times its flux [36]. The flux performances of the pore filled membranes were astonishing considering they ranged in thickness from 70 to 80 μm while the layer responsible for rejection and flux in Desal-51 is less than a micron thick!

The high fluxes of the gel-filled membranes, despite their large thicknesses, are not entirely surprising considering their exceedingly low gel polymer volume fractions indicate over 90% of the volume in the pores are filled with water! The high porosity of these filled membranes indicates the internal microstructure to be a very open polyelectrolyte network that allows unhindered passage of solvent and neutral solutes, smaller than the mesh size of the gel, but retards or blocks the passage of ionic solutes due to electrostatic repulsive interactions. A schematic showing the different pore sizes, as a function of charge, is shown in **Figure 2.13**. This of course, is a simplistic representation and does not take into account the effects of flux, valency and concentrations of the ions in solution.

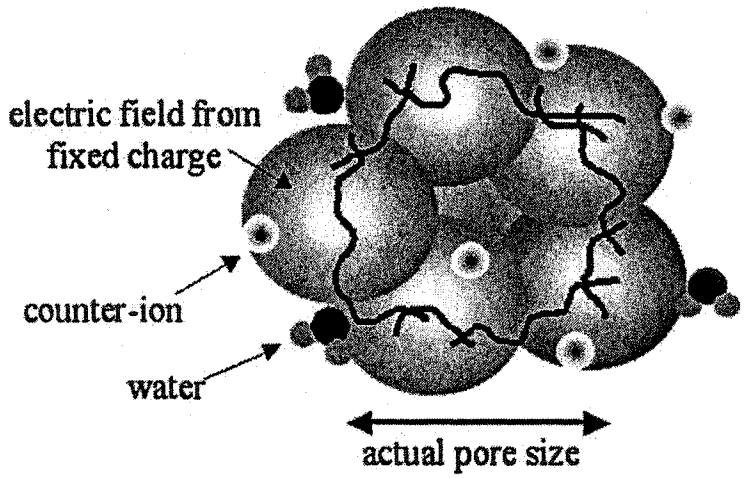

Figure 2.13 Schematic of a pore in a polyelectrolyte gel. The actual pore size determines hydrodynamic permeability and neutral solute separation. Co-ions see a much reduced *effective* pore size due to the electric field from the fixed charges

2.4.1 Determination of Membrane Charge

To determine a quantitative relationship between fixed charge concentration and salt rejection, poly(4-vinyl pyridine) membranes were characterized by potentiometric titration [68]. The titration behavior of the poly(4-vinyl pyridine) system was analyzed by the Henderson-Hasselbach equation as modified by Katchalsky and Spitnik **equation 2.13** [69]:

$$pH = pK_{\alpha=0.5} + n\log\left[\frac{1-\alpha}{\alpha}\right] \quad \textbf{(2.13)}$$

where $pK_{\alpha=0.5}$ and n are essentially constant for a given titration system and α is the degree of protonation. The titrations yielded $pK_{\alpha=0.5}$ values (the pH at which half of the polymer is protonated) of 2.57 and 3.73 for salt free and 0.1M NaCl conditions

respectively. Due to the low $pK_{\alpha=0.5}$ values, poly(4-vinylpyridine) membranes have virtually no charge at pH's > 6, thus, would be unable to reject salts to any significant degree. *N*-alkylation of the pyridine moiety was found to be essential for the membranes to be able to reject salts, without acidification of the feed.

Early work on poly(4-vinylpyridinium) systems established an empirical relationship between NaCl rejection and permeability, as depicted in **Figure 2.14** [34]. The data showed rejection of NaCl to be constant in the permeability range of 0.2×10^{-18} to 2×10^{-18} m^2 with a precipitous drop in separation above 2×10^{-18} m^2. Implicit in this finding was the insensitivity of polyelectrolyte volume fraction on separation, within the $< 2 \times 10^{-18}$ m^2 permeability range. This suggested the existence of a limiting membrane charge, exceeding which had no influence on the magnitude of separation; but below which, adversely affected separation. This finding was considered counter-intuitive at the time; however, has now been established to be entirely consistent with the Teorell-Meyer-Sievers (TMS) model that explains salt rejection by charged membranes.

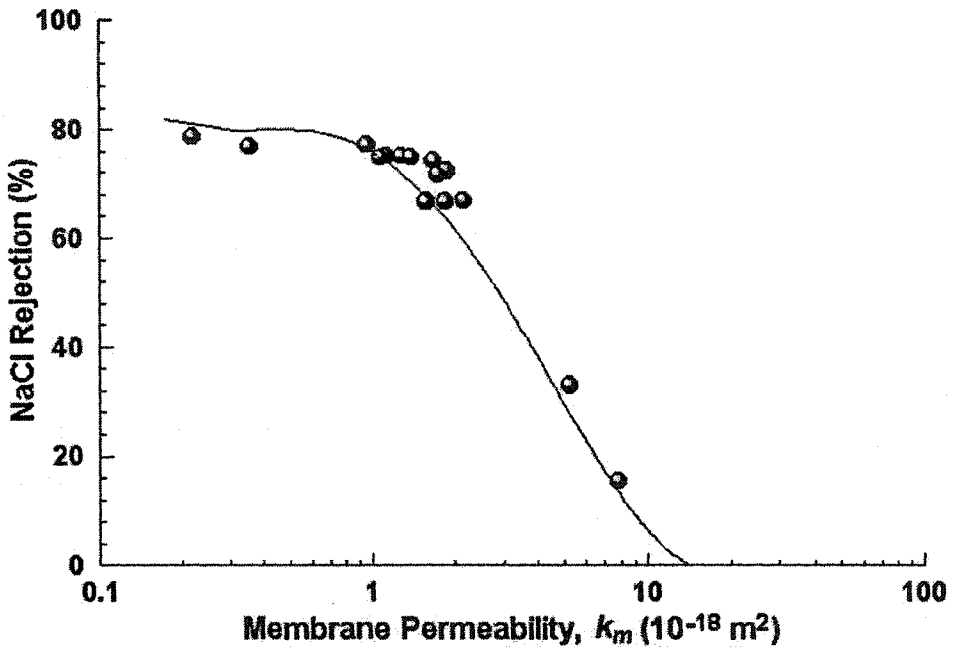

Figure 2.14 NaCl separation as a function of membrane permeability for poly(4-vinylpyridinium) membranes. Data obtained with 300 ppm NaCl feed at 300 kPa. Line is a polynomial fit [34]

2.4.2 Factors Determining Solute Rejection

The rejection of ionic solutes in charged nanofiltration membranes is explained by two models of electrolyte transport: the Teorell-Meyer-Sievers (TMS) model and the space-charge (SC) model (discussed in chapter one). The TMS model [70-73] assumes a homogeneous distribution of electrical potential and ion concentration throughout the membrane. This requires the pore (mesh) size to be smaller than the thickness of the double layer (Debye-Hückel screening length), κ^{-1}, at the ionic strength of the filtered solution [74,75]. If, however, the pores (or meshes) are larger than the Debye-Hückel

screening length, an ionic concentration gradient will be established in the radial direction across the pores. In such a case, the space-charge model developed by Osterle *et al.* is operative [76-79].

With the establishment of the permeability model, a very detailed understanding of the microstructure of the gel, such as its *mesh* size, could be determined. The gel polymer volume fraction for the $2x10^{-18}$ m^2 permeability, discussed previously, corresponded to ~ 0.08. The Debye-Hückel screening length (κ^{-1}) at 300 ppm NaCl was calculated to be greater than the calculated pore size for polymer volume fractions of 0.08 and above which justified the application of the TMS model [80].

At this time, the development of a model to predict separation of ionic solutes based on a combination of the hydrodynamic permeability model and the extended Nernst-Planck equation with the TMS or SC models appears to work with these polyelectrolyte filled membranes. A detailed study is underway, further comment cannot be given at this point.

2.5 Statement of Purpose

At the onset of this work, parameters governing salt separation and flux through pore filled membranes were not well understood and limited to poly(4-vinyl pyridine) (PVP) *in situ* polymerized membranes that were in the early stages of development. As discussed earlier in this chapter, these PVP ultrafiltration membranes were found to exhibit reverse osmosis performance properties upon acidification of the feed solution

[24]; a conversion that was reversible upon an increase of the feed pH. Cross-linking of the PVP created a non-collapsible polymer network within the membrane pores, but acidification of the feed or *N*-alkylation of the pyridine nitrogen was still required for these membranes to reject ionic solutes under pressure driven conditions [27].

At issue was the necessity of a permanent charge in the pore filler or acidification of the feed pH. More specifically, could a membrane filled with a formally neutral basic polymer- that can acquire charge through protonation by acid/base reaction with water- separate ionic solutes under pressure driven conditions? If so, what is the relationship between charge concentration and ionic solute separation performance? What are the pH ranges the membranes can effectively operate in rejecting ionic solutes? And, what are the effects of charge on permeability?

The most likely candidate for such an investigation was polyethylenimine, as shown in **Figure 2.15**.

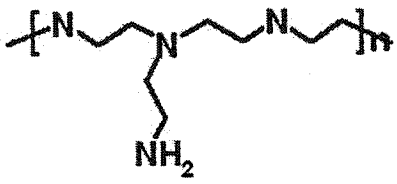

branched polyethylenimine
(BPEI)

Figure 2.15 Structures of branched polyethylenimine

Polyethylenimine is a basic polymer with reported pK values, ranging from as low as 5.01 to as high as 8.74 [80-82]. PEI is therefore expected to have a substantial degree of protonation at a neutral pH.

However, the incorporation of PEI into a microporous host by the *in situ* polymerization method posed many and severe challenges because branched PEI is prepared by ring opening polymerization of ethylenimine- a toxic and flammable gas **(Scheme 2.5)**.

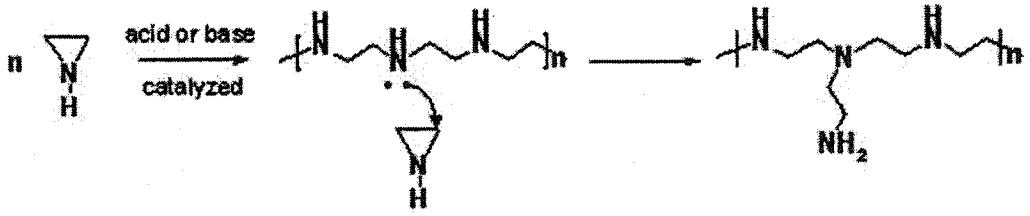

Scheme 2.5 Ring opening polymerization of ethylenimine to form BPEI

Clearly, the *in situ* polymerization method was not amenable to incorporation of PEI. An alternative method of membrane manufacture was thus required.

2.6 Objectives

There are two general goals of this work. The first is to establish that polyethylenimine can function effectively as a pore filler to change the properties of the

bulk polyolefinic host membrane and separate ionic solutes without prior acidification of the feed or induction of a permanent charge in the polymer by *N*-alkylation, due to its basicity. To accomplish this objective, the second goal, is to develop a new method for membrane fabrication since the *in situ* polymerization route cannot be used to incorporate polyethylenimine into a microporous host.

Underlying these general goals are the following detailed objectives.

1). To determine the relationship between charge and separation behavior of these membranes; that is, how do pH and salts affect performance?

2). Branched polyethylenimine, due to its highly branched, globular nature exhibits unique and interesting properties. The influence of branched polyethylenimine conformation on membrane performance will be investigated as a function of pH. Furthermore, because polyethylenimine contains a potential charge-bearing group in the backbone of the polymer, protonated PEI will be more sensitive to changes in persistence length and effective charge concentration than polyelectrolytes where the charge is localized on a pendant substituent. These effects on the polymer will be investigated with respect to their effects on membrane performance in permeability and salt separating abilities.

3). As will be discussed in later chapters, the method of PEI incorporation involves a method where the polymer is *in situ* cross-linked in the pores. This method is a highly versatile route for membrane fabrication and can be modified to incorporate PEI to coat the internal surfaces of the host substrate. Factors influencing this coating method

and the properties of these coated membranes will be discussed by permeability and microscopy analyses.

4). Fundamental to understanding the properties and performance behavior of PEI filled membranes is an understanding of PEI gel properties. The properties of PEI gels as a function of gel composition will be analyzed by swelling experiments, permeability and microscopy analyses.

2.7 Outline of This Thesis

This thesis contains six chapters. Chapters one and two are introductory in nature. Chapter one is a general overview of membrane technology and basic principles that both introduces and illustrates the pore filled concept and how it represents a new paradigm in membrane technology. Chapter two, developing upon the ideas introduced in the previous chapter, is a focused history of the research developments of the McMaster Membrane group and establishes a contextual framework for the chapters to follow.

Chapter three discusses the nanofiltration properties of polyethylenimine pore filled membranes. The chapter will focus on fabrication, characterization and salt separation of these membranes. A brief discussion of permeability will be presented as it relates to the salt separating abilities of these membranes.

Chapter four discusses the influence of the cross-linker on gel chemistry- in particular, heterogeneity. This chapter will focus on permeability in the context of the hydrodynamic permeability model presented in Chapter two and deviations from the

model will be discussed. Gel swelling as a function of cross-linker, pH and salt concentration, will be presented to elucidate the substantial differences in gel properties that can be attained with different cross-linking agents. The differences in the morphologies of these membranes and microstructure of these gels composed of different cross-linkers will be analyzed with permeability and microscopy data.

Chapter five discusses polyethylenimine gel coated ultrafiltration membranes. The discussion will focus primarily on methods of fabrication and their characterization by permeability, ultraviolet laser confocal microscopy and scanning transmission x-ray microscopy (STXM).

Chapter six concludes the thesis with a discussion of future work that can be borne from the work of this thesis.

2.8 Conclusion

In this chapter, an overview of the membrane technology developed at McMaster has been given from its auspicious beginnings, with thin film composite technology, to the groundbreaking research currently done on pore filled membranes. The challenges of understanding gel physical properties were overcome with creative and innovative methods of circumventing the limitations imposed by their inherent fragility. As indicated in chapter one, transport in membranes is a highly complex and often controversial issue. Models are essential in understanding membrane transport because models are abstractions that allow for attention to be directed at the essential core of the

problems. The validity and power of any model, therefore, is its ability to adapt to any system. With the establishment of the permeability model and development of the separations model the view of the pore has become increasingly clear at these higher magnifications of theory.

Although this chapter has dealt mostly with the published findings of poly(4-vinylpyridine), the models of permeability and salt separation have also been applied with equal success to a wide variety of other systems such as poly(acrylic acid), poly(vinylbenzyl ammonium) and as will be shown in the following chapters of this thesis, polyethylenimine.

2.9 References

1. Trushinski, B.J.; Dickson, J.M.; Smyth, T.; Childs, R.F.; McCarry, B.E. *J. Memb. Sci.* **1998**, *143*, 181
2. Ji, J.; Trushinski, B.J.; Childs, R.F.; Dickson, J.M.; McCarry, B.E. *J. Appl. Polym. Sci.* **1997**, *64*, 2381
3. Chadda, S.K.; McCarry, B.E.; Childs, R.F.; Rogerson, C.V.; Tse-Sheepy, I.O. Dickson, J.M. *J. Appl. Pol. Sci.* **1987**, *34*, 2713
4. Trushinski, B.J.; Dickson, J.M.; Childs, R.F.; McCarry, B.E. *J. Appl. Polym. Sci.* **1993**, *48*, 187
5. Sumitomo, H.; Hashimoto, K. *Adv. Polym. Sci.* **1985**, *64*, 63
6. Nolte, R.; Ledjeff, K.; Bauer, M.; Mulhaupt, R. *J. Memb. Sci.* **1993**, *83*, 211

7. Wolff, J.; Steinhauser, H.; Ellinghorst, G. *J. Memb. Sci.* **1988,** *36,* 207

8. Clarotti, G.; Schue, F.; Sledz, J.; Geckler, K.E.; Gopel, W.; Orsetti, A. *J. Memb. Sci.* **1991,** *61,* 289

9. Tsudenda, S.; Saito, K.; Furusaki, S. *J. Memb. Sci.* **1992,** *71,* 1

10. Saito, K.; Hori, T.; Furusaki, S.; Sugo, T.; Ishigaki, I. *Ind. Eng. Chem. Res.* **1987,** *26,* 1977

11. Nystrom, M.; Jarvinen, P. *J. Memb. Sci.* **1991,** *60,* 275

12. Ando, W. The Chemistry of Diazonium and Diazo Groups, Part 1. Patai, S. (ed.), New York, John Wiley and Sons, 1978, 341

13. Almstead, J.; Urwyler, B.; Wirz, J. *J. Am. Chem. Soc.* **1994,** *116,* 954

14. Rosenfeld, A.; Mitzner, R.; Baumbach; Bending, J. *J. Photochem. Photobiol. A: Chem.* **1990,** *55,* 259

15. Fisher, M.T.; Cernigliaro, G.J.; Sinta, R.; Scaiano, J.C. *J. Am. Chem. Soc.* **1992,** *114,* 2630

16. Vleggaar, J.J.; Huizer, A.H.; Kraakman, P.A.; Nijssen, W.P.; Visser, R.J.; Varma, C.A. *J. Am. Chem. Soc.***1994,** *116,* 11754

17. Reiser, A. Photoreactive Polymers: The Science and Technology of Resists, New York, John Wiley & Sons, 1989

18. Reichmanis, E.; Thompson, L.F. *Chem. Rev.* **1989,** *89,* 1273

19. Shipman, G. Eur. Patent. 105629, 1984

20. Lloyd, D. R.; Kinzer, K. E.; Tseng, H. S. *J. Memb. Sci.* **1990,** *52,* 239

21. Skouri, R.; Schosseler, F.; Munch, J.P. Candau, S.J. *Macromolecules.* **1995**, *28*, 197

22. Dickson, J.M.; Childs, R.F.; McCarry, B.E.; Gagnon, D.R. *J. Memb. Sci.* **1998**, *148*, 25

23. Rilling, K.; Dickson, J.M.; Childs, R.F.; Gagnon, D.R. US Patent 5,627,217, 1997

24. Mika, A.M.; Childs, R.F.; Dickson, J.M.; McCarry, B.E.; Gagnon, D.R. *J. Memb. Sci.* **1995**, *108*, 37

25. Uyama, Y.; Kato, K.; Ikada, Y. *Adv. Polym. Sci.* **1998**, *137*, 1

26. Xu, G.; Lin, S. *J.M.S. Rev. Macromol. Chem. Phys.*, **1994**, *C34*, 555

27. Hofmann, A.S. *Macromol. Symp.*, **1996**, *101*, 443

28. Chan, C.M. Polymer Surface Modification and Characterization, New York, Hanser Publications, 1994

29. Garbassi, F.; Morra, M.; Occhiello, E. Polymer Surfaces, New York, John Wiley & Sons, 1994

30. Casolaro, M. & Barbucci, R. *Coll. Surf.* **1993**, *77*, 81

31. Imaizumi, M.; Kubota, H.; Hata, Y. *Eur. Polym. J.* **1994**, *30*, 979

32. Mika, A.M.; Childs, R.F.; Dickson, J.M.; McCarry, B.E.; Gagnon, D.R. *J. Memb. Sci.* **1997**, *135*, 81

33. Childs, R.F.; Weng, J.F.; Kim, M.Y.; Dickson, J.M. *J. Pol. Sci. Part A: Polym. Chem.* **2002**, *40*, 242

34. Childs, R.F.; Mika, A.M.; Pandey, A.K.; McCrory, C.; Mouton, S.; Dickson, J. *Sep. Pur. Tech.* **2001**, *22-23*, 507

35. Pandey, A.K.; Childs, R.F.; West, M.; Lott, J.A.; McCarry, B.E.; Dickson, J.M. *J. Polym. Sci. A: Polym. Chem.* **2001**, *39*, 807

36. Mika, A.M.; Pandey, A.K.; Childs, R.F. *Desalination* **2001**, *140*, 265

37. Stachera, D.M.; Childs, R.F.; Mika, A.M.; Dickson, J.M. *J. Memb. Sci.* **1998**, *148*, 119

38. Stachera, D.M.; Childs, R.F. *J. Memb. Sci.* **2001**, *187*, 213

39. Kapur, V.; Charkoudian, J.C.; Kessler, S.B.; Anderson, J.L. *Ind. Eng. Chem. Res.* **1996**, *35*, 3179

40. Molymeux, P. Water-Soluble Synthetic Polymers: Properties and Behavior, Vol. II, Boca Raton, CRC Press, 1984

41. Mika, A.M.; Childs, R.F.; Dickson, J.M. *J. Memb. Sci.* **1999**, *153*, 45

42. Idol, W.K.; Anderson, J.L. *J. Memb. Sci.* **1986**, *28*, 269

43. Kim, J.T.; Anderson, J.L. *J. Memb. Sci.* **1989**, *47*, 163

44. Webber, R.M.; Anderson, J.L.; Jhon, M.S. *Macromolecules* **1990**, *23*, 1026

45. Kim, J.T.; Anderson, J.L. *Ind. Eng. Chem. Res.* **1991**, *30*, 1008

46. Anderson, J.T.; McKenzie, P.F.; Webber, R.M. *Langmuir.* **1991**, *7*, 162

47. Schmitz, K.S. Macroions in Solution and Colloidal Suspension, New York, VCH, 1993

48. Odijk, T.; Houwaart, A. *J. Polym. Sci., Polym. Phys. Ed.* **1978**, *16*, 627

49. Wang, L.; Yu, H. *Macromolecules* **1988**, *21*, 3498

50. Mika, A.M.; Childs, R.F.; Dickson, J.M. *Desalination* **1999**, *121*, 149

51. Johnson, E.M.; Berk, D.A.; Jain, R.K.; Deen, W.M. *Biophys. J.* **1996**, *70*, 1017

52. Tong, J.; Anderson, J.L. *Biophys. J.* **1996**, *70*, 1505

53. Sangani, A.S.; Acrivos, A. *Int. J. Multiphase Flow* **1982**, *8*, 193

54. Tsay, R.; Weinbaum, S. *J. Fluid Mech.* **1991**, *226*, 125

55. Spielman, L.; Goren, S.L *Environ. Sci. Technol.* **1968**, *2*, 279

56. Jackson, G.W.; James, D.F. *Can. J. Chem. Eng.* **1986**, *64*, 364

57. Mika, A.M.; Childs, R.F. *Ind. Eng. Chem. Res.* **2001**, *40*, 1694

58. Schaefer, D.W. *Polymer* **1984**, 25, 387

59. de Gennes, P. Scaling Concepts in Polymer Physics, Ithaca, Cornell University Press, 1979

60. Farnoux, B.; Boue, F.; Cotton, J.P.; Daoud, M.; Jannink, G.; Nierlich, M.; de Gennes, P.G. *J. Phys. (Paris)*, **1978**, *39*, 77

61. Odijk, T. *J. Polym. Sci., Polym. Phys.* **1977**, *15*, 477

62. Skolnick, J.; Fixman, M. *Macromolecules* **1977**, *10*, 944

63. Odijk, T. *Macromolecules* **1979**, *12*, 688

64. Sun, S.F. Physical Chemistry of Macromolecules. Basic Principles and Issues, New York, John Wiley & Sons, 1994

65. Happel, J.; Brenner, H. Low Reynold Number Hydrodynamics, Leyden, Noordhof International Publishing, 1973

66. Happel, J. *AIChE J.***1959**, *5*, 174

67. McCrory, C. Ph.D. Thesis: Impact of Gel Morphology on Pore Filled Membranes. 2001. McMaster University

68. Mika, A.M.; Childs, R.F. *J. Memb. Sci* **1999**, *152*, 129

69. Katchalsky, A.; Spitnik, P. *J. Polym. Sci.* **1947**, *2*, 432

70. Teorell, T. *Progr. Biophys. Biophys. Chem.* **1953**, *3*, 305

71. Meyer, K.H. & Sievers, J.F. *Helv. Chim. Acta.* **1936**, *19*, 649

72. Meyer, K.H. & Sievers, J.F. *Helv. Chim. Acta.* **1936**, *19*, 665

73. Meyer, K.H. & Sievers, J.F. *Helv. Chim. Acta.* **1936**, *19*, 987

74. Probstein, R.F.; Sonin, A.A.; Yung, D. *Desalination* **1973**, *13*, 303

75. Tsuru, T.; Nakao, S.; Kimura, S. *J. Chem. Eng. Jpn.* **1991**, *24*, 511

76. Morrison, F.A. & Osterle, J.F. *J. Chem. Phys.* **1965**, *43*, 2111

77. Gross, R.J. & Osterle, J.F. *J. Chem. Phys.* **1968**, *49*, 228

78. Fair, J.C. & Osterle, J.F. *J. Chem. Phys.* **1971**, *54*, 3307

79. Mika, A.M. unpublished data

80. Kobayashi, S.; Kazuhisa,H.; Masazumi,T.; Saegusa,T. *Macromolecues* **1987**, *20*, 1496

81. Weyts, K.F; Goethals, E.J. *Makromol. Chem., Rapid Commun.* **1989**, *10*, 299

82. Smits, R.G.; Koper, G.J.; Mandel, M. *J. Phys. Chem.* **1993**, *97*, 5745

CHAPTER THREE

FABRICATION, CHARACTERIZATION AND NANOFILTRATION PERFORMANCE OF POLYETHYLENIMINE PORE FILLED MEMBRANES

Abstract

This chapter is based on the contents of two papers- one published in the Journal of Polymer Science, Part A: Polymer Chemistry [1] and one prepared for publication in the Journal of Membrane Science. This chapter integrates the contents of both paper with some preliminary data obtained at a very early stage of the research.

This chapter discusses polyethylenimine pore filled membranes. The chemistry of the fabrication process, membrane characterization, materials and apparatus used and nanofiltration performances of the BPEI pore filled membranes are discussed in this chapter.

3.0 Introduction

The strong advantage offered by the pore filled construct is that membranes can be easily tailored for a given application by controlling the polymer volume fraction and the chemistry of the pore filled polymer. In the former case, the polymer volume fraction is a factor in controlling permeability so that membranes with high polymer volume fractions are suitable for reverse osmosis [2] or diffusion dialysis applications [3] and, conversely, membranes with lower polymer volume fractions can function effectively in nanofiltration [4] and ultrafiltration [5] applications. In the latter case, the chemistry of the pore filling plays an important role in ionic solute rejection. Positively charged gels can be used for solute rejections of feed solutions containing multi-valent cationic species, due to enhanced Donnan exclusion, and vice versa for negatively charged gels. Furthermore, because the active component in these pore filled membranes is a soft, solvent swollen, gel these membranes possess an innate self-repair mechanism; for example, dynamic "pin-holes" formed from flux breakthroughs due to over-pressurization can often be self-repaired by reorganization of the solvent swollen gel within the pores.

In this chapter, the effects of the chemistry of the pore filling on nanofiltration performance will be discussed using branched polyethylenimine (BPEI). Because BPEI is formed from ring opening polymerization of ethylenimine, both the primary nitrogen atoms (propagating nitrogens) and the secondary nitrogen atoms in the chain can react with another equivalent of ethylenimine to yield a secondary or tertiary nitrogen center

respectively (**Figure 2.16, Chapter 2**). For this reason, the polymer exists in a highly branched conformation with 25% primary, 50% secondary and 25% tertiary nitrogen centers [6]. The branched sites are separated by secondary amine groups, with on average one branch point for every 3-3.5 nitrogen atoms along a linear chain. This branching distribution is what gives BPEI a spheroid shape as determined by ^{13}C and ^{15}N NMR spin-lattice relaxation times [6-8]. It readily dissolves in water at the pH values and salt concentrations tested in this report. Furthermore, the aliphatic nitrogens in BPEI impart a basic character to the polymer so that a high charge concentration is expected at neutral pH's.

3.1 Experimental

3.1.1 Materials

Branched polyethylenimine (BPEI) with a weight average molecular weight (M_w) of ca. 25,000, Direct Red 23 dye (λ_{exc} = 507 nm and λ_{emm}=610 nm) [9] and naphthalene disulfonic acid were obtained from Aldrich Chemical Co. Naphthalene disulfonyl chloride (NDSC) was prepared using reported procedures [10]. Ethyleneglycol diglycidyl ether (EDGE) was obtained from Polysciences Inc. *N,N*-Dimethyl formamide (DMF), chloroform ($CHCl_3$), carbon tetrachloride (CCl_4) and 1-propanol were obtained from Caledon Labs. Ltd. and unless otherwise stated, all water used was carbon filtered and

deionized through a Barnstead/Thermolyne system (organic removal cartridge D8904 and deionization cartridge D8901). All reagents were used without further purification.

The host substrates used for the preparation of the membranes were polyolefinic based microporous membranes supplied by 3M Canada Company named PP3, PP4, PE1 and PE2. The acronyms represent polypropylene and polyethylene respectively. The physical properties of the host membranes are summarized in **Table 3.1**. The base membranes were extracted with acetone at room temperature (25 °C) for a minimum of one day prior to use to remove any oils or impurities.

Table 3.1 Properties of TIPS base substrates

Membrane	Average pore diameter[a] (μm)	Porosity (volume %)	Thickness (μm)
PP-3	0.82	81	79
PP-4	0.26	60	43
PE-1	0.19	80	55
PE-2	0.47	82	58

[a]Determined from bubble point technique

3.1.2 Fabrication of the membranes with naphthalene disulfonyl chloride

Discs (8.5 cm diameter) of PE-2 and PP-4 were immersed in a solution of BPEI in $CHCl_3$ (10% w/v concentration) for up to 30 minutes. The BPEI coated disc was dried and then immersed into a solution of NDSC in CCl_4 (0.02% w/w) for up to 30 minutes. Following the cross-linking with NDSC the membrane was washed sequentially with

$CHCl_3$, $CHCl_3$ containing 1% triethylamine, and CH_3OH, dried and the mass of the incorporated cross-linked polymer was recorded.

3.1.3 Fabrication of the membranes with a diglycidyl ether cross-linker

A 5 ml solution of BPEI in DMF (ranging from 10% to 20% w/v concentration) was rapidly mixed with a 5 ml solution of a calculated amount of EDGE in 1-propanol, total volume 10 ml. The polymer/cross-linker mixture was rapidly poured onto the base PP3 substrate (11x11 cm) resting on top of a sheet of polyethylene terephthalate (PET). The filled microporous membrane was then covered with another sheet of PET and a teflon bar was used to remove air bubbles and excess solution. The sandwiched membrane was held in place by another glass plate. The membrane was allowed to stand for gelling to occur, typically overnight (16 hours). After removing the membrane from the glass plate and PET sheets, the membrane was washed with methanol.

The mass increase was taken as the percentage mass increase of PEI anchored in the pores over the mass of the original membrane:

$$G(\%) = \frac{m_f - m_o}{m_o} 100\% \qquad (3.1)$$

where m_f is the mass of the filled, extracted and dried membrane and m_o the mass of the nascent base membrane. The concentration, or polymer volume fraction, of the cross-linked polyethylenimine in the pores was calculated as:

$$\phi = \frac{(m_f - m_o)v_2}{V_s \varepsilon} \qquad (3.2)$$

where ν_2 is the partial specific volume of the polymer (0.97 ml/g for branched PEI) [11], V_s is the substrate volume and ε is the substrate porosity (80.5% for PP3).

3.1.4 Characterization of the membranes

The length and width of the nascent membrane sheets were measured with a ruler. The length and width, of the membranes, were also measured after incorporation of the gels in various pH solutions. The thickness of the membranes was measured by using a digital micrometer (model MDC-1 "P, Mitutoyo Corp.) by multiple measurements across the surface of the membrane, variation +/- 5%. The ion-exchange capacity (IEC) was measured by placing the membrane sample into 25mL of 0.1M HCl. The acid solution was titrated with phenolphthalein indicator after the membrane was removed and residual acid, on the membrane, washed back into the acid sample. The IEC was calculated from equation **(3.3)**:

$$IEC(meq/g) = \frac{V_{HCl}N_{HCl} - V_{NaOH}N_{NaOH}}{m_d} x1000 \quad \textbf{(3.3)}$$

where V and N were the volumes and normalities of the acid and base solutions and m_d was the mass of the pore filled, extracted and dried membrane. The IEC is expressed as

milliequivalents of titratable nitrogen per unit mass of dried membrane. The procedure was repeated twice with reproducibility within 1-3%.

Water uptake (WU) was obtained from dividing the difference in weight of a dried membrane and water filled membrane by weight of the wet membrane.

$$WU = \frac{m_w - m_d}{m_w} 100\% \qquad (3.4)$$

3.1.5 Microscopic Studies

For confocal microscopic analyses, the membrane samples were soaked in an aqueous solution of Direct Red 23 dye (10^{-5} M) overnight (~16 h) at room temperature. The wet membrane samples were viewed in a Carl Zeiss laser fluorescence confocal microscope (LSM 510) (Carl Zeiss Corp., Germany). The nascent membrane was immersed in paraffin oil for imaging purposes. The laser wavelengths used to excite the fluorophores in the membrane samples were 488 nm and 543 nm for the argon and helium-neon lasers respectively.

The surface and internal morphology of the fluorescently labeled membrane, was imaged by exciting the Direct Red 23 fluorophore, electrostatically bound to the protonated PEI (at 543 nm) at pH 5.5. The base membrane was imaged by exciting the intrinsic fluorophore (at 488 nm) present in the TIPS substrate.

The atomic force microscopy (AFM) images of wet membrane samples were taken on a Nanoscope II (Digital Instrument, Inc) contacting mode atomic force microscope equipped with a fluid cell filled with a test solution and an Si_3N_4 cantilever.

3.1.6 Permeability measurements

Permeability experiments were carried out in a stirred ultrafiltration cell, depicted in **Figure 3.1**, with an active membrane area of 38.50 cm^2. To simulate the flow conditions in an actual filtration operation, a stir bar mounted above the membrane worked in conjunction with a speed adjustable stir plate, at a stir rate of 150-200 revolutions/second, to provide a constant fluid velocity parallel to the membrane surface. The pH of the feed solution was adjusted by HCl or NaOH. An Orion pH meter (model 720A) equipped with a ROSS combination pH electrode model 81-02 (Orion) was used to measure the pH of the solutions. All measurements of flux were carried out at pressures between 100 and 500 kPa. Permeate samples were collected over a given time period and weighed. The flux was calculated from the mass of permeate divided by the time and the membrane active area. Prior to each measurement, the membranes were equilibrated with the test solution under pressure until a stable flux was achieved. The interval between readings was at least one hour.

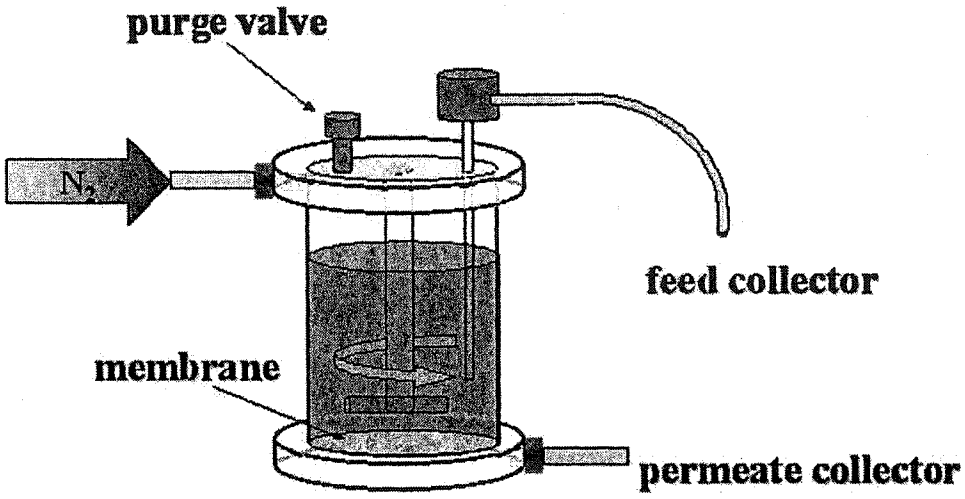

Figure 3.1 Schematic representation of the pressure cells used to test membranes

The membranes were tested with both single and mixed salt solutions for separation efficiency. The apparent rejection (R) was calculated by the following equation:

$$R(\%) = \left(1 - \frac{C_p}{C_f}\right) 100\% \qquad (3.5)$$

Where the C_p is the concentration of the permeate and C_f is the concentration of the feed. Single salt measurements were determined by conductivity measurements and mixed salt measurements were determined by inductively coupled argon plasma analysis (Jerrell-Ash, ICAP 9000). Sucrose concentration was measured by organic carbon analysis (Dorhmann, DC-190) and rejection was calculated in the same manner as the salt

separation. Each measurement was repeated a minimum of three times with a reproducibility of ±5%.

3.1.7 Potentiometric titrations

Potentiometric titrations were performed with the pH meter and pH electrode mentioned previously. A prepared solution of BPEI homopolymer was titrated in the presence of 5mM NaCl. A solution of BPEI (1.1 g/l) was stirred, capped with parafilm while bubbled with nitrogen gas. The pH change as a function of added acid was measured at 30 minute time intervals, or when the solution equilibrated as determined by the stabilization of the pH meter. The degree of protonation of the nitrogen centers was calculated as the difference between the proton equivalents added to the sample and the proton equivalents free in solution, as calculated from the measured pH values, divided by the number of nitrogen equivalents in the sample.

A duplicate set of membranes, with composition similar to those tested and reported in this chapter, was prepared for potentiometric titration. The membranes were titrated in the same manner as the homopolymer titration in the presence of 5mM NaCl. The membranes were cut into small pieces and were placed in a stirred beaker capped with parafilm and bubbled with nitrogen gas. 1 ml aliquots of 0.1M HCl were added, at 12 hour intervals, from a calibrated pipette (Eppendorf Research 1000 µl) and the changes in pH as a function of added acid were recorded. The degree of protonation was calculated in the same way described above.

3.2 Results and Discussion

The first series of BPEI filled membranes were based on a coating technology used to introduce a radical initiator (4,4'-azobis(4-cyanovaleryl chloride)) onto the coated layer as mentioned previously in **section 2.2.5** of **Chapter 2** [1]. BPEI concentrations of 2-4% w/v were used to coat the membranes and the deposited polymer was cross-linked into place in a subsequent step with NDSC (**Scheme 3.1**). The coating did not appreciably change the hydrophobic surface properties of the host substrate and ion-exchange capacities were difficult to determine. It was thus concluded that the procedure resulted in a BPEI coat that was a hard, dense coating that did not yield many titratable nitrogens.

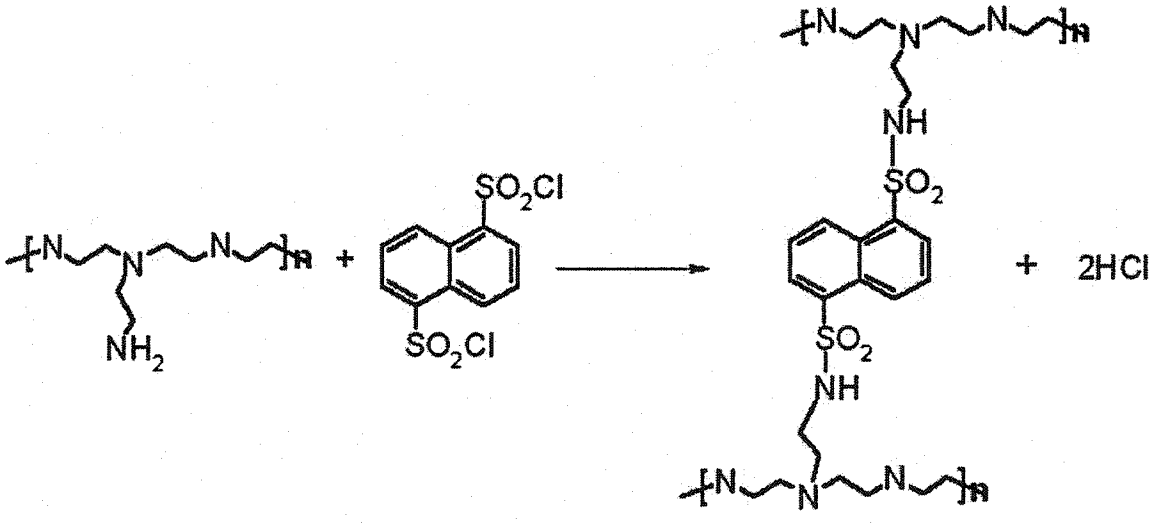

Scheme 3.1 Cross-linking of BPEI with NDSC

When the fabrication procedure was repeated with a higher concentration of BPEI (10% w/v) very high amounts of BPEI could be deposited in the base membrane (up to 142%). Pore filled membranes resulted when these membranes were cross-linked with NDSC. The differences in flux for nascent, coated and pore filled membranes are shown in **Figure 3.2.**

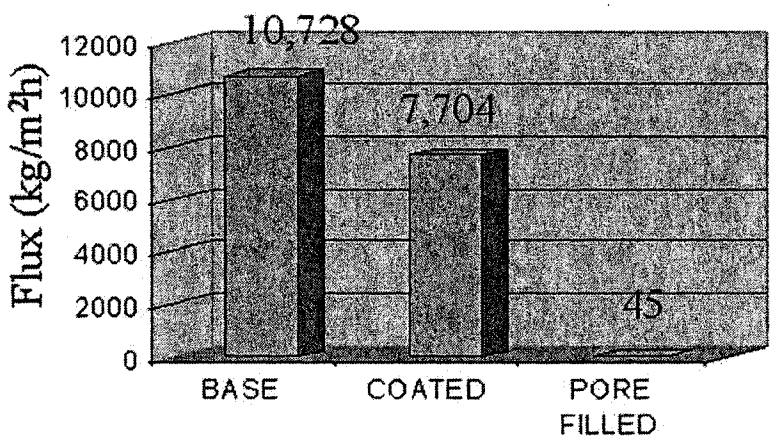

Figure 3.2 Differences in flux as a function of pore inclusion of BPEI measured at 100 kPa

3.2.1.1 Membrane Fabrication I: The Coating Process

The initial membrane fabrication method was based on differences in polymer-solvent interactions. Chloroform was chosen as the solvent for the coating procedure because it dissolves BPEI at all concentrations and can readily enter the pores of the host

substrate. To determine whether a relationship existed between the amount of coating that could be incorporated and time of coating, the mass gains of two membrane substrates were measured after coating in a solution of 10% BPEI (w/v) over a period of two hours. The results are shown in **Table 3.2**.

Table 3.2 Amount of BPEI coating as a function of time from a solution of 10% (w/v) BPEI

Membrane	Time of treatment with BPEI/$CHCl_3$ solution (min)	Mass increase on treatment with BPEI/$CHCl_3$ solution (%)
PE-1[a]	30	120
	60	116
	90	112
	120	139
PP-4[b]	30	65
	60	61
	90	60
	120	66

[a]Dimensions of strips: 5cm x 5cm x 0.005cm
[b]Dimensions of strips: 5cm x 5cm x 0.0058cm

The porosities of the two substrates are 82% and 60% for PE-1 and PP-4 respectively. Based on the measured dimensions and porosity, the porous volumes are 0.102 cm^3 for PE-1 and 0.087 cm^3 for PP-4. As can be seen from the data in **Table 3.2**, the amount of coating that can be incorporated into the membrane is independent of the duration of the coating process. Furthermore, the coated mass gains greatly exceeds the calculated expected mass gains of 37% and 20% for PE-1 and PP-4 respectively- based on the porous volumes and BPEI concentration (0.1 g/ml). Although the method of

calculation used to determine expected mass gains is reliable for fabricating pore-filled membranes, the method may have its limitations for coated membranes because it does not take into consideration the considerable surface area for coating; thus, it does not take into account the amount of polymer that can be coated on the top and bottom exterior surfaces of the membrane. This may explain the low values of the calculated mass gains.

A significant difference in substrate properties was noted when the coated membranes were dried under vacuum. The polyethylene based membranes exhibited remarkable and irreversible dimensional contractions. The results are shown in **Table 3.3**.

Table 3.3 Dimensional changes in the base substrate upon coating with BPEI and drying under vacuum

Membrane	Original volume (cm^3)	Volume after coating and drying (cm^3)	% change
PE-1	0.125	0.061	-51
PP-4	0.135	0.125	-7

The data in **Table 3.3** suggests the properties of the host substrate may play an important role in the performance of pore filled membranes constructed from them. Since the main role of the host substrate is confinement and protection of the gel from compression under pressure and osmotic swelling, structurally weak host substrates will have an adverse effect on the performance of the membrane under pressure. The dimensional changes were due to interactions within the coated polyethylenimine because a similar experiment conducted in the absence of BPEI resulted in a minor change in

volume (~3%) in PE-1 and no change in PP-4. BPEI filled membranes were not made with PE-1 substrate because of difficulties in working with the substrate. The membrane tore easily and was difficult to handle. The influence of the host substrate on membrane performance however has been confirmed with work on poly(4-vinylpyridine) based membranes [12].

3.2.1.2 Membrane Fabrication I: The Cross-linking Process

The deposited polymer could be extracted when immersed in a good solvent such as chloroform or methanol. Cross-linking of the coated polyethylenimine was therefore necessary for permanent incorporation within the membrane pores. It was essential to choose a solvent for the cross-linking reaction that did not dissolve the coated polymer such that diffusion (extraction) of the BPEI out of the membrane was prevented. Cross-linking was thus performed in CCl_4- a nonsolvent for BPEI. No loss of the coated material was observed after reacting BPEI with NDSC in CCl_4 and removal of the solvent under vacuum indicating that no BPEI polymer leached out of the membrane. After the cross-linking procedure, the membranes were extracted in a good solvent for BPEI (chloroform or methanol), to remove unincorporated polymer. Membranes fabricated by this process are reported in **Table 3.4**.

Table 3.4 Properties of BPEI-NDSC membranes[a]

Membrane	Mass gain[b] after cross-linking coated BPEI with NDSC[c] (%)	Ion exchange capacity (meq/g)
PE2-1	54	2.24
PE2-2	33	1.89
PP4-1	16	1.16
PE1-1	57	2.11

[a]Membranes made using 10% (w/v) BPEI in $CHCl_3$
[b]Mass gain after extraction in $CHCl_3$ and methanol
[c]0.02% (w/w) NDSC cross-linker in 50 mls of CCl_4

3.2.2 Nanofiltration Performance of PEI-NDSC Membranes

As mentioned earlier, and shown in **Figure 3.2**, the flux of the BPEI-NDSC membranes made from high concentrations of BPEI were three to four orders of magnitude lower than the base and coated membranes at 100kPa. As such these membranes had fluxes similar to other gel filled membranes [4]. As a result these membranes were investigated for their ability to separate salts from an ionic solution. The results are shown in **Table 3.5**.

Table 3.5 Single salt rejection capability of BPEI-NDSC membranes at 100kPa

Membrane	Feed composition (ppm)	Flux (kg/m^2h)	Rejection (%)
PE2-1	NaCl (15)	45	57
	NaCl (120)	45	24
	Na_2SO_4 (16)	26	11
PE2-2	NaCl (14)	58	46
	Na_2SO_4 (16)	61	8
PP4-1	NaCl (17)	16.3	68
	NaCl (122)	16	33
	Sucrose (50)	16	0

The solute rejection data in **Table 3.5** shows that separation, relative to NaCl (low concentration) rejection, is reduced at higher feed concentrations and in the presence of a bivalent counter-ion, SO_4^{2-}. Membrane PP4-1, furthermore, does not reject sucrose thus establishing sieving plays no role in the mechanism of separation. The solute rejection behavior of these membranes are entirely consistent with what is expected based on the Donnan exclusion mechanism discussed previously in **Chapter 1, section 1.2.2.1**. This important finding established that BPEI pore filled membranes can function effectively in nanofiltration applications without prior acidification of the feed or induction of a permanent charge in the gel by *N*-alkylation because BPEI is sufficiently basic to acquire a positive charge by an acid/base reaction with water. These membranes were investigated for their performance in mixed salt separations and the results are summarized in **Table 3.6**.

Table 3.6 Flux and Separation performance of PEI-NDSC membranes of a mixed salt feed at 100 kPa

Entry	Membrane	Feed composition and concentration (ppm)	Separation (%) Na^+	Mg^{2+}	Ca^{2+}	Flux (kg/m^2h)
1	PE2-1	Na (16), Mg (12), Ca (43)[a]	12	69	66	31
2	PP4-1	Na (15), Mg (7), Ca (47)[a]	18	93	83	13
3	PE2-1	Tap water[b]	-0.3	35	25	25
4	PE2-1	Tap water[c]	6	13	14	55

[a]mixture of cations, all as chloride salts, pH 6
[b]sampled after 14.5 hours of continuous flow, pH 7.5
[c]sampled after 112 hours of continuous flow at 345 kPa of pressure, pH 7.5

The higher rejections of bivalent co-ions (Mg^{2+} and Ca^{2+}) over the monovalent sodium ion are consistent with the Donnan exclusion mechanism already established. The third and fourth entries in **Table 3.6** show the effect of continuous flow of tap water as a function of time. The membrane exhibited much lower separation of ions in tap water than observed for the prepared salt solution shown in entry 1 for the same membrane. Tap water has a high concentration of bivalent counter-ions with a typical ionic composition, Na^+: 12 ppm; K^+: 0.8 ppm; Mg^{2+}: 8 ppm; Ca^{2+}: 40 ppm; F^-: 1 ppm; Cl^-: 25 ppm; NO_3^-: 2.8 ppm, and SO_4^{2-}: 26 ppm and unknown amounts of HCO_3^- and CO_3^{2-}; thus, a lower rejection of ionic solutes is expected. The membrane exhibited a green coloration after the flow tests, due to chelation of copper and other transition metals [13-16].

3.2.3 Membrane Fabrication II: *in situ* cross-linking with diglycidyl ether

The BPEI-NDSC membranes provoked much interest because of their ability to separate ionic solutes at ultra low pressures (100 kPa) with fluxes that were unprecedented in the literature. Despite their promise, the membranes were often inconsistent in their performance with long times required for equilibration. Furthermore, the method of fabrication allowed very little control over membrane properties such as the degree of cross-linking and mass loading. Membranes made by this route were often difficult to reproduce. As a result, different routes of membrane fabrication were examined. In particular, a process was developed in which the host substrate was filled with a solution of polymer and cross-linker and allowed to gel. This route provided a route to make robust membranes reproducibly with good control over membrane properties. Membranes were fabricated by sandwiching a filled microporous host between two poly(ethylene terephthalate) sheets, held in place by two glass plates, for gellation to occur.

Gel studies of cross-linked BPEI have been reported in the literature using diglycidyl cross-linking agents to form BPEI gels [17-20]. Ethyleneglycol diglycidyl ether (EDGE) was found to react with BPEI to give clear gels when a (50/50) mixture of 1-propanol and DMF were used as the solvent. The formation of an EDGE cross-linked BPEI system is shown in **Scheme 3.2**.

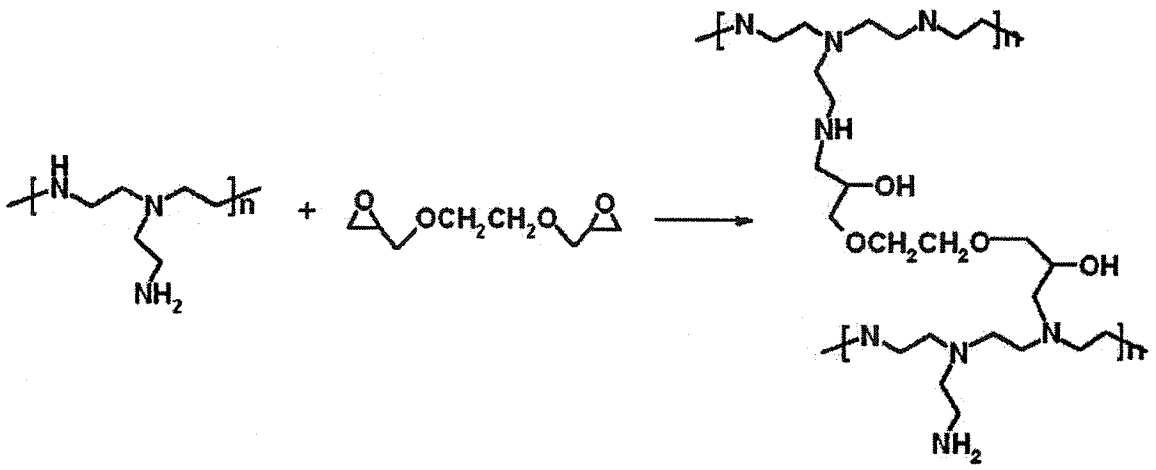

Scheme 3.2 Formation of BPEI-EDGE gel

The choice of solvent system was dictated by the requirements of solubility of the polymer and cross-linker and a high boiling point to mitigate evaporation. Membranes made with mixed solvents, methanol and DMF, were inconsistent in their performance. This was attributed to evaporation of methanol during the cross-linking process leading to inhomogeneity of the pore-filling. It was also found that cross-linking was completely inhibited when an aprotic solvent such as DMF was used without a protic solvent being present. No macro-syneresis was observed in any of the gels regardless of the polymer concentration or cross-linking ratio. The rate of the gellation reactions was sufficiently slow (typically 12-24 hours) such that the reagents could be conveniently mixed and introduced into the pores of the membrane before the viscosity of the solutions became too high.

3.2.4 Membrane characterization

A series of membranes were prepared, using PP-3 host substrate, with varying mass-gains and degrees of cross-linking as shown in **Table 3.7**. The mass-gains shown in **Table 3.8** were obtained after extraction of the membranes for 24 hours in methanol, deionized water for another 24 hours, then cycled twice through alternating 0.1 M HCl and 0.1 M NaOH for 12 hours each. The incorporated cross-linked BPEI could not be removed by the extraction procedures and no mass loss was observed even after large volumes of water were passed through the membranes under pressurized flow. It should be stressed that the BPEI is not chemically bonded to the poly(propylene) microporous substrate and is simply held in place by cross-linking and entanglement; furthermore, the surface of the host polypropylene membrane changed from highly hydrophobic prior to treatment to highly hydrophilic after the introduction of the BPEI gel.

Table 3.7 Properties of BPEI-EDGE pore filled membranes

Membrane	Mass gain (%)	Molar cross-linking (%)	Water uptake[a] (%)	Measured IEC[a] (meq/g)	Theoretical IEC (meq/g)	Gel polymer volume fraction at pH 5.5
BE1	53	10	85	2.86	5.73	0.0755
BE2	92	10	82	3.81	7.89	0.134
BE3	60	15	83	2.54	5.36	0.093
BE4	111	15	78	3.75	7.6	0.1687
BE5	72	20	81	2.75	5.38	0.115
BE6	118	20	75	3.8	7.0	0.1844

[a] Reproducibility was within 1% in all cases

Table 3.8 Thickness[a] as a function of pH of BPEI-EDGE filled membranes

	Thickness (μm)		
Membrane	pH 2	pH 5.5	pH 12
BE1	116 ± 6	104 ± 5	108 ± 5
BE2	132 ± 6	108 ± 4	107 ± 7
BE3	117 ± 7	97 ± 5	94 ± 3
BE4	113 ± 6	103 ± 6	103 ± 7
BE5	116 ± 6	101 ± 5	98 ± 5
BE6	112 ± 7	102 ± 5	104 ± 5

[a] Nascent membrane thickness: 75 μm

Information on two sets of membranes is given in **Table 3.7**, namely entries BE1, BE3, BE5 and BE2, BE4, BE6. Each membrane was formed using a constant concentration of BPEI in the filling solution but differing amounts of EDGE as cross-linker. The reported cross-linking ratios are nominal and based on the concentration of repeat units of BPEI present in the preparatory solution. The variation in mass gain in each series reflects the amount of EDGE present.

It was difficult to form membranes with mass-gains lower than those shown in **Table 3.7** unless much higher cross-linking ratios were used. Gels with lower formal cross-linking ratios (≤10 %) could only be formed when the polymer concentration was high and, conversely, low polymer concentrations (5-10 % w/v) necessitated a high cross-linker ratio (≥15%). The difficulties were attributed to the nature of the polymer and size of the cross-linker. More specifically, in order to form a gel, the concentration of the polymer must exceed the overlap concentration- the point at which the chains overlap. The overlap concentration is a function of the polymer's radius of gyration and molecular weight [21-23]. Because BPEI has a globular conformation, with a random distribution

of branch sites, the radius of gyration cannot be calculated by methods used for linear polymers [24]. Thus, an overlap concentration of BPEI cannot be calculated.

The size of the cross-linker also has an effect on gellation and is illustrated in **Figure 3.3**. EDGE is a small cross-linker that can react with BPEI in several ways. **Figures 3.3(a) and 3.3(b)** represent wasted cross-linking reactions because the EDGE cross-linker reacts with one polymer molecule of BPEI in an intramolecular fashion. At sufficiently high polymer or cross-linker concentrations, intermolecular cross-links can be formed as shown in **Figure 3.3(c),** which result in the formation of gels.

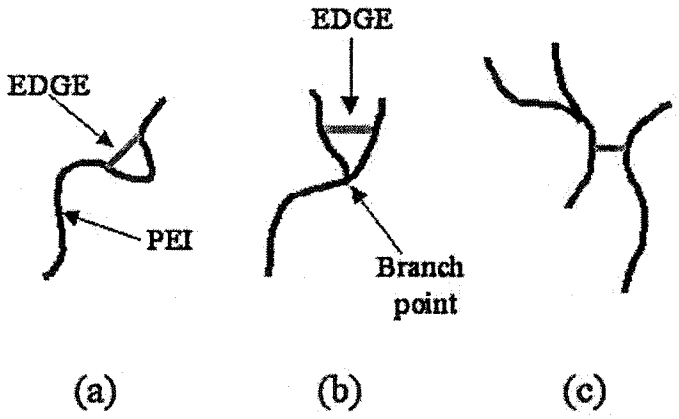

Figure 3.3 Different ways EDGE can cross-link BPEI. (a) Intra-chain cross-linking; (b) Intra-polymer cross-linking between branches; (c) Inter-polymer cross-linking

The thickness of all of the membranes were measured and compared to the original host material and shown in **Table 3.8**. No changes in the x and y dimensions were observed, but substantial increases in thickness, relative to the nascent membrane (75 μm average thickness), occurred with the incorporation of BPEI measured at pH 5.5.

There are little discernable trends in thickness as a function of mass gain or cross-linker ratio. On average and within experimental error, there are little changes in thickness within the pH range 2 to 12. This stands in stark contrast to the poly(4-vinylpyridine) membranes that show extreme dimensional sensitivity to ionization of the incorporated polymers [2,3,25]. The conformational stability of BPEI is consistent with what has been reported earlier by Kobayashi *et al.* [26,27] where it was shown that BPEI, due to its globular nature, does not undergo significant changes in conformation upon ionization.

The water uptake values in **Table 3.7** are a measure of the porosity of the gel-filled membrane. The water uptake values are correlated to the gel polymer volume fraction- which is the volume fraction occupied by the gel polymer in the pores (taking into account the thickness of the membrane). The water uptake values (or swelling of the gels) are high, ranging from 85% to 75% for low to high gel polymer volume fractions respectively. The high water uptake ratios clearly indicate these membranes, although filled with a gel, are still highly porous and are composed of mainly water. This is a critical factor in the performance of these membranes because hydrodynamic flow occurs solely through the porous regions and as the water content of a gel declines, the mobility of the solutes and solvent become restricted owing to a smaller average pore size of the gel network [28,29].

The ion exchange capacity (IEC) is a measure of the titratable nitrogens present within the filled membranes. The results, shown in **Table 3.7,** range from 2.5 to 3.8 meq of nitrogen per gram of membrane, indicating the potentially high fixed charge concentrations inside the membranes. The measured IEC's, however, are substantially

less than the calculated theoretical IEC's- typically 50%. Several factors combined may explain the low measured IEC in these membranes. For example, a similar result has been previously observed in poly(4-vinylpyridine) based membranes where an increase in divinylbenzene cross-linker (up to 4%) resulted in only 50% of the pyridine nitrogens accessible by titration [30]. The low measured IEC was attributed to an increased restriction of accessing the pyridine nitrogens because of the increased rigidity imposed by the cross-linking. Such an effect may be operative with the BPEI-EDGE filled membranes because the molar ratio of cross-linker is high (10-20%). Another factor is that BPEI, as will be discussed in more detail later, cannot exceed 75% degree of protonation. Since cross-linking of a polyelectrolyte has been shown to affect its ionization behavior [30] it is not surprising that the measured IEC for BPEI gel filled membranes is substantially lower than the calculated theoretical IEC. And finally, the low IEC's could be attributed to the salt-free conditions under which the titrations were performed, since salt has a shielding effect on the charges, which in turn would result in greater protonation of the nitrogens and a higher measured IEC. The titration behavior of BPEI will be discussed further in **section 3.2.6**.

3.2.5 Morphology and distribution of pore filling

The internal and surface morphologies of the membranes were examined with laser fluorescence confocal and atomic force microscopy. **Figure 3.4a** is a fluorescence

micrograph of the base, polypropylene substrate at a depth of 9.4 μm. The image resulted from fluorescence of an intrinsic trace impurity present in the polypropylene base membrane. Extraction of the base membrane, with trichloroethylene, rendered the polypropylene substrate invisible under identical imaging conditions.

A fluorescence micrograph of a BPEI pore filled membrane in deionized water, at a depth of 4.5 μm, is shown in **Figure 3.4b** imaged under identical conditions used for the base substrate. As can be seen, there is no evidence of the nodular/fibril morphology of the host substrate, but instead a blob morphology of the swollen BPEI gel is evident. The red color is due to the bound anionic fluorescent dye. The fibril structures, however, are imaged as yellow because the green dye of the base membrane is combined with the red dye in the PEI exterior coat to form a composite yellow signal.

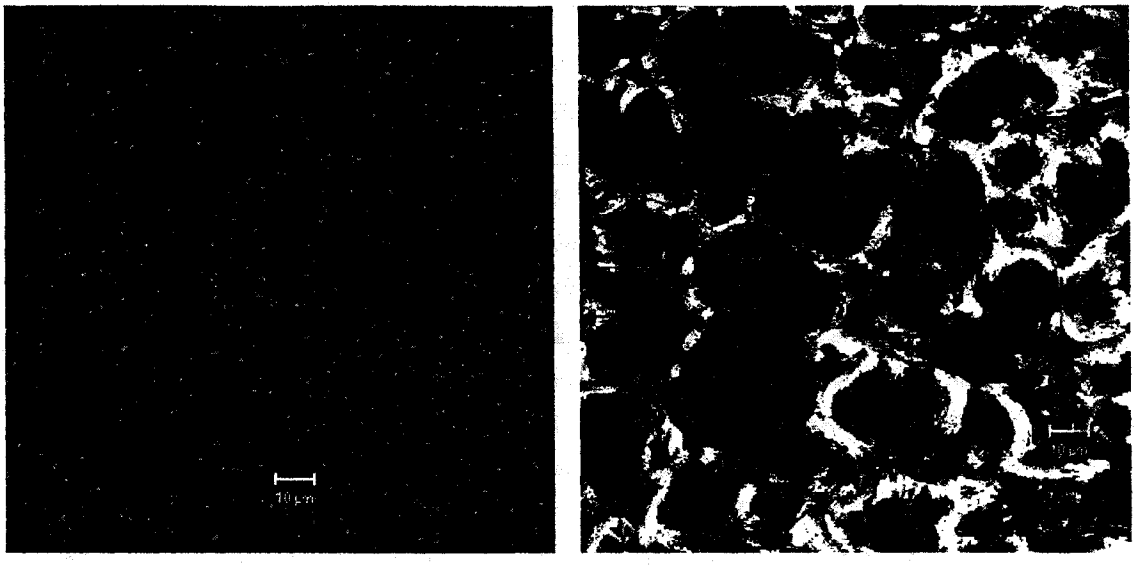

(a) (b)

Figure 3.4 Laser confocal micrographs of nascent PP-3 (a) and pore filled (b) membranes with 56% mass gain and 20% EDGE cross-linking. Magnification ~ 700x

The surface of a BPEI pore filled membrane in deionized water was imaged by atomic force microscopy and is shown in **Figure 3.5**. The micrograph clearly shows the blob morphology of swollen BPEI gels at the membrane surface. As can be seen, the fibular/nodular structure of the host membrane is covered by the soft undulating gel surface and no pores are visible. The AFM of the host substrate could not be performed because the surface was too coarse to image satisfactorily.

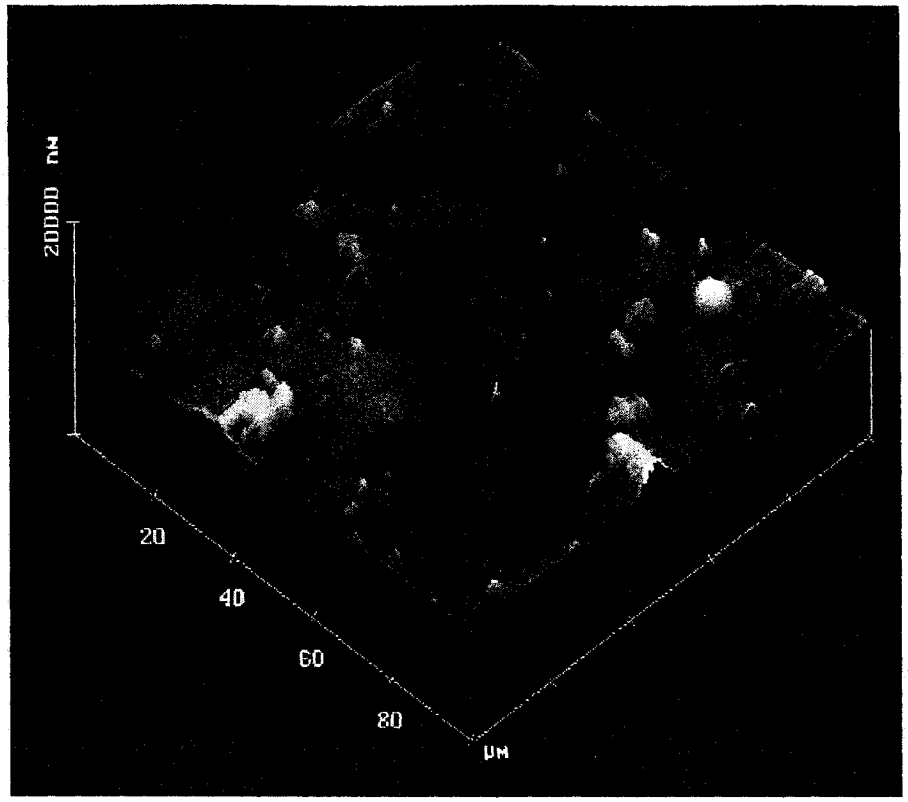

Figure 3.5 Atomic force micrograph of BPEI-EDGE pore filled membrane BE2

3.2.6 Degree of ionization

The presence of a nitrogen atom in the repeat unit of polyethylenimine imparts a basic character to the polymer. Titration of polyethylenimine has been reported by several researchers using calorimetric [31] and potentiometric [26,32-37] methods. Several authors have reported that 100% protonation of BPEI could not be achieved; but instead, degrees of protonation (α) reached limiting values of between 66% [32] to 75% [26,31,37].

An explanation for the limiting degrees of protonation behavior of PEI is the nearest neighbor interactions (NNI). Nearest neighbor interactions, are intrinsic properties of polymers that contain ionizable groups; that is, ionization of one group prevents ionization at a neighboring site. These NNI's are especially pronounced for PEI vs. ionizable polymers made from vinyl monomers because the charge resides in the backbone of the polymer whereas charge in polyvinyl systems reside in pendant groups that can orient themselves with respect to each other to minimize electrostatic interactions. Because the charges in PEI are in the backbone, the contour distance between them is fixed, and generally less than polyvinyl systems, resulting in greater electrostatic interactions. The extent and nature of these NNI's have been investigated by Lewis and St. Pierre [31], where they determined the thermodynamic parameters ΔG, ΔH and ΔS for proton ionization, and by Smits *et al.* [37] where they described the NNI in the context of the *Ising* [38] and *Katchalsky* [39] models of polyelectrolyte titrations.

pK values for protonated BPEI have been reported by Kobayashi *et al.* to range from 8.5 to 9.15 [26]; however, Bloys van Treslong and Staverman [36] established a dependence of pK values on salt and BPEI concentration and reported a range of pK values, from as low as 5.01 to as high as 8.52. Compared to the acid dissociation constant for protonated diethylamine (pKa 11) it is clear NNI have a substantial effect on pK values of BPEI.

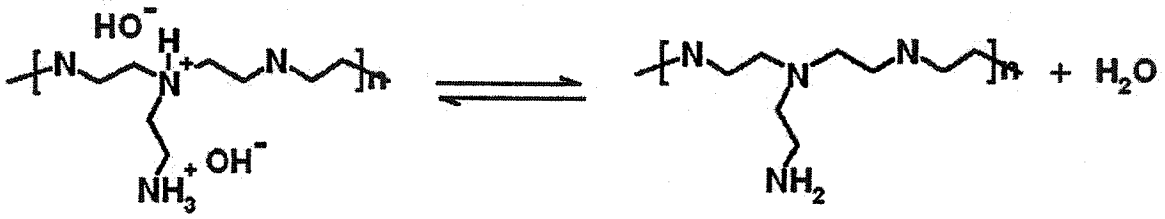

Figure 3.6 Acid dissociation of protonated BPEI in water

Potentiometric titrations of BPEI homopolymer and membranes containing cross-linked BPEI were undertaken in order to see how confinement of the polymer in a microporous membrane affects its pKa. In order to treat the data a modified Henderson-Hasselbach equation was used [29,40]

$$pH = pK_{\alpha=0.5} + n \log[(1-\alpha)/\alpha] \qquad (6)$$

where α represents the degree of ionization and n is a measure of the electrostatic interactions of neighboring groups on the chain. Typical titration curves obtained in 5mM NaCl are shown in **Figure 3.7.**

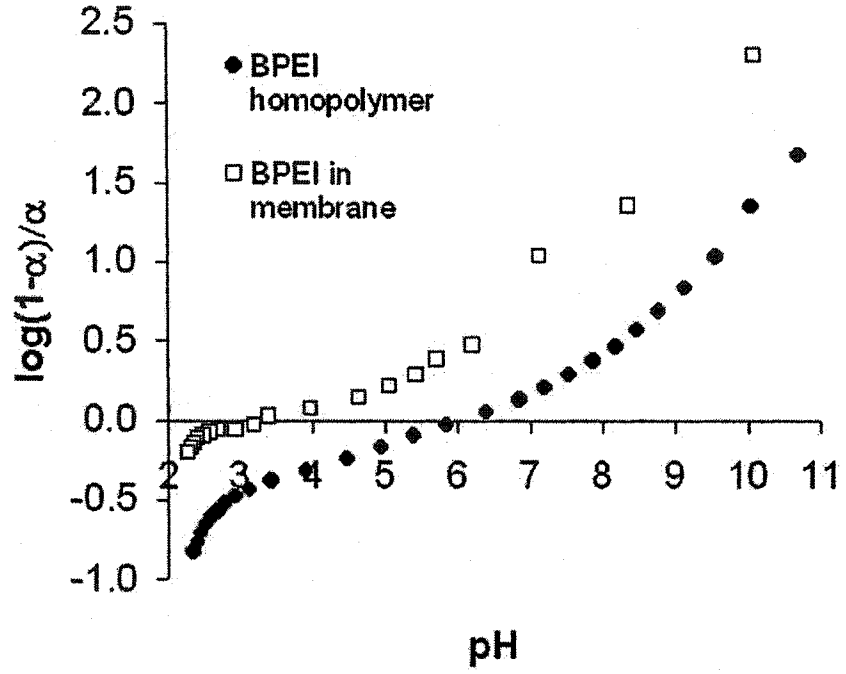

Figure 3.7 Titration plots of BPEI homopolymer in solution and BPEI incorporated in a membrane

In the context of **equation 6**, the acid dissociation term $pK_{\alpha=0.5}$ will be equated to pKa, used for small molecule systems, because it represents the pH at which the polymer is equal to $pK_{\alpha=0.5}$. It is clear from the data shown in **Figure 3.7** that the $pK_{\alpha=0.5}$ of the BPEI homopolymer is different when titrated in solution to when confined in a hydrophobic support. The $pK_{\alpha=0.5}$ value of 6.02 obtained here (concentration of BPEI repeat units = 2.56×10^{-2} M), in the presence of 5mM NaCl, closely matches the $pK_{\alpha=0.5}$ of 6.48 ([BPEI repeat unit] = 2.11×10^{-2} M), in 1mM NaCl, reported by Treslong and Staverman [36].

The values of $pK_{\alpha=0.5}$ obtained for the BPEI in the membranes are reported in **Table 3.9**. An increase in the BPEI concentration inside the membrane results in a decrease in $pK_{\alpha=0.5}$ values suggesting an inverse relationship; however, the results are contrary to what is expected. That is, an increase in polymer concentration should also be seen in an increase in $pK_{\alpha=0.5}$. There is, however, uncertainty in the BPEI concentration quoted in **Table 3.9** because the values were calculated based on the molar ratios of cross-linker used. Since degrees of cross-linking could not be verified experimentally, the cross-linking ratios are nominal values. The most significant finding in **Table 3.9**, however, is that encapsulation of BPEI in the membrane lowers the $pK_{\alpha=0.5}$ by over 2 orders of magnitude. A similar reduction in $pK_{\alpha=0.5}$, on incorporation of poly(4-vinylpyridine) in a membrane, has been previously observed [41]. This was attributed to both the effect of the higher local concentration of the polybase, when confined in the membrane as compared to that in dilute solution, as well as possibly the effect of the host. The lower $pK_{\alpha=0.5}$ for BPEI gel filled membranes cannot be attributed to concentration differences because the BPEI concentration inside the membrane is similar to the BPEI homopolymer concentration. The reduction in the $pK_{\alpha=0.5}$ for the membranes must therefore be due to the effects of the host or possibly the high degree of cross-linking.

Table 3.9 Titration data of BPEI-EDGE membranes

Polymer Volume Fraction	Cross-linking (%)	BPEI concentration inside the membrane (M)	$pK_{\alpha=0.5}$
BPEI homopolymer	-	2.56×10^{-2} [a]	6.02
0.055	10	9.51×10^{-3}	3.82
0.082	15	1.23×10^{-2}	3.25
0.097	20	1.3×10^{-2}	3.12
0.116	10	1.78×10^{-2}	3.25
0.13	15	1.94×10^{-2}	3.28
0.151	20	2.06×10^{-2}	3.01

[a]BPEI concentration in solution

3.2.7 Nanofiltration performance of BPEI-EDGE membranes

The pure-water fluxes of the membranes listed in **Table 3.7** were examined as a function of pressure and presented in **Figure 3.8**.

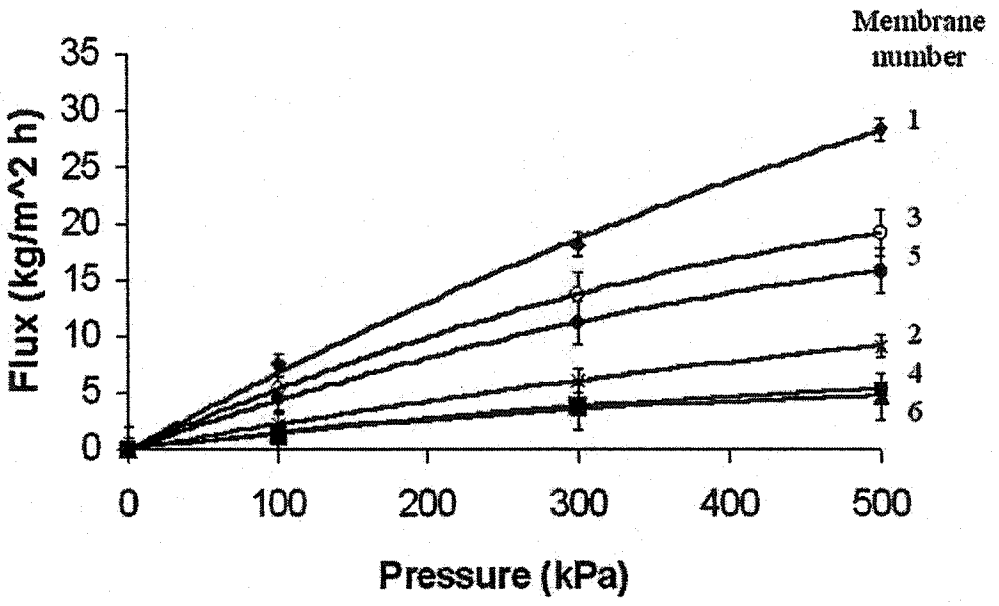

Figure 3.8 Flux as a function of applied pressure through BPEI-EDGE filled membranes

Each of the membranes exhibited, within experimental error, a fairly linear flux/pressure relationship through the origin over the pressure range (100-300 kPa); however, a slight curvature occurred at the higher pressure of 500 kPa. This indicates that the morphology of the membrane and the incorporated gel, for the most part, is not altered by hydraulic flow despite the relatively large pore sizes and porosities of the host membranes. The flux of the membrane decreases with an increase in mass load of gel polymer incorporated into the host membrane. These flux data were entirely reproducible with the same values being obtained after testing of the membranes with various solutes. This again points out the stability of this type of membrane construct.

Figure 3.9 shows the influence of pH on flux through three membranes.

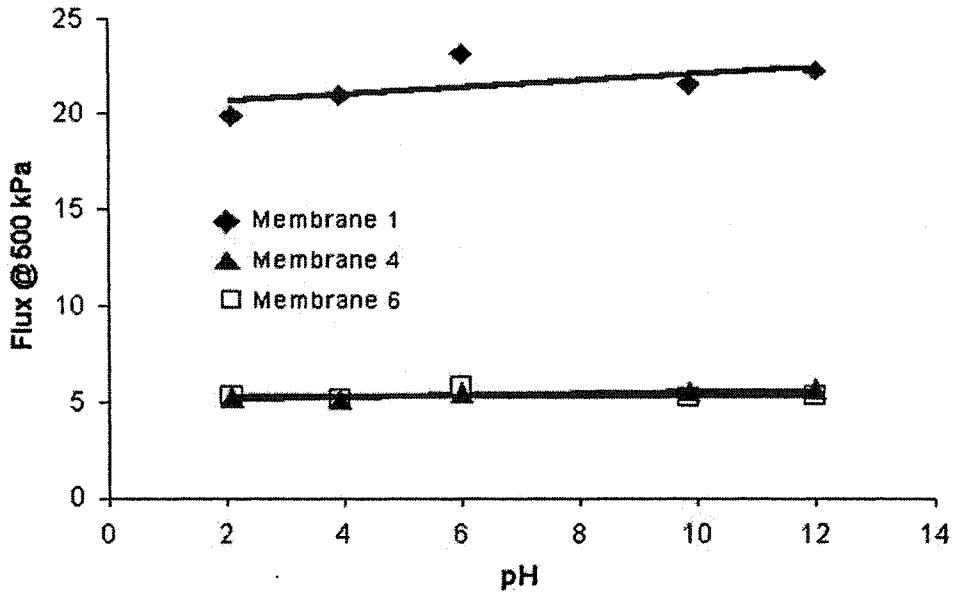

Figure 3.9 Flux as a function of feed pH of BPEI-EDGE filled membranes @ 500kPa

The most interesting feature of the data is the relative insensitivity of the gel to ionization. Regardless of the degree of cross-linking, the fluxes of the membranes are constant irrespective of the degree of ionization. Which, stands in stark contrast to the pH valve effect, discussed previously in **Chapter 2, section 2.2.3,** observed in poly(4-vinylpyridine) based membranes [2,25,41,42], where the pH sensitivity of these membranes on permeability can range from several orders of magnitude for uncross-linked pore fillings [2,25,42] to several fold for cross-linked pore fillings [41,43].

The flux-pH profile of BPEI filled membranes, although unusual, is consistent with the findings of Kobayashi *et al.* [26] who studied the viscosity behavior of BPEI over the pH range 2-12. They reported the viscosity values of BPEI were virtually

constant over a pH range of 2-12 as well as a range of ionic strengths, indicating the inherent globular structure of BPEI changed very little. This conformational stability results from its highly branched, globular nature [26,42].

3.2.8 Salt separation of BPEI membranes

BPEI pore filled membranes were tested for their ability to reject salt under pressure driven conditions. It can be seen in **Figure 3.10** that BPEI membranes reject NaCl, at a pH of 5.5, without the need for *N*-alkylation of the nitrogens in the polymer to provide charge in the gel. The rejection of NaCl is marginally diminished when the feed concentration is increased from 1mM to 5mM and multi-valent counter-ions (Na_2SO_4) are rejected to a lower level, which is consistent with the Donnan exclusion-based mechanism [45].

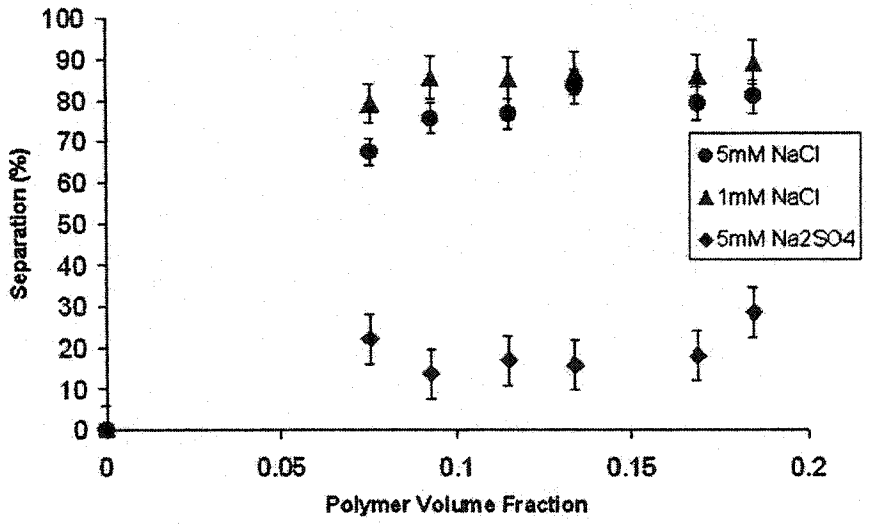

Figure 3.10 Donnan exclusion behavior of BPEI-EDGE membranes @ 500 kPa

As can be seen in **Figure 3.10**, the rejection profile of NaCl is relatively unaffected by the amount of BPEI present in the membranes. This suggests that the rejection of salt is determined by a limiting membrane charge density- exceeding which, does not contribute to an increased rejection of NaCl. At a pH of 5.5, the membranes have degrees of protonation of 30% ± 6% which correspond to uncondensed charge densities ranging from 0.43 to 1.22 mol/l of gel. The ionic strength of the 1 and 5 mM NaCl solutions are 0.001 and 0.005 mol/l respectively, so the ratios of the membrane charge concentration to the feed salt concentrations are very high (ca. 1220) so salt separation would be expected. This is consistent with the Teorell-Meyer-Sievers (TMS) model that predicts rejection of ionic species by charged membranes is dependent on the ratio of membrane effective charge to the salt concentration in the feed and not on their absolute values [46,47].

To verify that membrane separations are indeed regulated by the ratio of membrane charge density to the feed concentration, the separation of 5mM Na^+ as a function of pH was examined. The separation vs. pH profile is shown in **Figure 3.11**, where separation does not increase with an increase in degree of protonation (unlike the poly(4-vinylpyridine) pore filled membranes) and the separations were surprisingly consistently high, even up to the alkaline pH of 10 where the BPEI gel is expected to have very little charge. Indeed, the degree of protonation of the BPEI membranes at pH 10 is low (ca. 2%) and the charge densities of the membranes range from 0.02 to 0.06 mol/l of gel. The ionic strength of the solutions between the pH ranges of 4 and 10 was kept constant at 0.005 mol/l, thus still maintaining a relatively high membrane charge concentration to feed concentration ratio (4 to 12).

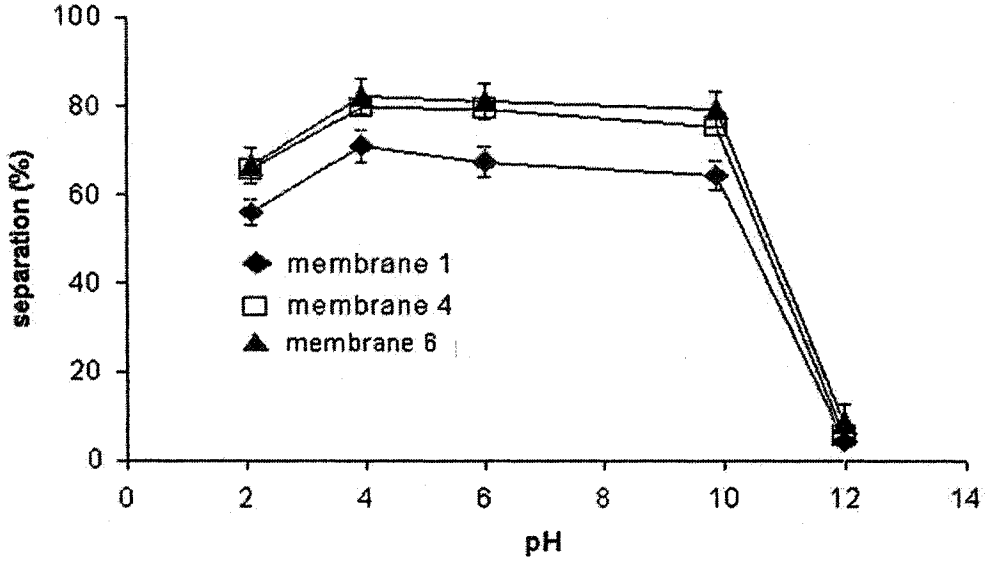

Figure 3.11 Separation as a function of pH of BPEI-EDGE membranes

The separation profile displays diminished separation at either pH extremes tested. The diminished separation at pH 2 is attributed to a lower Donnan potential established at the gel/feed interface due to a 10-fold increase in feed solute concentration. It is worth noting at this point that an increased proton concentration does not translate to a higher charge density within the gel. At a pH of 2, a phenomenon known as counter-ion condensation occurs. The counter-ion condensation theory developed by Manning [49] and Sato [50] postulates that the spacing of the fixed charge, along a polyelectrolyte chain, below the Bjerrum length (7.13 Å in water at 25 °C) results in association of counter-ions with the macro-ion, effectively shielding the charge and nullifying the effects of any further increase in charge. The net effect is that an increase in degree of

ionization of a polyelectrolyte will result in a corresponding linear increase in charge density until the counter-ions condense- at which point the charge density reaches an asymptotic maximum and levels off. The nitrogen to nitrogen distance along the backbone is 3.48 Å and at a pH of 2, the calculated degree of protonation exceeds 80% which results in the spacing of charges to fall below the Bjerrum length and thus condensing the counter-ions in BPEI.

The abrupt drop in separation at pH above 10 is due to the removal of charge and the increasing concentration of sodium ion. Both of these factors combined would have a severe effect in reducing the Donnan potential within the gel. The BPEI-EGDGE gel, furthermore, is unstable to highly basic solutions and material loss was observed over a prolonged exposure to highly alkaline conditions (pH >12). No such loss was observed in highly acidic conditions (pH 2).

Based on the high single salt rejection capabilities, the BPEI pore filled membranes were tested for mixed ion rejection (tap water) abilities. The measured pH of tap water prior to use was 7.5 so the charge concentrations in the membranes are lower than in the single salt rejection case where the pH was 5.5. The rejection of bivalent cations (Mg^{2+} and Ca^{2+}), however, is extremely high as shown in **Figure 3.12** indicating a large fixed charge concentration is not necessary for ionic solute separation. Sucrose, a small neutral organic, was not rejected to an appreciable extent indicating sieving does not play a role as a mechanism for separation, further establishing the basis of separation to be Donnan exclusion.

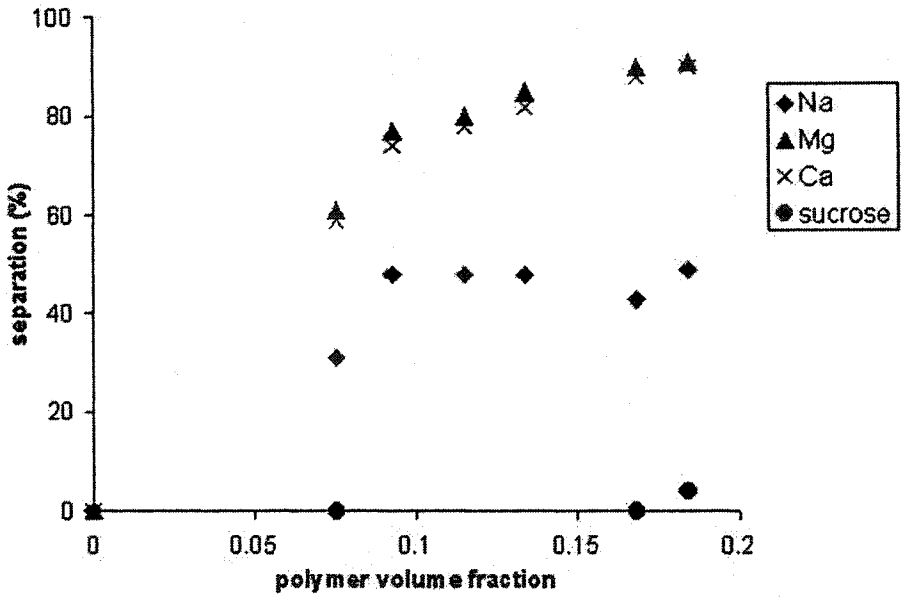

Figure 3.12 Tap water and sucrose (50 ppm) separation by BPEI-EDGE membranes. Tap water composition- Na^+: 12 ppm; K^+: 0.8 ppm; Mg^{2+}: 8 ppm; Ca^{2+}: 40 ppm; F^-: 1 ppm; Cl^-: 25 ppm; NO_3^-: 2.8 ppm, and SO_4^{2-}: 26 ppm and unknown amounts of HCO_3^- and CO_3^{2-}

The results in **Table 3.10** also compare the performances of BPEI pore filled membranes with commercial membranes in separation of ionic solutes in tap water. The data clearly shows that the BPEI membranes are competitive with the commercial membranes in their performances with the advantages of cost effectiveness and ease of manufacture. There are, however, limitations to BPEI pore filled membranes because long term, continuous flow, tests of tap water rejection showed a marked decrease in performance over time. This was attributed to chelation of transition metals [29,51], present in trace amounts in the tap water, accumulating and concentrating within the BPEI gel. Chelation of the metals reduces the number of nitrogens available for protonation and thus, the Donnan potential; furthermore, the metals may act as cross-

linkers changing the gel morphology. The chelated transition metals, however, could be removed by cleaning the membrane with 0.1 M HCl and the performance of the membrane restored.

Table 3.10 Comparison of BPEI-EDGE membranes with commercial nanofiltration membranes in tap water separation

Membrane	Flux[a] (kg/m^2h)	NaCl Rejection (%)	$MgCl_2$ Rejection (%)	$CaCl_2$ Rejection (%)
1	28	30	60	57
6	4.8	50	91	89
Desal 51	23.3	41	87	81
Hydranautics 7450	8.4	33	65	68

[a]Flux measured at 500kPa

3.3 Conclusion

The work in this chapter has contributed to many significant developments in the evolution of the pore-filled membrane technology at McMaster. First, the *in situ* cross-linking method of fabrication has provided a means to make a wide variety of gel filled membranes with excellent reproducible properties. The *in situ* cross-linking technique has many advantages; for example, it is a highly versatile technique because it can be used to make gel filled membranes that could not otherwise be made by the *in situ* polymerization technique. The *in situ* cross-linking technique, furthermore, does not

cause structural damage to the host substrate as is speculated to occur in the *in situ* polymerization process. Interpenetration of the monomer into the bulk polypropylene or degradation of the host substrate caused by the exothermicity of the polymerization could result in a compromise of the structural integrity of the host substrates.

The BPEI gel filled membranes have also been shown to permanently change the surface properties of the host polypropylene substrate from hydrophobic to hydrophilic. The membranes are highly porous despite the large amount of gel that can be loaded into the pores. The membranes have high ion-exchange capacities because of the large number of titratable nitrogens present in the gel.

The results in this chapter also conclusively prove that a permanent, static charge is not required to reject salts in a pore-filled nanofiltration membrane under pressure driven separations. The separations achieved with PEI-EGDGE membranes are higher than those achieved by the commercial membranes at ambient pH's and are excellent in water softening applications. The degree of protonation required to function in salt separation is quite low and is achieved by the relative high basicity of the PEI aliphatic nitrogen centers. A dynamic, mobile charge, as is present in PEI can be advantageous when used in the separation of potential fouling agents that are attracted to cationic centers. The removal of the charge by deprotonation can facilitate cleaning and is a cheap, fast process.

3.4 References

1. Childs, R.F.; Weng, J.F.; Kim, M.Y.; Dickson, J.M. *J. Pol. Sci. Part A: Polym. Chem.* **2002**, *40*, 242
2. Mika, A.M.; Childs, R.F.; Dickson, J.M.; McCarry, B.E.; Gagnon, D.R. *J.Memb.Sci.* **1995**, *108*, *37*
3. Stachera, D.; Childs, R.F.; Mika, A.M.; Dickson, J.M. *J.Memb.Sci* **1998**, *148,119*
4. Mika, A.M.; Pandey, A.K.; Childs, R.F. *Desalination* **2001**, *140*, 265
5. Kim, M.Y.; Lee, E.; Childs, R.F. *manuscript in preparation*
6. Hosteller, R.E. & Swanson, J.W. *J. Polym. Sci., Polym. Chem. Ed.* **1974**, *12*, 29
7. Axelson, D.E. & Blake, S.L. *J. Polym. Sci., Polym. Chem. Ed.* **1985**, *23*, 2507
8. St. Pierre, T. & Geckle, M. *J. Macromolec. Sci.* **1985**, *A22*, 877
9. F.J. Green. The Sigma-Aldrich Handbook of Stains, Dyes and Indicators. Aldrich Chemical Co. Milwaukee, Wi (1990). P. 270
10. Caesar, P.D. *J. Am. Chem. Soc.* **1951**, *73*, 1097
11. The partial specific volume of branched PEI was determined by taking the inverse of the density as reported by Aldrich Chemical Co. The value is similar to that calculated by method of H. Durchschlag, H. & Zipper, P. *Prog. Colloid. Pol. Sci.* **1994**, *94*, 20
12. Childs, R.F. & Mika, A.M. *The Design of High Performance, Gel-filled Nanofiltration membranes*, In: Proceedings of the North American Membrane Society 2001 conference, *in press*

13. Rivas, B.L.; Maturana, H.A.; Perich, I.M.; Angne, U. *Polym. Bull.* **1985**, *14*, 239

14. Rivas, B.L.; Maturana, H.A.; Perich, I.M.; Angne, U. *Polym. Bull.* **1985**, *15*, 121

15. Rivas, B.L.; Canessa, G.S.; Pooley, S.A. *Makromol. Chem.* **1986**, *187*, 71

16. Rivas, B.L.; Maturana, H.A.; Bartulin, J.; Catalan, R.E.; Perich, I.M.; Angne, U. *Polym. Bull.* **1986**, *16*, 299

17. Kobayashi, S.; Shirasaka, H.; Suh, K.; Uyama, H. *Polymer J.* **1990**, *22*, 442

18. G Figuly, G.; Royce, S.; Khasat, N.; Schock, L.; Wu, S.; Davidson, F.; Campbell, G.; Gillies, P. *Macromolecules* **1997**, *30*, 6174

19. Kokufuta, E.; Suzuki, H.; Yoshida, R.;Yamada, R.; Hirata, M.; Kaneko, F. *Langmuir* **1998**, *14, 788*

20. Kokufuta, E.; Suzuki, H.; Yoshida, R.;Yamada, R.; Hirata, M.; Kaneko, F. *Colloids and Surfaces* **1999** *147,* 179

21. Schmitz, K.S. Macroions in Solution and Colloidal Suspension. VCH, New York, NY (1993)

22. Sedlak, M.; Amis, E.J. *J. Chem. Phys.* **1992**, *96*, 817

23. Sedlak, M.; Amis, E.J. *J. Chem. Phys.* **1992**, *96*, 826

24. Benoit, H.; Doty, P. *J. Phys. Chem.* **1953**, *57*, 958

25. Mika, A. M.; Childs, R.F. *J.Memb.Sci* **1998**, *152, 129*

26. Kobayashi, S.; Kazuhisa, H.; Masazumi, T.; Saegusa, T. *Macromolecules* **1987**, *20, 1496*

27. Kobayashi, S. *Prog.Polym.Sci.* **1990**, *15, 751*

28. Feil, H.; Bae, Y.H.; Feijen, J.; Kim, S.W. *J.Memb.Sci.* **1989**, *64, 283*

29. Bae, Y. H.; Okano, T.; Kim, S.W. *Pharmaceutical Res.* **1991**, *8*, *624*

30. Mika, A.M.; Childs, R.F.; Dickson, J.M.; McCarry, B.E.; Gagnon, D.R. *J. Memb. Sci.* **1997**, *135*, *81*

31. Lewis,E.A.; Barkley,J.; St.Pierre,T. *Macromolecules* **1981**, *14,* 546

32. Theiele, H. & Gronau, K.H. *Die Makromolekulare Chemie* **1963**, *59*, 207

33. Shepherd, E.J. & Kitchener, J.A. *J. Chem. Soc.* **1956**, 2448

34. Saber,T.M.H.; Shams El Din,A.M. *J. Electroanal. Chem.* **1969**, *20*, 311

35. Weyts, K.F; Goethals, E.J. *Makromol. Chem., Rapid Commun.* **1989**, *10*, 299

36. Bloys van Treslong, C.J. & Staverman, A.J. *Recl. Trav. Chim. Pays-Bas.* **1974**, *93*, 171

37. Smits, R.G.; Koper, G.J.; Mandel, M. *J. Phys. Chem.* **1993**, *97*, 5745

38. Nishio, T. *Biophys. Chem.* **1991**, *40*, 19

39. Katchalsky, A.; Mazur, J.; Spitnik, P. *J. Polym. Sci.* **1957**, *23*, 513

40. Morawetz, H.; Wang, Y. *Macromolecules*, **1987**, *20*, *194*

41. Mika, A.M.; Childs, R.F. *J. Memb. Sci.* **1999**, *152*, 129

42. Mika, A.M.; Childs, R.F.; Dickson, J.M. *J.Memb.Sci in press*

43. Mika, A.M.; Childs, R.F.; Dickson, J.M. *J.Memb.Sci* **1999**, *153, 45*

44. Mika, A.M.; Childs, R.F.; Dickson, J.M. *Desalination* **1999**, *121,149*

45. Kobayashi, S.; Shirasaka, H.; Suh, K.; Uyama, H. *Polymer J.* **1990**, *22, 442*

46. Boom, J.M.; Mulder, M.H.V; Strathmann, H.; Peeters, J. *J.Memb.Sci* **1998**, *145, 199*

47. Hoffer , E.; Kedem, O. *Desalination* **1967**, *2*, 25

48. Tsuru, T.; Nakao, S.; Kimura, S. *J.Chem.Eng.Jpn.* **1991**, *24*, 511

49. Manning, G.S. *Acc.Chem.Res.* **1979**, *12,* 443

50. Satoh, M.; Kawashima, T.; Komiyama, J; Iijima, T. *Polym.J.* **1987**, *19*, 1191

51. Steinman, L.; Porath, J.; Hashemi, P.; Olin, A. *Talanta* **1994**, *41*, 1707

CHAPTER FOUR

EFFECT OF CROSS-LINKER ON POLYETHYLENIMINE GEL PROPERTIES AND PORE FILLED MEMBRANES MADE FROM THEM

Abstract

The concept of the pore filled membrane was introduced in **Chapter 1** and discussed in depth in **Chapter 2**. Building on the established contextual framework, **Chapter 3** dealt with the unique properties and pressure driven performances of BPEI gel filled membranes. The BPEI-EDGE membranes had morphologies typical of gel-filled membranes and were very effective in the nanofiltration of ionic solutes.

In this chapter an understanding of the effects of cross-linker on BPEI gel chemistry is approached on several fronts. First, the effects of cross-linker on gel morphology and their effects on the swelling capabilities are analysed at different pH and salt concentrations. Second, the effect of cross-linker on membrane morphology and physical properties are analysed. Third, the microstructure of the gels/membranes are analysed by permeability and salt separation measurements.

4.0 Introduction

The physical property of the pore-filled hydrogel is one of the key parameters affecting the properties and performance capabilities of pore-filled membranes. Much work has been done on determining factors that control morphologies of polymeric materials, such as porous beads [1-7] and gels [8-14]. Recently, the influence of gel heterogeneity on membrane performance was reported in a doctoral thesis submitted by McCrory [15]. Gel heterogeneity could be induced to varying degrees by changing the solvency during the uv-photoinitiated polymerization of acrylic acid. The consequences of inducing heterogeneity were morphological changes in the microstructure of the gel that were manifested in increased permeability and decreased separations of ionic solutes.

It has been shown in **Chapter 3** that a formally neutral polymer could be incorporated into the pores of a microporous host, acquire a charge by an acid/base reaction with the solvent (water) and thereby reject ionic solutes by a Donnan exclusion mechanism. These membranes exhibited high rejections of sodium chloride over a large pH range (2-10) and had linear pressure-flux relationships between 100-300 kPa's with a slight deviation at higher pressures (500 kPa). The permeability through the BPEI-EDGE gels, in the membranes, obeyed Darcy's law (**Chapter 2, Section 2.3.3**) in that the fluid velocity was directly proportional to the applied pressure.

The BPEI-EDGE gels used to make the membranes were clear with no evidence of phase separation at any molar ratio of cross-linker. Since the physical properties of the gel determine the properties of the membrane, two main questions arise from the work in

Chapter 3. The first concerns the influence of cross-linker properties on the gel properties. Specifically, how do the size and hydrophobicity of a cross-linker affect the gel properties such as swelling capacity and morphology? Weiss *et al.* [8] argued that a cross-linked gel could be considered a two-phasic system with both phases gels, but of different average concentration and average degree of cross-linking. Much of the literature reports on gels have been studied from this perspective with attention focused on the degree, or extent, of cross-linking. Reports on the influence of the chemical nature of the cross-linker on gel properties have not been found. Second, how do the differences in gel properties relate to the properties and performance capabilities of the membranes made from those gels?

To this end, this chapter reports an investigation of how three different crosslinkers- ethyleneglycol diglycidyl ether (EDGE); polypropyleneglycol diglycidyl ether (PODGE); and bis-phenol-A-diglycidyl ether (BADGE)- chosen because of their differing size, hydrophobicity and rigidity affects the properties of the BPEI gel and ultimately the membranes filled with those gels.

Central to this discussion are methods of characterization. As described in **Chapter 2**, the hydrodynamic permeability model developed by Mika and Childs [16] could successfully predict the permeability of poly(4-vinylpyridine) based membranes. This model has subsequently been applied successfully to characterize poly(acrylic acid) filled membranes [15]. The model provides a means to calculate the intrinsic gel properties such as mesh size from the permeabilities allowing a detailed perspective of the microstructure of the gel. The model combined with microscopy techniques such as

electron, confocal fluorescence and scanning transmission x-ray microscopy (STXM) provides a good means to analyze gel/membrane morphologies and properties.

4.0.1 Characterization of Gel Filled Membranes: Scanning Transmission X-Ray Microscopy (STXM)

Scanning transmission x-ray microscopy is a very powerful technique for determining the chemical composition of a material while also providing spatial imaging of up to 50nm resolution. This technique has been reviewed extensively elsewhere [17-21] so the following section will be a brief introduction necessary for the understanding of the STXM data presented in this work.

As x-rays pass through an object, the intensity of the beam will be attenuated by the amount of photons adsorbed. The adsorbed photons cause excitations of the inner shell electrons of the atoms in the substance. These excited inner shell electrons can be promoted to unoccupied energy levels to form a short lived excited state or can be removed completely resulting in ionization of the atom. X-ray absorption spectroscopy has been traditionally described in absorption edges, which are the onset of inner-shell ionization. There is an absorption edge associated with each inner shell level of an atom, such that all elements have an X-ray absorption edge in the soft X-ray energy range (100-1200 eV).

Near Edge X-ray Absorption Fine Structure (NEXAFS) [22], which is the basis of STXM, can identify and quantitate the chemical structure of the element from the fine

scale details of the absorption spectrum that occurs at each edge. These features correspond to electronic excited states in which an inner-shell electron has been excited to unfilled molecular orbitals or conduction bands. The unoccupied electronic structure and thus the inner-shell excited states are determined by the geometric and electronic structure of the sample.

One key advantage provided by the NEXAFS technique is that the spectra of polymers differ significantly, even for polymers with similar molecular structures. The spectrum of each polymer can thus serve as a fingerprint and unknown species can be easily identified by the NEXAFS spectra. Comparison with NEXAFS spectra of pure standards provides a means to derive quantitative composition maps of the components of a complex material from a series of X-ray microscopy images. The amount of a particular element can be determined quantitatively from the differences in the x-ray absorption just above and just below its absorption edge.

4.0.2 Singular Value Decomposition (SVD) Methodology

As x-rays pass through an object, the extent to which the photons are absorbed is determined by the following equation:

$$I = I_o e^{-\alpha(E)t} \quad \textbf{(4.1)}$$

where I_o is the initial beam intensity, I is the intensity of the absorbed attenuated beam, t is the thickness of the material and $\alpha(E)$ is the linear attenuation coefficient at energy E.

The linear attenuation coefficient is dependent upon the material's mass absorption coefficient $\mu(E)$ and density ρ.

$$\alpha(E) = \mu(E)\rho \quad \textbf{(4.2)}$$

For quantitative image analysis, the transmitted signal is converted to an optical density (*OD*) according to:

$$OD(E) = \ln (I_o/I) \quad \textbf{(4.3)}$$

and is linearly related to the sample properties by

$$OD(E) = \mu(E) \cdot \rho \cdot t \quad \textbf{(4.4)}$$

The *OD* of a multi-component sample containing i non-interacting components is given by

$$OD(E) = \mu(E)_1 \cdot \rho_1 \cdot t_1 + \mu(E)_2 \rho_2 \cdot t_2 + \ldots + \mu(E)_i \cdot \rho_i \cdot t_i \quad \textbf{(4.5)}$$

In this case, the variable t_i refers to the thickness of the component i with mass absorption coefficient μ_i and density ρ_i. The total optical density is thus a summation of the optical densities of the all of the components the x-ray beam passes through. By measuring the *OD* for different energies E and determining the energy dependent mass absorption coefficients μ from a reference spectra of the pure compound, component maps $\rho \cdot t(x,y)$ can be derived by solving **equation 4.5** for every pixel (x,y) of the image set. After correcting for density, the vertical scale of the derived component maps (thickness t) of each component required to reproduce the total *OD* at each pixel in the region sampled can be determined.

The X-ray photoabsorption response of a multi-component sample is a superposition of the response of each compound present in the column- weighted by its mass absorption coefficient at the photon energy employed. Spatially resolved X-ray absorption signals can be used for quantitation because of the linear relationship between optical density and concentration.

The mass absorption coefficients are derived from measurements of the pure components; for example, reference spectra in this work was recorded from regions of the sample known to be pure in one of the components. In practice, however, spectra are obtained by first recording an energy scan I from the spot of interest and subsequently the incident flux I_o measured with the same detector and optical path but with the sample out of the beam. The spectra are converted to OD by using **equation 4.3** and conversion to a mass absorption scale is accomplished by matching the signal in the pre-edge and post-edge regions to the sum of the tabulated atomic mass absorption coefficients [23] for the elemental composition of the pure component (ex: C_3H_6 for polypropylene and C_2H_5N for polyethylenimine).

Component maps are derived from the application of SVD analysis to a sequence of X-ray images- each of which is a plot of the density-thickness product (density-weighted relative path) for a given component. These maps provide component distributions in the thin section once corrections are made for density.

4.1 EXPERIMENTAL

4.1.2 Materials

Branched polyethylenimine (BPEI) with a weight average molecular weight (M_w) of ca. 25,000, polypropyleneglycol diglycidyl ether (PODGE) with a number average molecular weight (M_n) of ca. 640, bis-phenol-A-diglycidyl ether and Direct Red 23 dye (λ_{exc} = 507 nm and λ_{emm}=610 nm) [24] were obtained from Aldrich Chemical Co. Ethyleneglycol diglycidyl ether (EDGE) was obtained from Polysciences Inc. Methanol was obtained from Caledon Labs. Ltd. Unless otherwise stated, all water used was carbon filtered and deionized. All reagents were used without further purification.

The microporous host substrate, fabricated by a thermally induced phase separation process used for the preparation of pore coated anion-exchange membranes was a polypropylene microporous membrane supplied by 3M Canada Company, details of which are given in **Table 3.1, Chapter 3**. The base membrane was extracted with acetone at room temperature for a minimum of one day prior to use.

4.1.3 Membrane Preparation

Separate solutions, of equal volume and known concentrations (10% and 20% w/v) BPEI in DMF and diglycidyl cross-linkers in 1-propanol were prepared. The solutions were rapidly mixed and spread across the polypropylene host membrane (12 x

12 cm) kept on a polyethylene terephthalate (PET) sheet on top of a glass plate. The filled membrane was immediately covered with another PET sheet and the polymer/cross-linker solution was distributed evenly throughout the entire porous polypropylene host membrane by rubbing the top PET sheet with a rubber roller. The sandwiched, filled, membrane was left undisturbed at room temperature, overnight (16 h) for gelling to occur. After removal of the membrane from the PET sheet, the membrane was washed with deionized water and then with methanol to remove soluble, unincorporated components.

The membranes were characterized by mass gain, polymer volume fraction, thickness, ion exchange capacity, water content and permeability as described in **Chapter 3**.

4.1.4 Gel Swelling Studies

Separate solutions, of equal volume and known concentrations (10% and 20% w/v) BPEI and cross-linkers (10% & 20% molar cross-links based on concentration of BPEI repeat unit) were prepared. The polymer/cross-linker solutions were rapidly mixed and poured into a plastic disposable 5mL syringe with a diameter of 1.3 cm. The solutions were allowed to stand at room temperature, for 48 hours for gellation to occur. The gels were removed from the syringe by cutting the syringe at the base with a hacksaw and pushing out the gel with the plunger. The gel cylinders were sectioned to approximately 1 cm thickness. The gels were then placed into separate vials containing

solutions of different pHs (2, 5.5 and 12) adjusted by addition of HCl or NaOH and salt concentration (5mM NaCl) and allowed to stand for one week at room temperature. Each swelling experiment was performed in duplicate with two gel slices in two different vials of the same solution. The water-swollen gels were then removed from the vials, patted dry to remove excess surface water and weighed. The swollen gels were weighed after being dried under a vacuum at 65 °C, for 3 days. The gels were dried for further periods of time until a variation of less than 5% in their dried mass was obtained (less than three dryings were required). The degree of swelling is expressed as

$$\text{Degree of Swelling} = (M_w - M_d)/M_d \times 100\% \quad \textbf{(4.6)}$$

where M_w is the mass of the wet, swollen gel and M_d is the mass of the dry gel.

4.1.5 Microscopy Studies

For confocal microscopy analyses, the membrane samples were soaked in an aqueous solution of Direct Red 23 dye (10^{-5} M) overnight (~16 h) at room temperature. The wet membrane samples were viewed in a Carl Zeiss laser fluorescence confocal microscope (LSM 510) (Carl Zeiss Corp., Germany) using the 63x magnification water immersion objective lens. The laser wavelengths used to excite the fluorophores in the membrane sample were 488 nm and 543 nm with argon and helium-neon lasers respectively.

The surface and internal morphology (to a depth of 7nm) of the coated, fluorescently labeled membrane, was imaged by exciting the Direct Red 23 fluorophore,

electrostatically bound to the protonated PEI (at 543 nm) at pH 5.5. The base membrane was imaged by exciting an intrinsic fluorophore (at 488 nm).

Environmental scanning electron micrographs (ESEM) were taken in an Electroscan model 2020 Environmental Scanning Electron Microscope (Electroscan Corporation). Wet membrane samples were cut and glued to an aluminum stub using an epoxy adhesive. Images were obtained at pressures of 2.9 Torr to 4.0 Torr in a water-saturated atmosphere (99%) at 20 kV.

4.1.6 STXM Analysis

A cross-section of the wet gel was frozen at -120°C and cryo-microtomed, to approximately 150 nm thickness. While frozen, the section was laid flat on a (750μm x 750μm) Si_3N_4 window and a second Si_3N_4 window was placed on top. The sample was warmed to room temperature to create the wet sample, which was analyzed at room temperature.

The C 1s images were recorded with beam line 7.0 STXM at the Advanced Light Source (ALS) [25]. The transmitted x-ray photon flux is measured on single photon counting basis using a scintillation converter and a high-performance photomultiplier tube (Hamamatsu 647P). To avoid any absorption by the air, the microscope chamber is completely filled with helium at atmosphere pressure after the sample is installed. Typical count rates are about 2×10^7 photons/s transmitted through the helium at 300 eV,

with the ALS storage ring running at 1.9 eV, 400 mA. Counting periods (dwell times) of 0.2 ms per pixel are typical used for analytical imaging. Currently the best spatial resolution of the microscope is about 100 nm, mainly due to mechanical vibration, rather than the zone plate, which has a diffraction-limited resolution of about 50 nm. The entrance and exit slits of the monochromator were set to obtain an energy resolution of about 100 meV in the carbon 1s region ($E/\Delta E$ ~3000).

Images were recorded at selected energies through the carbon edge region. Images at a photon energy particularly sensitive to radiation damage were recorded after each image sequence to monitor damage. Post-acquisition image alignment [26] was used to correct for drift of the field of view associated with lateral run-out of the zone plate as it is moved along the optical axis to maintain focus.

The reference mass absorption coefficient signal for the polyethyleneimine gel was derived from regions of a separately recorded image sequence as well as from the set of images recorded for this SVD analysis. The reference mass absorption coefficient signal for polypropylene was obtained from a spectrum of pure polypropylene recorded at the ALS STXM. The incident flux signal used to convert the measured transmission intensity to optical density was recorded through the wet cell structure adjacent to the membrane. Therefore explicitly accounting for water was not required or the Si_3N_4 window absorption in the quantitative analysis.

4.1.7 Permeability Testing of BPEI Gel Filled Membrane

Hydrodynamic permeability and salt separation measurements of the BPEI gel filled membranes were obtained by methods previously discussed in **Chapter 3, Section 3.1.6.**

4.2 Discussion

Three types of cross-linkers were examined for their effect on the properties of BPEI gels, measured through performance under pressure driven conditions, microscopy and swelling experiments. The three cross-linkers, ethyleneglycol diglycidyl ether (EDGE), polypropyleneglycol diglycidyl ether (PODGE) and bis-phenol-A-diglycidyl ether (BADGE), were used to study the effects of cross-linker properties such as size, rigidity and hydrophobicity on the PEI gel properties (**Figure 4.1**).

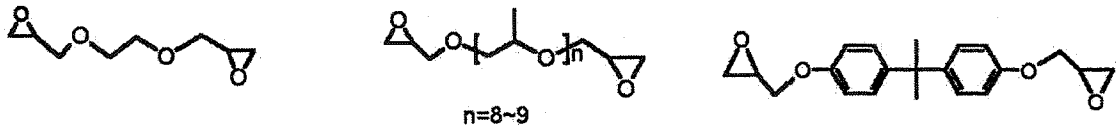

Ethylene glycol diglycidyl ether (EDGE) | Polypropylene glycol diglycidyl ether (PODGE) | Bis-phenol A digylcidyl ether (BADGE)

Figure 4.1 Structures of cross-linkers used for formation of BPEI gels

4.2.1 BPEI Gels: Physical Morphology

Work by Janda *et al.* has shown the influence of cross-linker size on polymer network properties; larger cross-linkers create softer and more pliable cross-linked networks than small cross-linkers [27]. PODGE, a polypropyleneglycol oligomer, used in this work, has approximately 9 repeat units with an end to end distance of 92.4 Å- calculated from the law of cosines, bond angles and bond distances- for a fully extended chain. This is larger than EDGE, which has a calculated end-to-end distance of 22.9 Å using the same method. In addition to the larger size, PODGE allows for greater flexibility and mobility because of the reduced barrier of rotation around the greater number of carbon-oxygen bonds. Based upon this data, it was believed the PODGE cross-linked system would result in a looser gel coating than the EDGE cross-linked system.

To contrast the effects a flexible and hydrophilic cross-linker may have on gel properties, bisphenol-A-diglycidyl ether (BADGE), was also investigated as a cross-linker to investigate its effects on BPEI gel/membrane properties. Unlike PODGE and EDGE, the BADGE cross-linker is highly hydrophobic and structurally rigid.

A photograph of PODGE, EDGE and BADGE cross-linked BPEI gels of varying cross-link ratios is shown in **Figure 4.2**. As can be seen, the BPEI-EDGE gels are clear at both the low and high cross-linking ratios; however, there is a noticeable coloration in

the BPEI-PODGE gels with an increased color intensity reflected in the concentration of the PODGE cross-linker. No solvent syneresis was observed in either system. The source of the coloration in the PODGE gels is unknown. Both BPEI and PODGE are clear liquids.

The BPEI-BADGE gels show a completely different morphology. At 10% cross-linking, the BPEI-BADGE gels show a slight opalescence with complete opacity observed at 20% cross-linking; furthermore, both BADGE cross-linked gels exhibited dimensional contraction and solvent syneresis as shown in **Figure 4.3**. Storage of the BPEI-BADGE gels in deionized water for several months showed no change in their translucence/opacity.

No indications of light scattering or syneresis were observed with increased cross-linking in the EDGE and PODGE systems suggesting that these gels are homogeneous.

Figure 4.2 Photograph of 10% and 20% EDGE, PODGE and BADGE cross-linked BPEI gels. Distortions in the 20% EDGE and PODGE gels were caused by removal of samples for microscopic analyses and were not defects in gel structure. All gels made with same polymer concentration

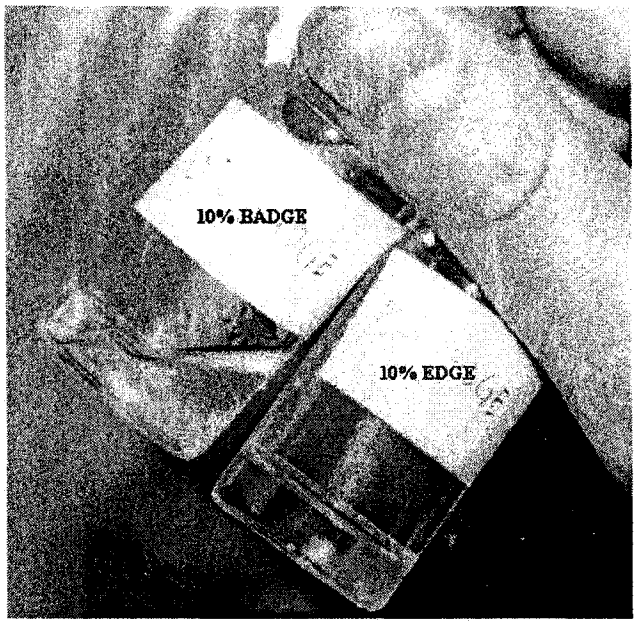

Figure 4.3 Dimensional contraction and solvent syneresis of BPEI-BADGE gel contrasted against a homogeneous BPEI-EDGE gel. Thumb courtesy of J. Zhou

Light scattering due to inhomogeneities in gel microstructure is well known [27-31] and has been previously reported in our group in the formation of cross-linked polyacrylic acid gels, by free radical copolymerization of acrylic acid with *N,N*-methylenebisacrylamide, in different solvents [15]. The present work shows that heterogeneity can also be induced into gels formed from pre-formed polymers by varying the cross-linker.

Phase separation is the main reason for the formation of inhomogeneities in the polymeric gel network [8,28,30]. If a gel is considered as a semi-dilute polymer solution, the introduction of cross-linking creates areas of localized high polymer chain concentration [8]. This point was further clarified by Evmenenko *et al.* [32] who stated

that changes in polymer spatial distribution induced by cross-linking lead to the increase of local polymer concentration in the vicinity of the network junctions which exceeds the mean polymer concentration in the gel; thus, the cross-linked junctions appear as static, frozen regions in a network which have a liquid nature. These static junction points, when clumped together and unevenly distributed through a gel, lead to micro-domains that can scatter light. The increased light scattering observed with increased cross-linking in the BADGE gels implies that the micro-domains responsible for light scattering are larger.

4.2.2 STXM Analysis of BPEI Gels

The spectroscopic basis for distinguishing the polymer components is presented in **Figure 4.4**, where the linear absorption of C 1s and N 1s NEXAFS spectra is given at various photon energies. Each spectra consists of two curves- which represents the absorption curve of the BPEI gels plotted against a reference curve of pure BPEI- and a calculated elemental absorption curve [22] which were used to convert both spectra to mass absorption units. The BPEI spectrum is dominated by strong transitions at 289 eV, which is attributed to C 1s $\rightarrow \sigma^*_{C\text{-}H}$ transitions. The broad peak at 293 eV is associated with $\sigma^*_{C\text{-}C}$ resonances. The broad peak at 406.5 eV is associated with the N 1s $\rightarrow \sigma^*_{N\text{-}H}$ transitions.

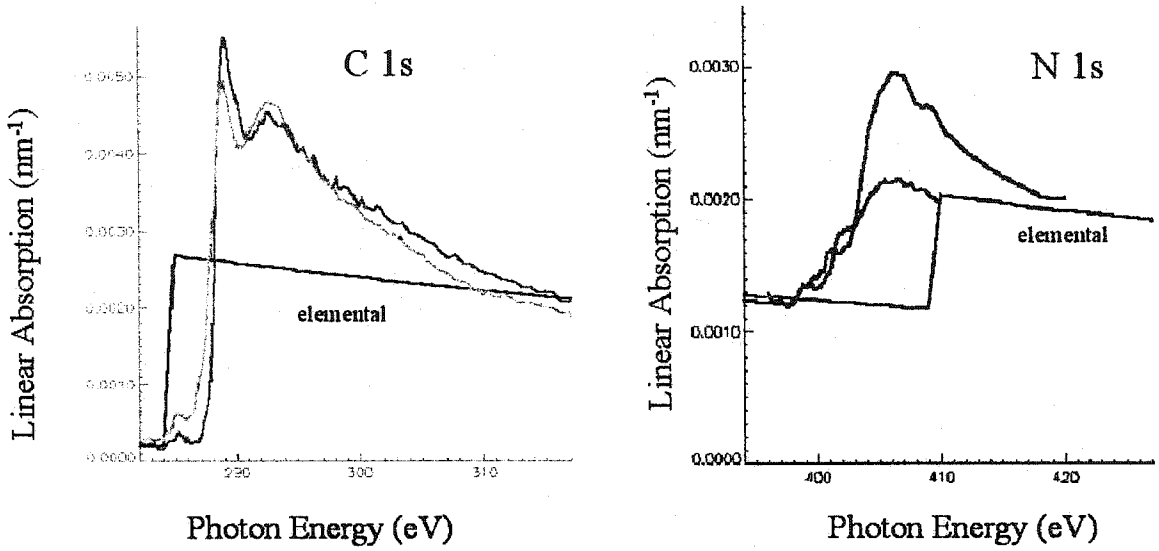

Figure 4.4 Linear absorption curves for the C 1s and N 1s NEXAFS spectra of PEI. Green curve is the elemental absorption curve

Microtomed sections of the hydrated gel samples, sandwiched between two Si_3N_4 windows, were analyzed by STXM at 289 and 420 eVs. The linear absorption at various photon energies was measured over a 20 μm x 20 μm region of the gel by a linescan method. The optical density of the sample was calculated from the measured mass absorption and density of the sample. The C1s and N1s absorption spectra are given in **Figure 4.5**.

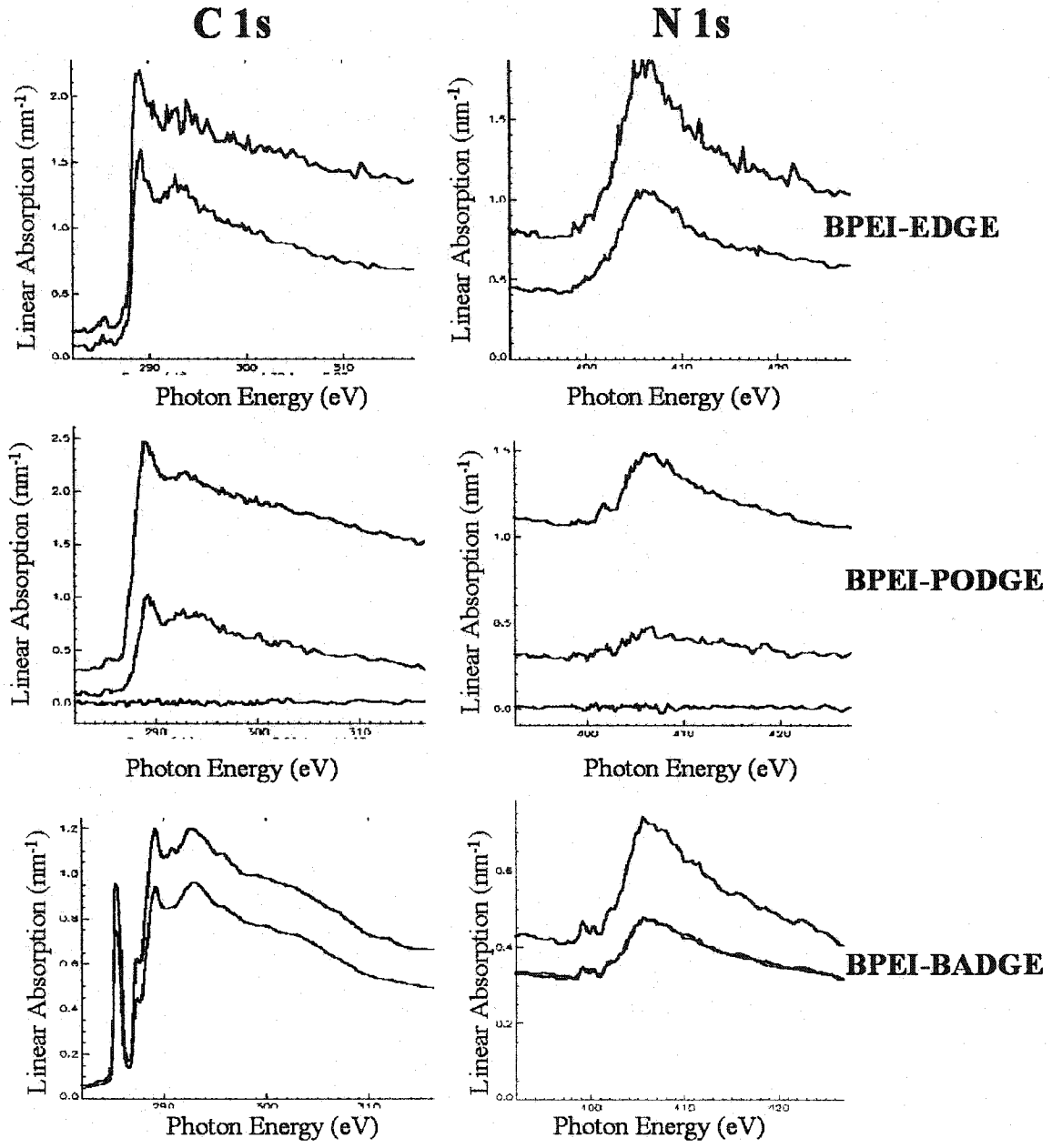

Figure 4.5 Linear absorption spectra at various photon energies for the C1s and N1s excitations for BPEI gels with three different cross-linkers

The blue and green curves in each spectrum refer to two regions of the gels scanned with differing levels of absorption. The most significant finding is in the BPEI-PODGE spectrum. The pink curve is representative of what would be expected for a hole; that is, no absorption. The green curve has reduced signal intensity in both the C1s and N1s spectrum indicating the possibility of a microhole, or microheterogeneity. Component maps derived from the SVD analysis of the absorption spectra given in **Figure 4.5** is shown in **Figure 4.6**.

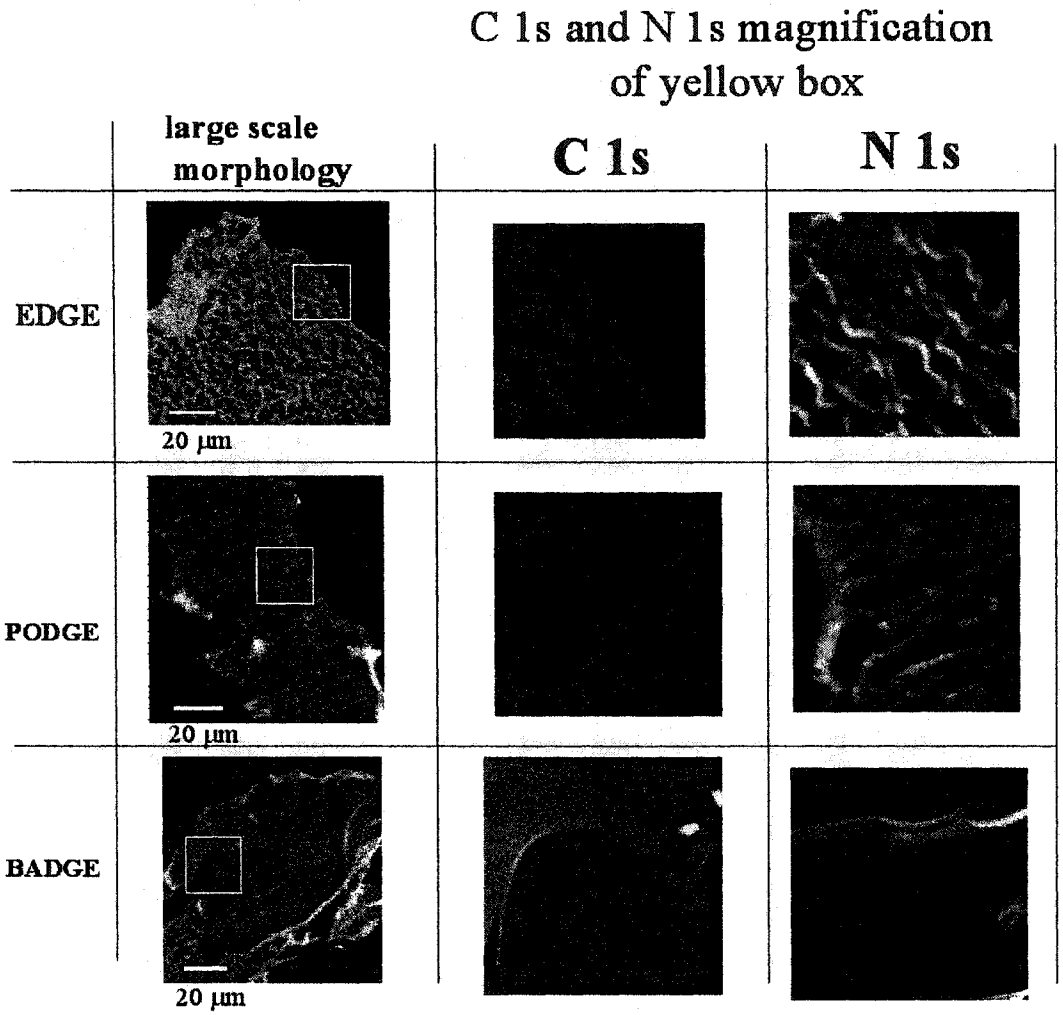

Figure 4.6 STXM chemical maps of EDGE, PODGE and BADGE cross-linked BPEI gels. Red signal corresponds to PEI and green signal corresponds to cross-linker. Brown signal is a composite of both colors

The STXM images in **Figure 4.6** shows a fairly uniform distribution of polymer and cross-linker for the EDGE and BADGE cross-linked systems. Of the gels made from the three cross-linkers, only BPEI-PODGE gels showed visible micropores or signs of micro-heterogeneity from the STXM analysis. Although the holes could be due to

microtoming artifacts, the C1s component map shows highly localized concentrations of cross-linkers around the holes. The inability to find similar evidences of micro-heterogeneity in the BADGE cross-linked system is surprising since macro-heterogeneity (defined as opaque gels with syneresis) was observed in the bulk gels. Although STXM should be able to detect changes in phase [20], the findings of this work confirms the difficulties previously encountered in detection of heterogeneity in poly(acrylic acid) based membranes [15]. This difficulty could be due to heterogeneous domains being smaller than the resolving power of the techniques employed. A suggestion for future work is to use a technique such as small angle neutron scattering, with a resolution limit of 1 nm, to resolve structures that cannot be seen through STXM or electron microscopy [33].

4.2.3 Cross-linked BPEI Gel Swelling Properties

One of the most remarkable properties of polyelectrolyte gels is their ability to absorb several hundred to several thousand times their weight of water, while retaining structural integrity and elasticity. Many reports exist describing the high degrees of swelling of polyelectrolyte gels, which have been monitored by changing the salt concentration and pH. This swelling property is at the origin of the applications of these gels as superabsorbents [34-37]. The swelling behavior of charged gels has been described by Katchalsky *et al.* [38] and Flory and Rehner [39] as resulting from a balance between the elastic energy of the network and the osmotic pressure of the ions. In salt-

free charged gels this osmotic pressure is due to the counter-ions that are confined inside the gel.

Heterogeneity can have a substantial influence on the gel's swelling abilities. Basil and Gupta [40] suggested that heterogeneity within the gel microstructure would result in an uneven distribution of elastic forces over all the subchains when the gel swells. As discussed previously, heterogeneity from cross-linking is manifested as the presence of pockets of high and low polymer concentration interspersed throughout the gel. The elastic forces, therefore, have a complicated profile connected with the local cross-link density because of the induced inhomogeneity of the cross-linking process during the synthesis of the gel [41]. These effects alter the overall elastic modulus and affect swelling properties.

It is interesting to note that the EDGE cross-linker yields a clear, isotropic gel at all molar cross-linking ratios. The swelling data presented in **Table 4.1** suggests that an increase in EDGE concentration results in greater interchain cross-linking. It was argued in **Chapter 3, section 3.2.5**, that intrachain and interchain cross-linking of BPEI by EDGE are equally probable because of its small size with the net consequence being a lower effective cross-linking of the gel than the cross-linking suggested by the molar ratio of EDGE to the polymeric repeat units. The extent to which a molar increase in EDGE actually contributes to an increase in interchain cross-linking and whether that increase is linear with concentration is not known.

Table 4.1 Swelling data of BPEI gels as a function of polymer concentration and molar cross-linker ratio measured at differing pH's and salt concentration. C and D represent Concentrated (20% w/v) and Dilute (10% w/v) of the polymer solutions respectively.

		No Salt			5mM NaCl		
Entry	Gel composition	pH 2	pH 5.5	pH 12	pH 2	pH 5.5	pH 12
1	10% EDGE D	Unable to form Gel					
2	10% EDGE C	4269	2314	1762	1489	921	905
3	20% EDGE D	Unable to form Gel					
4	20% EDGE C	1098	718	601	786	566	576
5	10% PODGE D	3410	2376	630	1195	945	567
6	10% PODGE C	605	379	279	501	314	263
7	20% PODGE D	1899	1391	291	513	307	311
8	20% PODGE C	189	147	100	178	145	115
9	10% BADGE D	3461	1336	286	430	169	153
10	10% BADGE C	360	206	179	147	117	110
11	20% BADGE D	349	274	261	174	130	120
12	20% BADGE C	106	94	80	109	89	91

Low concentration BPEI solutions (10% concentration) with EDGE did not form gels (entries 1&3) but instead resulted in an increase in solution viscosity. This is suggestive of the wasted cross-linking reaction previously discussed previously. BPEI-EDGE gels made with the concentrated (20%) polymer solutions resulted in clear gels that absorbed many thousand times their dry weight in water. The differences in the degree of swelling (measured by the mass increase from water absorption) between the pH extremes of 2 to 12, under salt-free conditions were relatively small (2.4x and 1.8x for the 10% and 20% cross-linked gels respectively). The higher EDGE cross-linking, in entry 4, shows its effect in the reduced swelling at all pH's. The presence of 5mM NaCl reduces the swelling capacity of these gels relative to the gels in salt-free conditions as a

result of the shielding effect of NaCl on the charge. The effect of salt on mitigating the swelling of BPEI gels has been previously reported by Kobayashi *et al* [43].

The 10% cross-linked BPEI gels for both the PODGE and BADGE systems made with dilute polymer concentration exhibited very large swelling abilities; however, substantial decreases in swelling were observed with increased cross-linker and increased polymer concentrations. Decrease in gel swelling, with increased polymer concentration, has been previously reported by several authors [32,43,44]. Once more decreases in swelling were observed for these gels in 5mM NaCl.

Several important points emerge when comparing the effects the different cross-linkers have on the swelling properties of their respective gels. The EDGE cross-linked gels, made with high polymer concentration at both degrees of cross-linking, have significantly greater swelling capabilities than the PODGE and BADGE gels of similar composition. The physical properties of EDGE are unlikely to affect the properties of the BPEI-EDGE gels appreciably since the EDGE cross-linker is a small molecule that dissolves readily in water. The PODGE and BADGE cross-linkers, however, are much larger with varying degrees of hydrophobicity (PODGE is slightly soluble in water, BADGE is completely insoluble).

Analysis of the PODGE and BADGE gel swelling data shows some interesting trends. PODGE and BADGE gels made at dilute polymer concentration and 10% cross-linking show a similar swelling percentage in salt free acid; however, the relative swelling percentages differ substantially at neutral and basic conditions in the presence or absence of salt and the magnitude of swelling is related to the hydrophobicity . This

suggests that the swelling properties of the gel are largely determined by the protonated BPEI; however, as the charge is reduced, the influence of the cross-linker has a more noticeable effect. This trend is especially evident in entries 6-8 and 10-12, where the concentration (or mass fraction relative to BPEI) of the cross-linker is higher than in entries 5 and 9. The lower swelling capacity of the BADGE gels, relative to the PODGE and EDGE gels reflect the hydrophobic nature of the cross-linker.

4.2.4 BPEI Gel Filled Membranes: Physical Properties

A series of membranes were prepared from the gels previously discussed to determine the effects of cross-linkers on membrane properties and performance. The properties of the membranes are given in **Table 4.2**.

Table 4.2 Properties of BPEI gel filled membranes

Membrane[a]	Polymer volume fraction	Degree of Cross-linking (%)	Water uptake[b] (%)	Thickness at pH 5.5, no salt[c] (μm)	Ion exchange capacity[d] (meq/g)	Theoretical IEC (meq/g)
BP1	0.0738	10	81	76	1.59	1.98
BP2	0.0768	10	81	79	1.4	2.55
BP3	0.147	10	78	75	1.78	3.07
BP4	0.204	10	75	72	2.14	3.48
BP5	0.097	20	79	75	1.35	1.78
BP6	0.134	20	79	79	1.58	2.2
BP7	0.214	20	76	76	1.62	2.5
BB1*	0.206	10	70	116	3.2	8.7
BB2*	0.411	10	52	109	3.5	16.4
BB3*	0.268	20	64	111	3.13	9.9
BE1	0.0755	10	85	104	2.86	5.73
BE2*	0.0917	10	82	132	3.76	6.02
BE3	0.134	10	82	108	3.81	7.89
BE4*	0.116	10	80	134	3.79	6.55
BE5	0.126	10	78	108	3.41	6.82
BE6*	0.132	10	80	143	4.06	7.66
BE7*	0.174	10	75	152	4.28	8.52
BE8	0.093	15	83	97	2.54	5.36
BE9	0.169	15	78	103	3.75	7.6
BE10	0.115	20	81	101	2.75	5.38
BE11	0.184	20	75	102	3.8	7.0

*Membranes fabricated from PP5 host substrate. All others fabricated from PP3
[a]BP ~ PEI-PODGE; BE ~ PEI-EDGE; BB ~ PEI-BADGE
[b]Each water uptake measurements performed 5 times to a precision of +/- 2%
[c]Average thickness of nascent PP3 ~ 75 μm; average thickness of nascent PP5 ~ 119 μm. All thickness values measured to within < +/- 5%
[d]Titrations performed twice with a reproducibility of < 5%

Both the BPEI-EDGE and BPEI-PODGE filled membranes wetted immediately with water. The BPEI-BADGE membranes also wetted with water, however, were less hydrophilic as evident in the initial formation of beads of water at the surface.

The properties of the BPEI gel filled membranes within each set (cross-linkers) are consistent with each other in terms of water uptake, thickness and ion exchange measurements; however, noticeable differences are seen when comparisons are made among sets.

The water uptake values for the PODGE and EDGE series of membranes are high (75-85%) again reflecting the highly porous nature of these membranes. Dramatic reductions in water uptake (swelling) are seen for the high polymer volume fraction BADGE membranes BB2 & BB3. The low water uptake reflects the high polymer volume fraction of these membranes and the hydrophobicity of the BADGE cross-linker [46].

Large differences in thickness can be seen among the PODGE, BADGE and EDGE sets. The thickness values of the water swollen, BPEI-PODGE membranes are almost unchanged from the nascent membrane thickness. The thicknesses of the BPEI-EDGE membranes, however, are up to 35% greater than the thickness of the nascent membrane. The most startling observation is seen in the thickness values of the water swollen BPEI-BADGE filled membranes. A contraction in membrane thickness is observed upon incorporation of the BADGE cross-linked gel, even at the very high polymer volume fractions.

The thickness values are consistent with the gel swelling data presented earlier in **Table 4.1**. The EDGE gels were observed to swell the largest amount at pH 5.5 and as such, the EDGE membranes have the largest thicknesses. It should be noted that the large swelling observed in the bulk gels is mitigated when confined in the pores of the

membrane; again, showing the stabilizing effect of the host on gel properties. The thickness of the PODGE based membranes did not change much from the thickness of the nascent membranes and will be discussed in greater detail in the following section. Gel syneresis and dimensional contractions were observed with the BPEI-BADGE gels and it is therefore not surprising to observe contraction in the thickness of the BPEI-BADGE membranes. No changes in the *x* and *y* dimensions, for any of the membranes, were observed.

The ion exchange capacities of the PODGE cross-linked membranes range between 50-80% of the theoretical values, indicating that not all the nitrogens can be titrated. The IEC's of the EDGE cross-linked membranes are only 50-60% of the theoretical values as reported previously in **Chapter 3**. The largest attenuation of IEC, however, is observed in the BADGE cross-linked membranes where only 21-37% of the theoretical IEC could be measured. This clearly indicates that a substantial amount of nitrogens are not accessible, which is consistent with the macroscopic gel heterogeneity, solvent syneresis and dimensional contractions observed in both the bulk gels and the BPEI-BADGE filled membranes.

4.2.5 BPEI Gel Filled Membranes: Morphology

BPEI-PODGE pore filled nanofiltration membranes, described in **Table 4.2**, were made according to methods described in **chapter 3** as a basis of comparison to the BPEI-EDGE membranes. Analysis of the confocal fluorescence microscopy images of

membrane BP5 in **Figure 4.7** clearly shows the presence of a coated layer on both sides of the membrane.

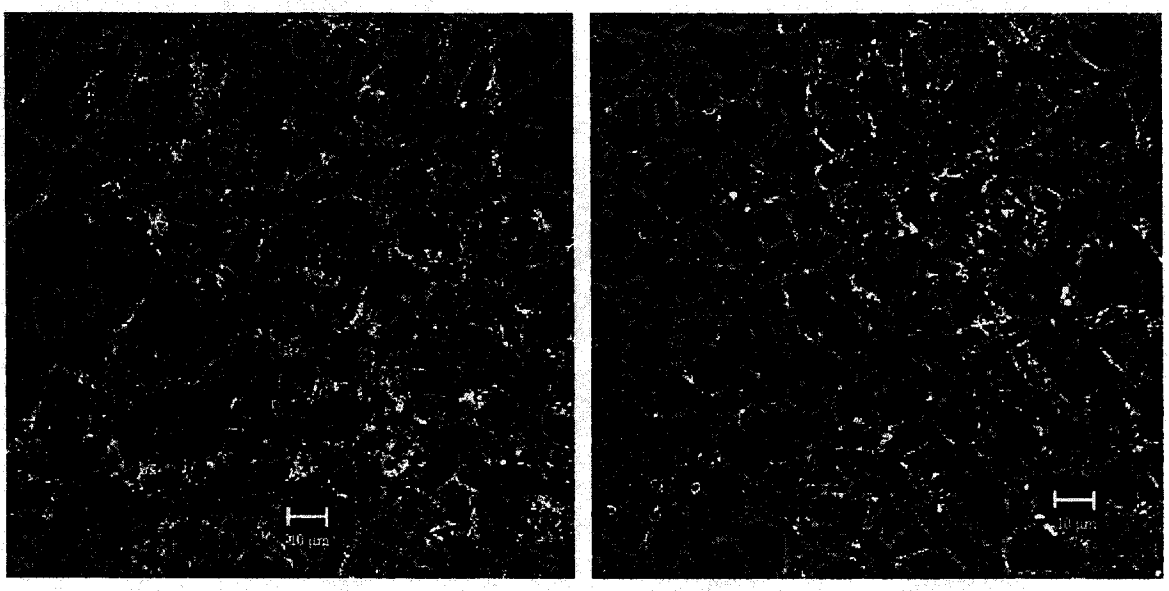

Figure 4.7 Top and Bottom laser confocal fluorescence micrograph of BPEI-PODGE filled membrane BP5 (distance bars- 10 μm)

One possible explanation for the results of **Figure 4.7** was that solvent evaporation occurred during the BPEI-PODGE membrane fabrication. Both Mika and Ge observed similar results during work on asymmetric membranes [47]. Mika and Ge attempted to fabricate membranes with an asymmetric distribution of gel by allowing evaporation of the solvent to occur during the cross-linking of a polymer solution inside the pores of an asymmetric host substrate. It was assumed that evaporation of the solvent would result in a concentration of the polymer/cross-linker solution in the smaller pore

sized areas of the starting asymmetric host, due to capillary forces, resulting in an asymmetric distribution of the gel through the thickness of the membrane.

The morphology shown in **Figure 4.7** is consistent with what would be observed if solvent evaporation did indeed occur during the gellation process. The host substrate (PP3) has an asymmetric distribution of pore sizes through its thickness. The pores through the thickness of the membrane resemble an hourglass shape- smallest in the center and largest on the outer surfaces, as depicted in **Figure 4.8** [48]. Solvent evaporation from one side would cause capillary forces to act upon the polymer/cross-linker solution wicking it into the central depths of the membrane where a thin gel would form with large voids on the outer surfaces.

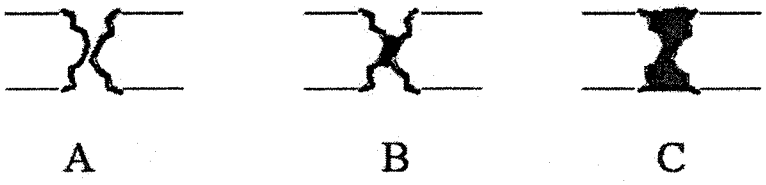

Figure 4.8 Cross-sectional representation of different membrane morphologies that can arise from different gel chemistries and fabrication procedures. (A) is a completely coated pore; (B) is a coated/filled pore observed in the BPEI-PODGE system; (C) is a completely filled pore observed in the BPEI-EDGE system

Although solvent evaporation could explain the results of **Figure 4.7**, evaporation was considered an unlikely explanation because care was taken to ensure evaporation did not occur during any stage of the fabrication procedure; furthermore, similar morphologies were not observed in BPEI-EDGE and BPEI-BADGE membranes made by

the same fabrication protocol as is evident, for example, in **Figure 4.9**, a laser fluorescence confocal micrograph of a BPEI-EDGE filled membrane; **Figure 4.10**, a laser fluorescence confocal micrograph of a BPEI-BADGE filled membrane; and **Figure 4.11a**, an environmental scanning electron micrograph of a BPEI-EDGE membrane. All the images exhibit the continuous blob morphology expected of a pore-filled membrane.

Figure 4.9 Laser fluorescence confocal micrograph of BPEI-EDGE filled membrane

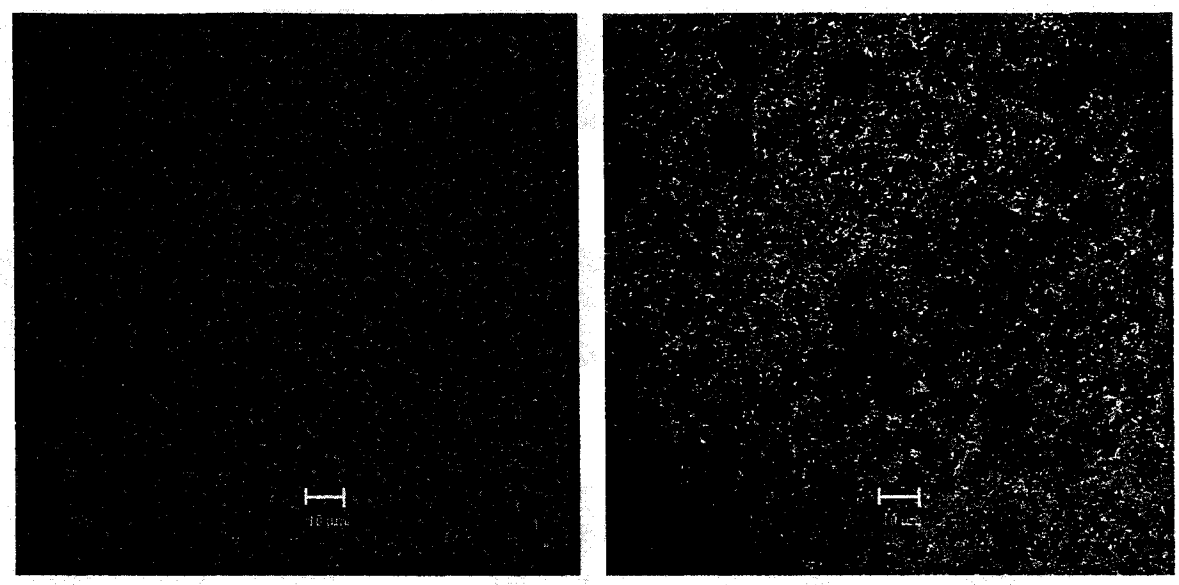

Figure 4.10 Laser fluorescence confocal micrograph of a nascent PP-5 and BPEI-BADGE filled membranes BB1

(a)

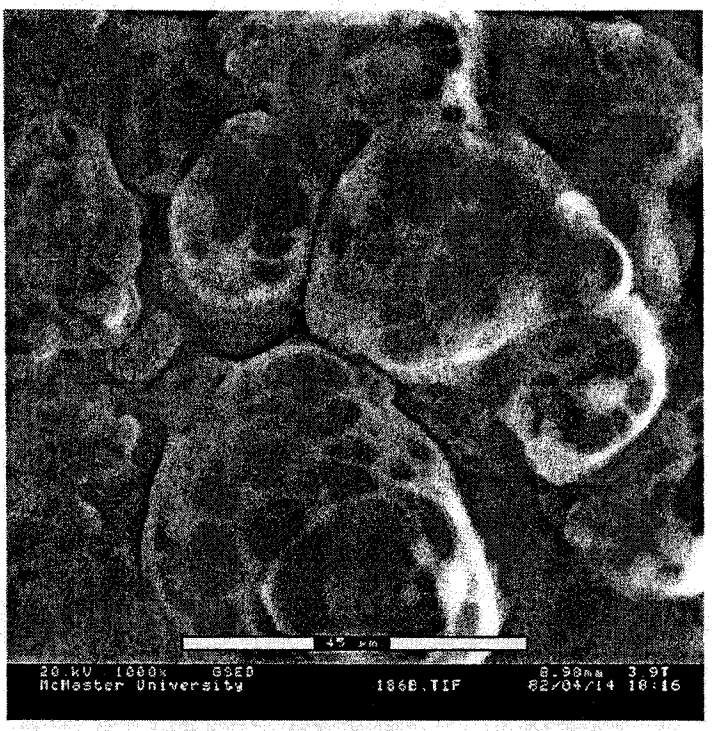

(b)

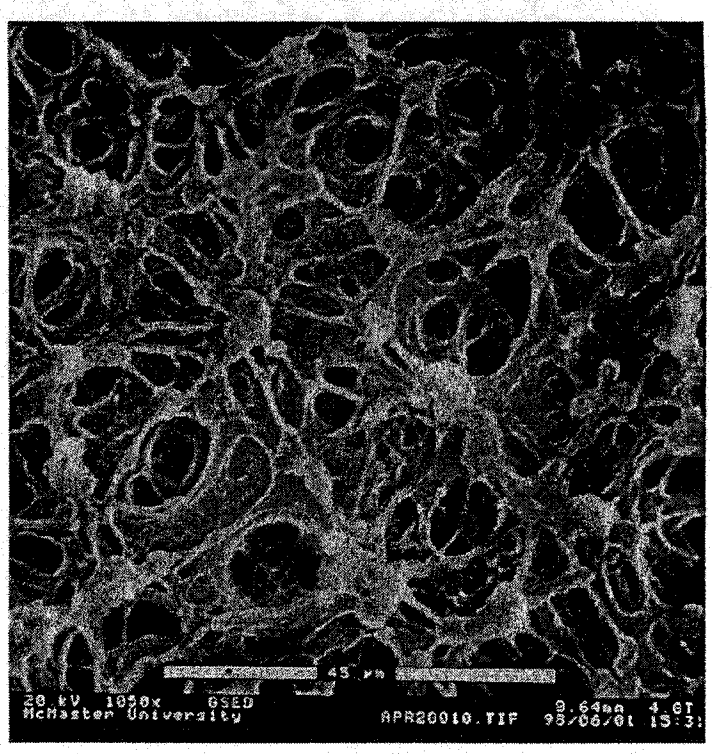

Figure 4.11 Environmental scanning electron micrographs of BPEI-EDGE (a) and BPEI-PODGE (b) filled membranes

Figure 4.11b is an ESEM image of a BPEI-PODGE filled membrane fabricated several years prior to the BPEI-PODGE membranes shown in **Figure 4.7**. As can be seen, the morphology observed under ESEM supports the morphology observed under confocal microscopy. The coated morphology has, in fact, been observed in the entire series of BPEI-PODGE pore filled membranes.

The presence of a coated gel layer in the absence of solvent evaporation suggests that the PODGE cross-linker may have a specific affinity for the host polypropylene. A similar phenomenon has been previously observed in the interfacial polymerization of a diamine with a disulfonyl chloride [49,50]. As discussed very briefly in **Chapter 2, Section 2.2.2**, only 1,8-octanediamine (selected from several possible diamines) yielded a smooth coating in the interfacial polymerization with NDSC on the surface of a polypropylene membrane; whereas polymerization with other α,ω–diamines resulted in the formation of granules. It was thought that a specific affinity between 1,8-octanediamine and the polypropylene resulted in the smooth, homogeneous polysulfonamide coating.

If such an affinity of PODGE for the polypropylene occurred, diffusion and accumulation of the PODGE molecules around the pore walls would result in a concentration gradient being established in the radial direction across the pore. The increased concentration of the cross-linker near the pore walls would increase the rate of the cross-linking reaction and form a gel while the cross-linker depleted region in the center of the pore would simply wash out in the post extraction step.

This hypothesis was tested in an adsorption experiment of PODGE coating on polypropylene as a function of PODGE concentration. **Figure 4.12** shows the relationship between adsorption and concentration.

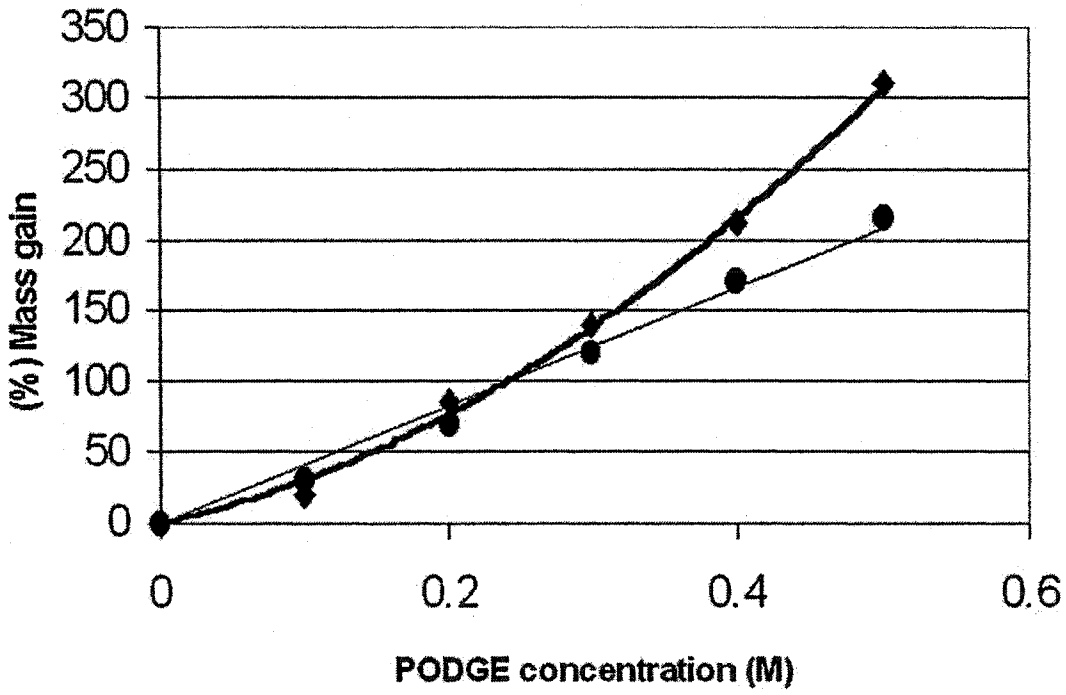

Figure 4.12 Adsorption of PODGE on polypropylene as a function of concentration. Each (♦) data point is an average of three measurements to a precision of < 3%

The circular points represent the mass gains expected from the porosities of the membrane samples and the concentrations of PODGE. The diamond shaped points refer to the actual mass gains measured from the adsorption of PODGE at each concentration. As can be seen, there is a significant departure of the actual mass gain from the expected

mass gain at the higher concentrations of PODGE. The coated mass gain of PODGE as a function of concentration is exponential, suggestive of an affinity relationship between the PODGE and polypropylene. The amount of PODGE that could be adsorbed was independent of the time of adsorption. The concentration of PODGE within membranes BP1 to BP7, however, ranged from 0.11 M to 0.32 M. The curves in **Figure 4.12** overlap in that PODGE concentration regime; however, the concentrations of PODGE within the membrane were calculated based on the mass fraction of the cross-linker in the starting pre-gel solution and assuming the concentration remained unchanged in the gelled phase. If phase separation occurred during the gellation process- induced by an affinity between PODGE and polypropylene- the actual concentration of PODGE in the membrane could be significantly higher than the calculated concentration. The PODGE concentration could, therefore, be in the region of **Figure 4.12** where the curves diverge.

An interesting observation was made during an experiment involving the formation of BPEI-EDGE and PODGE gels during solvent evaporation. **Figure 4.13** shows gels formed during solvent (methanol) evaporation.

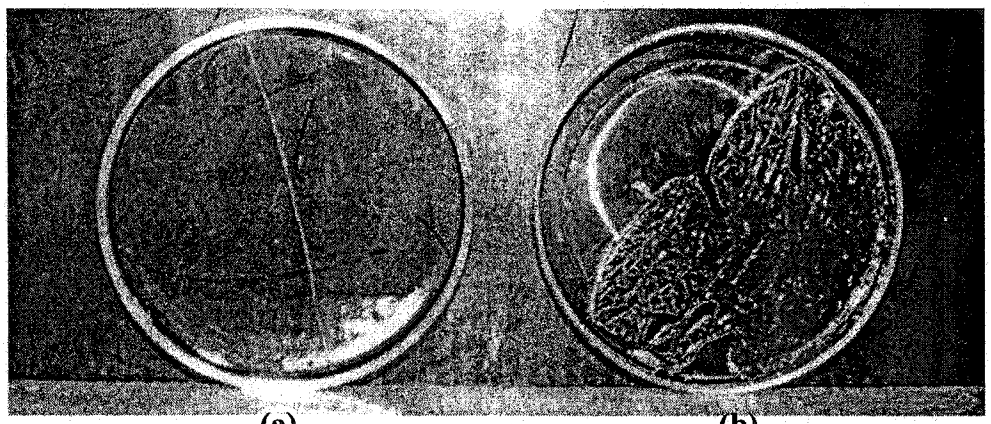

Figure 4.13 BPEI-EDGE (a) and BPEI-PODGE (b) gels formed during solvent evaporation under identical conditions

The BPEI-EDGE and BPEI-PODGE solutions were prepared with the same polymer concentration and molar ratio of cross-linker. The solutions were then poured into two separate petri dishes, laid side by side, from which solvent was allowed to evaporate. As can be seen in **Figure 4.13**, the two resulting gel films are very different in their morphologies. A scratch was made in the BPEI-EDGE gel film to show that a gel was indeed present because of its smooth, homogeneous and blemish free morphology. The gel made from the PODGE cross-linker, on the other hand, had a wrinkled, coarse morphology. Since the gels were formed under identical conditions, the differences in morphologies must arise solely from differing cross-linker/polymer interactions. The BPEI-PODGE gels shown in **Figure 4.13b** are suggestive of a heterogeneous distribution of PODGE cross-linker resulting from a phase separation of the two polymeric systems.

4.2.6 BPEI Filled Membranes: Nanofiltration Performance

The BPEI filled membranes were tested for their ability to reject salt under pressure driven conditions. The flux and rejection data for several of the membranes reported in **Table 4.2** are provided below.

Table 4.3 Flux and rejection of 5mM NaCl feed through BPEI gel filled membranes

Membrane	Mass gain (%)	Polymer volume fraction	Cross-linking (%)	5mM NaCl solution flux @ 500 kPa	5mM NaCl rejection @ 500 kPa (%)
BE1	53	0.076	10	26 +/- 1.6	68
BE3	91	0.134	10	5.5 +/- 0.3	83
BE10	72	0.115	20	14 +/- 0.6	77
BE11	118	0.184	20	8.3 +/- 0.3	81
BP2	35	0.077	10	46 +/- 0.1	56
BP3	56	0.147	10	25 +/- 0.7	53
BP5	43	0.097	20	65 +/- 0.6	38
BP6	57	0.134	20	47 +/- 0.3	48
BP7	74	0.214	20	28 +/- 0.04	53
BB1	119	0.206	10	48 +/- 0.9	43
BB3	144	0.268	20	44 +/- 0.2	36

Several important points emerge from the data in **Table 4.3**. First, the fluxes of the BPEI-PODGE membranes are within the nanofiltration range typically observed for pore filled membranes and not in the ultrafiltration range ($10^3 \sim 10^4$ kg/m^{2}h) expected for a completely coated membrane [51]. The flux data indicates that the PODGE cross-linked BPEI gel must be present as a pore-filling plug despite the gel coating, observed in **Figures 4.7 & 4.11b** confirming the model presented in **Figure 4.8b**.

Second, there are significant differences in flux among the different cross-linked membranes. For example, comparison of BE1 with BP3 (membranes with similar mass gains and cross-linking) does not show much difference in flux; however, comparison at higher cross-linking between BE10 and BP7 show a two-fold difference in flux indicating the effect of the cross-linker on gel morphology. The most significant differences in flux are observed in comparisons with the BADGE cross-linked membranes. The BADGE cross-linked membranes, despite their very large mass gains, have very high fluxes that exceed the fluxes of the EDGE and PODGE cross-linked membranes.

Third, the separation of 5mM NaCl is affected greatly by the cross-linker used to make the BPEI gel. As reported in **Chapter 3**, the BPEI-EDGE filled membranes function effectively in the nanofiltration of ionic solutes. The separations are high (68-83% rejection) and is unaffected by the degree of cross-linking. The separations of the BPEI-PODGE membranes, however, are significantly lower than the BPEI-EDGE membranes. Compare, for example, membranes BE1 and BP3- an EDGE two BPEI membranes cross-linked with the same molar ratio of EDGE and PODGE. The fluxes are the same; however, the PODGE cross-linked membranes have a significantly reduced NaCl rejection.

The PODGE membranes, in each case, have significantly lower salt rejection, ranging from 38-56%. This behavior is typical of membranes affected by concentration polarization- a phenomenon characteristic to all pressure driven membrane processes. Concentration polarization, as the name implies, is the presence of a solute concentration gradient in the feed with the maximum concentration established at the membrane

interface [52]. Concentration polarization can be mitigated by increasing the rate of mixing in the feed; however, this phenomenon is intrinsic to all pressure driven membrane processes and the effects are decreased rejection of solutes- arising from an increased localized feed concentration at the membrane interface. This effect is observed, and indeed magnified, with BPEI-PODGE membranes because the open, porous structure of the surface effectively entraps the salt solution preventing it from properly mixing with the bulk feed. Because mixing is diminished within the pores, the salt solution becomes increasingly concentrated with continuing convective flow of the salt solution through the pores. The high, localized salt concentration in the pores greatly diminishes the Donnan potential of the BPEI-PODGE gel, thus decreasing the separations.

The salt separations observed in the BPEI-BADGE membranes are also low, despite the large amount of gel polymer that could be loaded. Membranes BB1, BB3, BP2 and BP6 all have similar fluxes; however, the salt rejections observed in the BADGE cross-linked membranes (BB1) are the lowest despite the mitigating effect of concentration polarization on separations in BP2 and BP6. The nanofiltration performance of the membranes as a function of cross-linker, in the PODGE and BADGE membranes, shows that an increase in cross-linking results in a decrease in salt separations and an increase in flux- unlike what was observed in the EDGE system.

The confocal micrograph of BB1 shown in **Figure 4.10** shows that the gel fills the membrane pores; however, there are small pores throughout the gel evident in the pockmarked appearance. Concentration polarization would also be operative in the

BADGE membranes; however, the effect is not expected to play as significant a role as in the case of the PODGE cross-linked membranes because the surface pores are not as large. The reduced separation, however, is mostly attributable to the heterogeneity of the BADGE cross-linked gel [15,53].

The gel opacity, syneresis, reduced swelling capabilities of the bulk BADGE cross-linked gel and the lower than expected ion exchange capacities of the BPEI-BADGE membranes reported earlier suggests that the gel morphology consists of pockets of high density, polymer rich regions and pockets of low polymer lean regions as depicted in **Figure 4.14b**.

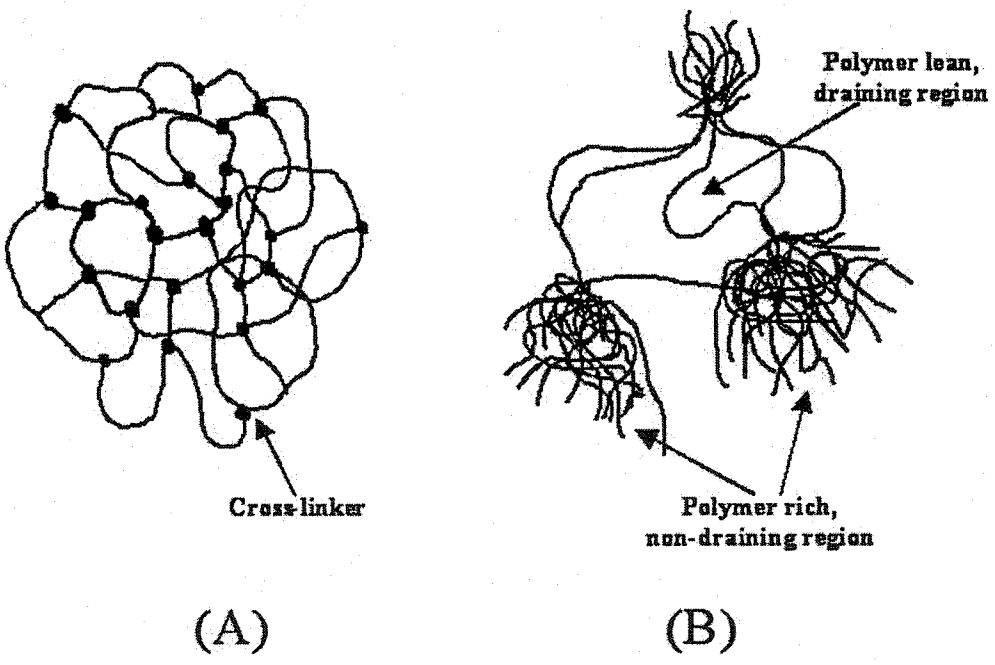

Figure 4.14 Schematic representation of an isotropic (A) and a heterogeneous (B) gel

The gel network depicted in **Figure 4.14b** has a significant fraction of the polymers located in highly dense domains. The nitrogens in those domains are mostly inaccessible because diffusive and convective flow of solvent and electrolytes do not occur significantly within the time scales involved in membrane characterization and testing. The nitrogens in those *non-draining regions* therefore do not contribute to the membrane charge and thus do not participate in the Donnan exclusion of ionic solutes.

The physical basis of the low separations observed in the BPEI-BADGE membranes can be explained in the context of a model currently being developed [53,54] that correlates charge and gel mesh size based on the Teorell-Meyers-Sievers (TMS) [55-58] and space charge models [59-61] of electrolyte interactions. The TMS model assumes a homogeneous distribution of electric field throughout the pores of the membrane. For this model to be effective, the mean spacing between chains (**Figure 4.14a**- a depiction of an isotropic gel) must be relatively constant and smaller than the thickness of the double layer of the polyelectrolyte (Debye-Hückel screening length), κ^{-1}, at the ionic strength of the filtered solution [62,63]. The TMS model cannot be operative in a gel with a morphology depicted in **Figure 4.14b** because there would be a non-uniform distribution of the electric field.

In the case where the pores are larger than the Debye-Hückel screening length of the polyelectrolyte, the space charge model is operative. In such a case, an ionic concentration gradient is established in the radial direction across the pore and the magnitude of the salt rejection is greatly affected by the size of the pores. The low separations observed in the BADGE membranes suggest that the mesh sizes, created by

the heterogeneity, in the BADGE gels are at the limit where the space charge model can be applicable. Furthermore, the large open spaces- depicted as polymer lean, draining regions- contributes to the high fluxes observed within the BPEI-BADGE gel filled membranes. This will be discussed further in the following section.

4.2.7 Hydrodynamic Permeability of BPEI Gel Filled Membranes

As described in **Chapter 2** the hydrodynamic permeability model developed by Mika and Childs [16] is a very powerful model for understanding gel properties. The hydrodynamic permeability model allows for an *a priori* prediction of gel/membrane permeability against which experimentally obtained permeabilities can be compared and verified. Information such as the mesh size ($\sqrt{k}$) can be extracted from the permeabilities and deviations from the model can give a perspective of the microstructure of the gel.

One such deviation could arise from gel heterogeneity, which has been shown to have a substantial effect on gel hydrodynamic permeability [8,15]. Weiss *et al.* [8] discussed the effects of gel heterogeneity- a nonuniform distribution of monomer- on permeability in the context of freely draining and nondraining regions. Gels with increasing levels of heterogeneity have shown increased permeability [8,15,53]. This is consistent with the fluxes observed in the BPEI-BADGE membranes of the previous section, where the flux through the heterogeneous gel was observed to be very high due to the presence of polymer lean (freely draining) regions (heterogeneity).

To determine how the cross-linkers affect the microstructure of the gel- and thus, the permeability- the hydrodynamic permeability of the BPEI gel filled membranes were measured and compared to the predicted permeabilities obtained from the model. **Table 4.4** lists the membranes and **Figure 4.15** shows the correlation of measured vs. predicted permeabilities as a function of polymer volume fraction.

Table 4.4 Properties of BPEI cross-linked with PODGE (BP), BADGE (BB) and EDGE (BE) filled membranes

Membrane	Degree of Cross-linking (%)	Water uptake (%)	Polymer volume fraction	Hydrodynamic Permeability (10^{-18} m^2)
BP1	10	81	0.0738	2.76
BP2	10	81	0.0768	2.74
BP3	10	78	0.147	1.35
BP4	10	75	0.204	0.33
BP5	20	79	0.097	3.92
BP6	20	79	0.134	2.73
BP7	20	76	0.214	1.56
BB1*	10	70	0.206	3.35
BB2*	10	52	0.411	0.098
BB3*	20	64	0.268	2.66
BE1	10	85	0.0755	1.68
BE2*	10	82	0.0917	1.25
BE3	10	82	0.134	0.51
BE4*	10	80	0.116	0.64
BE5	10	78	0.126	0.54
BE6*	10	80	0.132	0.45
BE7*	10	75	0.174	0.21
BE8	15	83	0.093	0.99
BE9	15	78	0.169	0.29
BE10	20	81	0.115	0.28
BE11	20	75	0.184	1.79

*Membranes fabricated from PP5 host substrate. All others fabricated from PP3

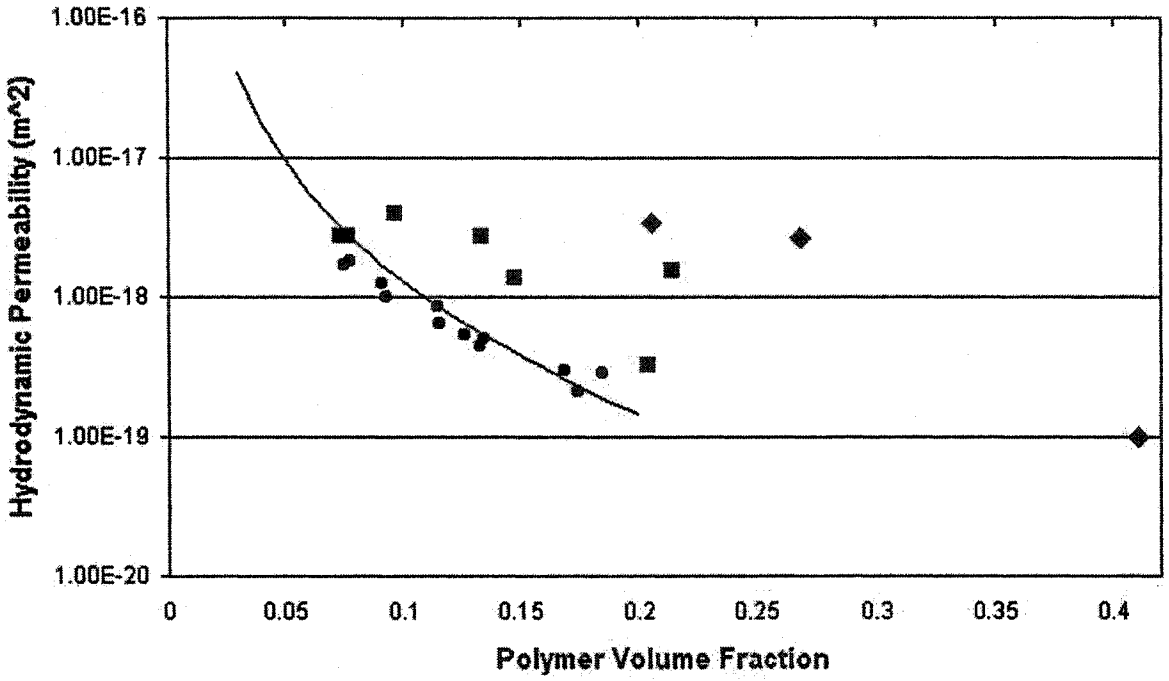

Figure 4.15 Hydrodynamic permeability of BPEI gel filled membranes with (•)-EDGE, (♦)-BADGE, and (■)-PODGE cross-linkers compared to hydrodynamic permeability model (-) for BPEI

As can be seen in **Figure 4.15**, the permeabilities of BPEI-EDGE membranes correlate very well to the modeled permeability obtained using **Equation 2.11** and **2.12** over the gel polymer volume fraction range of $0.0755 \leq \phi \leq 0.184$, with the PEI characteristic ratio $C_\infty = 16.1$ [64]. The model matches well with the experimental permeability data for the BPEI-EDGE membranes and cross-link density does not appear to have any effect on permeability since BE8-11 all fit the model line. This is consistent with what has been observed in the bulk gels since there are no visible evidences of heterogeneity in either the 10% and 20% EDGE cross-linked gels. Furthermore, as

discussed in **Chapter 3, Figure 3.10**, separation of NaCl is not affected by the degree of EDGE cross-linking suggesting that an increase in EDGE cross-linker does not contribute to an increase in gel heterogeneity.

Large deviations from the model, however, are observed for permeabilities through BPEI-PODGE and BPEI-BADGE membranes, although the water uptake and polymer volume fractions are within the range of BPEI-EDGE membranes. The higher permeabilities of the BPEI-PODGE membranes are due to the lower thicknesses of the gel layer. The hydrodynamic permeability of a gel is dependent upon its thickness since the hydrodynamic resistance of the polymer network, which is transmitted through the viscous solvent, will be affected by both the spacing of the polymer chains (polymer volume fraction) and the length of the pathway the solvent must travel (thickness) [65,66]. As discussed previously, the BPEI-PODGE filled membranes exhibit a coating on either side with a pore-filling plug in the center. The thickness of the plug is unknown but is less than the thickness of the membrane. The thickness of the membrane was used to calculate the hydrodynamic permeability of the BPEI-PODGE membranes; therefore, there is much uncertainty with the permeability data and hence the deviation from the model. It is worthy to note, however, that the permeabilities of the BPEI-PODGE filled membranes are affected by the relative concentration of PODGE cross-linker. The three membranes with 20% PODGE cross-linker BP5, BP6 and BP7 all have higher permeabilities than the 10% PODGE cross-linked membranes. Furthermore, membrane BP7, with the highest polymer volume fraction (0.214) and the largest concentration of PODGE, shows the greatest deviation from the model further giving credence to the

hypothesis that PODGE has an affinity for the polypropylene base membrane resulting in a thinner gel plug.

The BPEI-BADGE membranes show the largest deviation from the model. As discussed previously, the BPEI-BADGE gels are very heterogeneous. It stands to reason then, in the context of draining and nondraining domains in heterogeneous gels previously discussed (**Figure 4.11**), that BPEI-BADGE gel filled membranes should have a markedly enhanced permeability compared to BPEI-EDGE gels that are isotropic. The majority of the solvent flow occurs through the draining regions, which results in a high membrane permeability despite the high polymer volume fractions.

4.3 Conclusions

The choice of cross-linker has been found to have a substantial effect on the morphology of the gel and the performance capabilities of the gel-filled membrane. The swelling capabilities of BPEI gels made from EDGE, PODGE and BADGE reflect the degree to which they are hydrophilic. The EDGE based gels swell the greatest amounts and the EDGE based membranes are well behaved with no evidence of heterogeneity.

The properties of rigidity and hydrophobicity of the BADGE cross-linker is manifested in the BPEI-BADGE gels. The gels swell very little and display visible signs of heterogeneity. Heterogeneity induced by the BADGE cross-linker is reflected in the increased permeability and decreased salt separation of the BPEI-BADGE membranes.

The formalism of draining and non-draining regions within a heterogeneous gel can account for such effects.

The use of PODGE cross-linker- a highly flexible, large molecule- results in membranes with unusual morphologies unlike those observed for other gel filled membranes. The enhanced permeabilities of these membranes are due to the smaller thickness of the gel layer located in the interior of the membrane. The nature of the PODGE-PEI-polypropylene interactions is not fully understood; although there is some evidence to suggest the PODGE molecule has affinity for the polypropylene in the host substrate.

4.4 References

1. Gehrke, S.H. & Lee, P.I. *Hydrogels for drug delivery systems.* In: Specialized Drug Delivery Systems: Manufacturing and Production Technology. Tyle, P. (ed), New York, Marcel Dekker, 1988; pp. 333-392
2. Guyot, A. *Synthesis and Structure of Polymer Supports.* In: Syntheses and Separation using Functional Polymers. Sherrington, D.C.; Hodge, P. (eds), New York, John Wiley & Sons, 1988; pp. 1-42
3. Horak, D.; Pelzbauer, Z.; Bleha, M.; Ilavsky, M.; Svec, F.; Kalal, J. *J. Appl. Polym. Sci.* **1981**, *26, 411*
4. Hradil, J. & Svec, F. *Angew. Makromol. Chem.* **1985**, *135, 85*

5. Hradil, J. & Svec, F. *Angew. Makromol. Chem.* **1985**, *130, 81*

6. Svec, F. & Frechet, J.M. *Macromolecules* **1995**, *28, 7580*

7. Smigol, V.; Svec, F.; Frechet, J.M. *Macromolecules* **1993**, *26, 5615*

8. Weiss, N.; Van Vliet, T.; Silberberg, A. *J. Polym. Sci.: Polym. Phys. Ed.* **1979**, *17*, 2229

9. Weiss, N.; Van Vliet, T.; Silberberg, A. *J. Polym. Sci.: Polym. Phys. Ed.* **1981**, *19, 1505*

10. Righetti, P.G.; Caglio, S.; Sarachi, M.; Quaroni, S. *Electrophoresis* **1992**, *13, 587*

11. Righetti, P.G.; Gelfi, C. *J. Chromatog. B* **1996**, *699, 63*

12. Zhu, S. & Hamielec, A. *Makromol. Chem., Macromol. Symp.* **1992**, *63, 135*

13. Dusek, K. *Inhomogeneities induced by cross-linking in the course of crosslinking copolymerization.* In: Polymer Networks: Structural and Mechanical Properties. Chmopff, A.E. (ed). New York, Plenum Press, 1971, pp. 245-260

14. Sedlack, B. & Konak, C. *J. Colloid. Interf. Sci.* **1982**, *90, 60*

15. McCrory, C.T.M. Ph.D. Thesis: Impact of gel morphology on pore filled membranes. 2001. McMaster University

16. Mika, A.M.; Childs, R.F. *Ind. Eng. Chem. Res.* **2001**, *40*, 1694

17. Kirz, J.; Ade, H.; Jacobsen, C.; Ko, C.H.; Lindaas, S.; McNulty, I.; Sayre, D.; Williams, S.; Zhang, X.; *Review of Scientific Instruments* **1992**, *63*, 557

18. Howells, M. *Review of Scientific Instruments* **1992**, *63*, 557

19. Jacobsen, C.; Williams, S.; Anderson, E.; Brown, M.T.; Buckley, C.J.; Kern, D.; Kirz, J.; Rivers, M. *Optics Communications* **1991**, *86, 351*

20. Warwick, T.; Padmore, H.; Ade, H.; Hitchcock, A.P.; Rightor, E.G.; Tonner, B.P. *J. Electron Spectroscopy* **1997**, *84, 85*

21. Ade, H.; Smith, A.P.; Zhang, H.; Zhuang, G.R.; Kirz, J.; Rightor, E.; Hitchcock, A.P. *J. Electron Spectroscopy* **1997**, *84, 53*

22. Stohr, J. NEXAFS Spectroscopy, Berlin, Springer-Verlag, 1992

23. Henke, B.L.; Gullikson, E.M.; Davis, J.C. *At. Nucl. Data Tables* **1993**, *54, 181*

24. F.J. Green. The Sigma-Aldrich Handbook of Stains, Dyes and Indicators. Aldrich Chemical Co. Milwaukee, Wi (1990). P. 270

25. Warwick, T.; Franck, K.; Kortwight, J.B,; Meigs, G.; Moronne, M.; Myneni, S.; Rotenberg, E.; Seal, S.; Steele, W.F.; Ade, H.; Garcia, A.; Cerasari, S.; Denlinger, J.; Hayakawa, S.; Hitchcock, A.P.; Tyliszczak, T.; Rightor,; Shin, H.J; Tonner, B.P. *Rev. Sci. Inst.* **1998**, *69, 2964*

26. Jacobsen, C.; Wirick, S.; Flynn, G.; Zimba, C. *J. Microscopy.* **2000**, *197, 173*

27. Toy, P.H.; Reger, T.S.; Janda. K.D. *Aldrich.Acta.* **2000**, *33, 87*

28. Lai, Y.C.; Quinn, E.T. *Photopolymerization: Fundamentals and Applications.* ACS Symposium Series 673. In: Photopolymerization: Fundamentals and Applications, Scranton, A.B., Bowman, C.N., Peiffer, R.W. (eds.), Washington, American Chemical Society, 1997; pp. 35-50

29. Dusek, K. *Inhomogeneities induced by cross-linking in the course of cross-linking copolymerization.* In: Polymer Networks: Structure and Mechanical Properties, Chompff, A.J., Newman, S. (eds.), New York, Plenum Press, 1971; pp. 245-260

30. Dusek, K.; Seidl, J.; Malinksy, J. *Collection Czech. Chem. Commun.* **1967**, *32*, 2766

31. Dotson, N.A.; Macosko, C.W.; Tirrel, M. *Cyclization during cross-linking free radical polymerizations.* In: Synthesis, characterization and theory of polymeric networks and gels, Aharnoi, S.M. (ed.), New York, Plenum Press, 1992; pp. 319-336

32. Lukas, J.; Bleha, M.; Svec, F.; Kalal, J. *Angew. Makromol. Chem.* **1981**, *95*, 129

33. Schroder, U.P. & Opperman, W. *Properties of Polyelectrolyte Gels.* In: Physical Properties of Polymeric Gels, Cohen-Addad, J.P. (ed.), New York, John Wiley & Sons, 1996; p. 185

34. Evmenenko, G.; Alexeev, V.; Budtova, T.; Buyanov, A.; Frenkel, S. *Polymer* **1999**, *40*, 2975

35. Schroder, U.P. & Opperman, W. *Properties of Polyelectrolyte Gels.* In: Physical Properties of Polymeric Gels, Cohen-Addad, J.P. (ed.), New York, John Wiley & Sons, 1996; p. 19

36. Chujo, Y.; Yoshifuji, Y.; Sada, K.; Saegusa, T. *Macromolecules* **1989**, *22*, 1074

37. Kobayashi, S.; Shirasaka, H.; Suh, K.; Uyama, H. *Polym. J.* **1990**, *22*, 442

38. Figuly, G; Royce, S; Khasat, N.; Schock, L.; Wu, S.; Davidson, F.; Campbell, G.; Keating, M.; Chen, H.; Shimsick, E.; Fischer, R.; Grimminger, L.; Thomas, B.; Smith, L.; Gillies, P. *Macromolecules* **1997**, *30,* 6174

39. Katchalsky, A.; Lifson, S.; Heisenberg, H. *J. Polym. Sci.* **1951**, *7*, 571

40. Flory, P. J. The Principles of Polymer Chemistry. Cornell University Press, Ithica, NY, 1953

41. Bansil, R.; Gupta, M.K. *Ferroelectrics* **1980**, *30*, 63

42. Zeldovich, K. B.; Khoklov, A. R. *Macromolecules* **1999**, *32*, 3488

43. Kobayashi, S.; Shirasaka, H.; Suh, K.D.; Uyama, H. *Polym. J.* **1990**, *22*, 442

44. Forster, S.; Schmidt, M.; Antonietti, M. *Polymer* **1990**, *31*, 781

45. Nierlich, M.; Boue, F.; Lapp, A.; Oberthur, R. *J. Physique* **1995**, *46*, 649

46. Stachera, D. Ph.D. Thesis: Poly(4-vinylpyridine) filled microporous membranes: Factors affecting transport and selectivity. **2000**. McMaster University

47. Mika, A.M.; Ge, G.; Childs, R.F. *Fabrication of asymmetric membranes,* US patent *in preparation* **2001**

48. Fang, L; Childs, R.F. *unpublished results*

49. Wang, L. Ph.D. Thesis: Internal surface coating and photochemical modification of polypropylene microfiltration membranes. 1997. McMaster University

50. Dickson, J.M.; Childs, R.F.; McCarry, B.E.; Gagnon, D.R. *J. Memb. Sci.* **1998**, *148*, 25

51. Childs, R.F.; Weng, J.F.; Kim, M.Y.; Dickson, J.M. *J. Pol. Sci. Part A: Polym. Chem.* **2002**, *40*, 242

52. Mulder, M. Basic Principles of Membrane Technology, 2nd ed. Dordrecht, Kluwer Academic Publishers, 1996, p. 418

53. Mika, A.M.; Childs, R.F.; Dickson, J.M. *J. Memb. Sci. in press*

54. Mika, A.M.; Childs, R.F. Development of model for ionic solute separation in polyelectrolyte pore filled membranes. *Manuscript in preparation*

55. Teorell, T. *Progr. Biophys. Biophys. Chem.* **1953**, *3*, 305

56. Meyer, K.H. & Sievers, J.F. *Helv. Chim. Acta.* **1936**, *19*, 649

57. Meyer, K.H. & Sievers, J.F. *Helv. Chim. Acta.* **1936**, *19*, 665

58. Meyer, K.H. & Sievers, J.F. *Helv. Chim. Acta.* **1936**, *19*, 987

59. Morrison, F.A. & Osterle, J.F. *J. Chem. Phys.* **1965**, *43*, 2111

60. Gross, R.J. & Osterle, J.F. *J. Chem. Phys.* **1968**, *49*, 228

61. Fair, J.C. & Osterle, J.F. *J. Chem. Phys.* **1971**, *54*, 3307

62. Probstein, R.F.; Sonin, A.A.; Yung, D. *Desalination* **1973**, *13*, 303

63. Tsuru, T.; Nakao, S.; Kimura, S. *J. Chem. Eng. Jpn.* **1991**, *24*, 511

64. Wang, S.; Debolt, L.; Mark, J.E. *Polym. Prepr.* **1993**, 34, 478

65. Kapur, V.; Charkoudian, J.C.; Kessler, S.B.; Anderson, J.L. *Ind. Eng. Chem. Res.* **1996**, *35*, 3179

66. Kapur, V.; Charkoudian, J.; Anderson, J.L. *J. Memb. Sci.* **1997**, *131*, 143

CHAPTER FIVE

COATING THE INTERNAL MICROSTRUCTURE OF MICROPOROUS MEMBRANES WITH CROSS-LINKED POLYETHYLENIMINE GELS

Abstract

The incorporation of a hydrophilic gel into the pores of a polyolefinic microporous membrane changes its surface properties from hydrophobic to hydrophilic. **Chapter 3** dealt with the incorporation of BPEI gels into a polypropylene host membrane to create effective nanofiltration membranes. The membranes easily wetted with water and high water uptake values were observed. **Chapter 4** dealt with the effect of various cross-linkers on BPEI membranes in terms of the properties of these membranes. One such cross-linker, polypropyleneglycol diglycidyl ether, created membranes with a thick gel coating on the exterior walls of the surface pores. Although the PODGE based membranes still functioned in the nanofiltration regime, the observed coating morphology motivated work towards developing an ultrafiltration membrane where all the pores were coated with a thick gel layer. This chapter reports the work of coating the pores of a microfiltration host with a swellable cross-linked gel.

5.1 INTRODUCTION

There is considerable interest in coated membranes as evident in the large number of disclosures in the patent and scientific literature. There are varieties of coating methods and coated membranes with, perhaps, thin film composites the best understood and most common [1]. Coating is a versatile method for changing the surface properties and chemistry of a material. The application of an adherent coat to the entire surface of a base support structure- instead of just one face, as in the case of thin film composites- allows for a wide range of applications based upon the morphology and properties of the starting material. Such coated membranes are widely used in microfiltration and, to a lesser extent, ultrafiltration processes such as food, beverage, biotechnology, pulp and paper industries and water purification/recovery systems [2]. In all of these processes, there is a need to modify the membrane surface properties as microfiltration substrates are typically formed from water-insoluble polymers. Such polymers are usually rigid and physically strong but are hydrophobic and are readily fouled by the adsorption of hydrophobic particles and solutes from feed streams [3,4]. Fouling is a major problem in the industrial use of membranes leading to low rates of throughput and making frequent cleansing or costly pretreatment necessary.

Many reports of 'hydrophilizing' hydrophobic membrane surfaces by coating with a hydrophilic polymer have been made [5-16]. However, there is frequently considerable variability in these coatings and improved methods of coating microporous host substrates to make novel coated membranes would be one of great value.

The previous chapters have dealt with gel filled membranes developed here at McMaster University [17-25]. As discussed previously, these membranes are composed of a structurally rigid microporous host filled with a polyelectrolyte hydrogel, the chemical properties of which, determining the properties and performances of the membrane. The microporous host membranes- polyolefin based structures formed by a thermally induced phase separation (TIPS) [26] process- have many very desirable properties such as, good structural strength, ease of manufacture, high void volumes, well controlled porosities and chemical inertness. The polyethylene and polypropylene membranes, however, are extremely hydrophobic so their potential uses in aqueous applications are quite limited. The incorporation of a polyelectrolyte hydrogel irreversibly changes the surface properties of the base membrane from highly hydrophobic to hydrophilic; thus, the pore-filled nanofiltration membranes, as discussed in the previous chapters, readily absorb water [17,18, 21,23]. The polyelectrolyte gel, in these membranes, fills the entire void volume of the microporous host; therefore, the permeability through the gel-filled membrane is determined by factors such as the polymer volume fraction, physical properties of the polyelectrolyte and limited to the nanofiltration regime [27]. These membranes are, therefore, not practical for microfiltration applications where a large throughput of material is required at low operating pressures.

Previously a process of coating the internal surface of a microporous membrane by a modified interfacial polymerization process was reported [28,29]. It was found that a polysulfonamide layer deposited on a microporous polypropylene membrane increased

the surface hydrophilicity. The method, however, did not provide a means for controlling the thickness of the coating. A modified coating method, as described in **Chapter 2, Section 2.2.5**, was subsequently developed where BPEI was coated and cross-linked into place, with naphthalene-1,5-disulfonyl chloride, on the surface of a polypropylene membrane [30]. The coated BPEI layer was described as a "hard coating" because the fluxes of the coated membranes did not differ substantially from the flux of the nascent membrane and the nitrogens in the coated polymer layer were difficult to detect by titration.

In this chapter, a new method of developing pore-coated membranes with properties in between a pore-filled and a "hard coated" membrane is reported. The membranes are based on a permanently coated gel layer that expands into the pores because of its highly swellable nature, but can also be collapsed onto the pore walls by drying. It is important to distinguish this "soft coated" construct with membranes with brush lined pores that may also have similar properties. In the latter case, polymers are end grafted, or adsorbed, to the surface of a host substrate to form a brush morphology and can either contract to the substrate surface or expand into the pores depending upon the composition of the solution passing through the pores [31-38]. To establish the coating technique an *in situ* solvent evaporation of a polymer/cross-linker solution within the pores of a microporous host was employed. The conditions and materials required to manufacture this new architecture of "soft coated" membranes are described.

5.2 EXPERIMENTAL

5.2.1 Materials

Branched polyethylenimine (BPEI) with a weight average molecular weight (M_w) of ca. 25,000, polypropyleneglycol diglycidyl ether (PODGE) with a number average molecular weight (M_n) of ca. 640 and Direct Red 23 dye (λ_{exc} = 507 nm and λ_{emm}=610 nm) [39] were obtained from Aldrich Chemical Co. Ethyleneglycol diglycidyl ether (EDGE) was obtained from Polysciences Inc. Methanol was obtained from Caledon Labs. Ltd. Unless otherwise stated, all water used was carbon filtered and deionized. All reagents were used without further purification.

The microporous host substrate, used for the preparation of pore coated anion-exchange membranes was a polypropylene microporous membrane supplied by 3M Canada Company. Details of the support membrane are given in **Table 1, Chapter 3.** The base membrane was extracted with acetone at room temperature for one day prior to use to remove any oils remaining from the manufacturing process.

5.2.2 Coated Membrane Preparation

Separate methanol solutions, of equal volume and known concentrations, of BPEI (10 and 15% w/v) and the cross-linker (EDGE or PODGE) were prepared at 10 and 20% molar ratios with respect to the ethylamine monomeric repeat unit in the polymer. The

solutions were rapidly mixed and spread across the polypropylene host membrane (12 x 12 cm) kept on a polyethylene terephthalate (PET) sheet on top of a glass plate. The wetted membrane was immediately covered with another PET sheet and the polymer/cross-linker solution was distributed evenly through the pores of the polypropylene host membrane by rubbing the top PET sheet with a rubber roller. The top PET sheet was removed and the wetted membrane was placed in a methanol vapor rich chamber, shown in **Figure 5.1**, and the system was allowed to stand at room temperature, overnight (16 h) for gelling to occur.

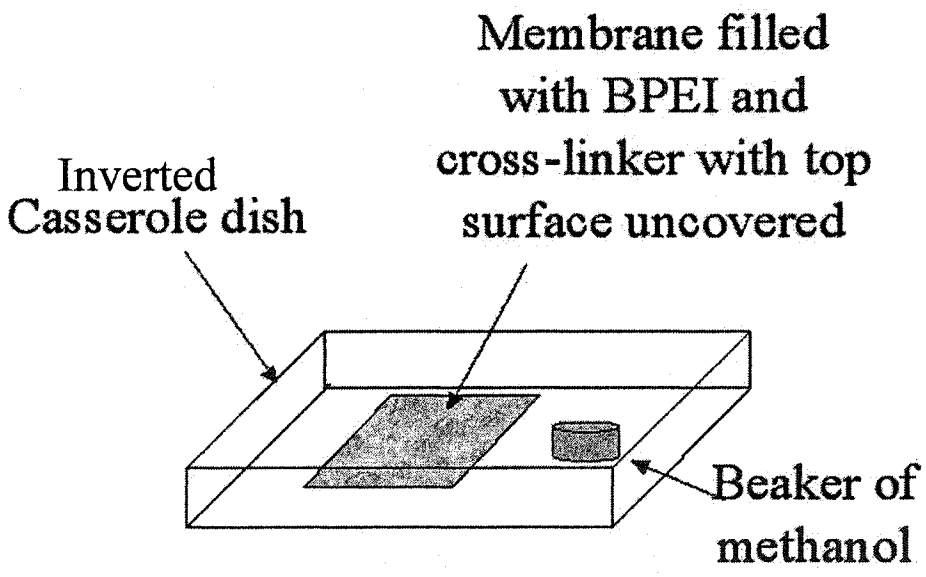

Figure 5.1 Schematic of methanol vapor rich vessel used to fabricate soft coated BPEI membranes

After removal of the membrane from the PET sheet, the membrane was washed with deionized water and then with methanol to remove soluble, unincorporated components. The membrane was then dried under vacuum, at room temperature, and the mass gain was determined. The mass gain is expressed as

$$\text{Mass Gain} = (M_c - M_b)/M_b \; x \; 100\% \quad \textbf{(5.1)}$$

where M_b is the mass of the base, dry, unfilled membrane and M_c is the mass of the dry, coated membrane.

The membranes were conditioned by twice cycling through acid and base (typically 12 hours each) during the determination of ion exchange capacity. After the final base cycle, the membranes were washed with deionized water, vacuum dried and stored until the permeability tests.

5.2.3 Membrane Characterization

The thickness of the dry membrane was measured with a digital micrometer (model MDC-1 "P, Mitutoyo Corp.) by repeated measurements across the surface of the membrane until a variation of less than 5% was obtained. Other dimensions were measured with a ruler with an accuracy of ± 1mm. The thickness of the wet membranes was determined as previously described with the aid of a pycnometer [17,18].

The ion exchange capacities of the membranes and water uptake were determined by procedures described in **Chapter 3, Section 3.**

5.2.4 Microscopic Studies

Membrane samples for confocal microscopy were were soaked in an aqueous solution of Direct Red 23 dye (10^{-3} M) overnight (~16 h) at room temperature. The acquisition of the confocal microscopic images was obtained by procedures previously described in **Chapter 4, Section 4.1.5.**

5.2.5 STXM Analysis

Acquisition of the STXM data on cryomicrotomed membrane samples of approximately 200nm thickness was obtained by methods previously described in **Chapter 4, Section 4.1.6.**

5.2.6 Permeability Measurements

Water permeability measurements were carried out in a stirred dead-end ultrafiltration cell with an active membrane area of 38.5 cm^2 as described in **Chapter 3, Section 3**. Flux measurements were carried out at pressures ranging from 50 to 150 kPa, pressurized with a nitrogen cylinder. To ensure consistency among different membranes,

permeability was measured after each membrane was characterized, dried and rewetted. The rewetting procedure was accomplished by first soaking the dried membrane in methanol for less than 1 minute, then deionized water for 1~2 minutes. To ensure internal consistency and reliability of data, the collection of each permeate sample (300 ml) was commenced and finished at precise intervals determined by calibrated markings on the cell. The flux, J_m, at 25 °C was calculated from the mass of the permeate divided by the time and membrane-active area.

$$J_m = \frac{m_p}{A_m T} \quad \textbf{(5.3)}$$

Where m_p is the mass of the permeate in kg, A_m is the area of the membrane in m^2, and T is the time in hours.

5.3 RESULTS AND DISCUSSION

5.3.1 Mechanism of Coating

Since BPEI is an inexpensive, readily available polymer rich in chemical functionality, it has been studied extensively in coating applications. BPEI has been used to coat silica [43-46]; mica surfaces [47]; porous zirconia [48]; polystyrene cross-linked with divinylbenzene [49,50] and porous support structures for use in composite membranes [51,52]. In most of the cases mentioned, the coating of BPEI is held in place by coulombic interactions with a charged surface or chemically grafted to the surface.

BPEI coatings have also been used to 'hydrophilize' hydrophobic microfiltration membranes [14,53]. Recently, Pall Corporation developed a method for coating, and cross-linking into place, BPEI onto the surface of a microporous membrane [54]. This process involved coating the surface of a porous substrate with a solution of BPEI and cross-linker by a dip-coating method. The membranes were then cured (cross-linked) at elevated temperatures (50 - 130° C). The coated BPEI layer changed the surface properties of the base substrate such that a negatively charged solute, such as Bovine serum albumin (BSA) protein, could bind due to electrostatic interactions at a pH of 7.

The method of coating developed in this report involves a modification of the pore-filling method described in the previous chapters. The modification involves an *in-situ* gellation process under controlled solvent evaporation. The rate of solvent evaporation during the gellation step was found to be a crucial parameter in making coated membranes. Preliminary experiments, where methanol evaporation was not controlled, resulted in membranes with extremely inconsistent physical properties and flux performances, as will be shown in the following section. Evaporation of solvent results in an increase in polymer/cross-linker concentration which, in turn, will increase the rate of the cross-linking reaction. The consequence of an enhanced rate of cross-linking is a non-even distribution of the gel coating due to gellation occurring before deposition onto the pore walls. The unincorporated gel washes out in the post fabrication extraction stage. By evaporating the solvent in a closed chamber, under a methanol-saturated atmosphere, the cross-linked polymer could be deposited more evenly throughout the base substrate and yield membranes that had reproducible physical

properties and performances. The PEI gel coat, although not chemically bonded to the base membrane, was permanently anchored by cross-linking and could not be removed, even when extracted in boiling methanol for 48 hours.

5.3.2 Coated Membranes- Physical Properties

Since a soft coated morphology was desired, two cross linkers- polypropylene glycol diglycidyl ether (PODGE) and ethyleneglycol diglycidyl ether (EDGE) (**Figure 4.1, Chapter 4**)- were chosen based on their large swelling capabilities as discussed in **Chapter 4**. Two sets of membranes, one set based on the PODGE cross-linker and the other based on EDGE, were thus prepared using the evaporative coating technique. The coated membranes, listed in **Table 5.1**, were made with mass gains ranging from 18% to 91%.

Table 5.1 Properties of BPEI coated membranes

	% PODGE cross-linker	% EDGE cross-linker	Expected mass gain (%)	Actual mass gain (%)	Thickness of wet membranes (μm)[a]	Ion exchange capacity (meq/g)	Theoretical IEC (meq/g)
P1	10	/	63	18	71 +/- 2	1.09+/-0.13	1.52
P2	10	/	46	53	81 +/- 7	3.08+/+0.03	3.06
P3	10	/	93	77	93 +/- 2	3.71+/-0.03	3.87
P4	10	/	80	84	91 +/- 5	3.02	4.05
P5	20	/	99	91	76 +/- 3	2.15+/-0.24	3.11
E1	/	10	35	49	78 +/- 4	2.99	5.64
E2	/	10	60	71	83 +/- 4	2.86	6.04

[a]Average thickness of nascent membrane 75 +/- 3 μm

As discussed in the previous section, membranes made without controlled evaporation- that is, in the absence of a methanol saturated atmosphere- resulted in uneven coatings. The lower than expected mass gain for membrane P1 is due to it being made without controlled evaporation. All other membranes were made under controlled evaporation conditions and the actual mass gains are closer to the calculated expected mass gains.

In each case, the membranes could be easily wetted with water indicating a permanent change in the surface properties of the hydrophobic polypropylene host. The nitrogens in the incorporated BPEI were titrated and the measured ion exchanges were compared to the theoretical values. The IECs for BPEI-PODGE membranes were very close to the theoretical values but approximately half of the nitrogens could be titrated for the BPEI-EDGE membranes as observed previously in **Chapter 3**. The reasons for the differences in the titration behavior of these two membranes are not known since the measured IECs of BPEI-PODGE filled membranes, as reported in **Chapter 4**, were 50-80% of the theoretical values. A possible reason for the differences in titration behavior may be due to the estimation of the BPEI concentration in the PODGE membranes. The theoretical IECs were calculated based on the assumption that the concentration ratio of BPEI and PODGE in the gel is the same as the solution they were prepared from. If phase separation occurs during the gellation stage with removal of unincorporated gel, as suggested in **Chapter 4**, the concentration ratios of BPEI and PODGE remaining in the membrane will be different and could thus result in an incorrect theoretical IEC.

Despite the high mass gains and large ion exchange capacities, only membranes P3 and P4 had significant wet thickness changes (21% & 24%) relative to the nascent membrane; the thickness of the other membranes were- within error- the same as the nascent. This stands in clear contrast to wet BPEI pore filled membranes where thickness changes of up to 44% were observed in pH 5.5. Although it is surprising that a thin coating should yield any change in membrane thickness, a possible explanation could be that the membranes had significant coatings on either surface that swelled and did not collapse during the conditioning/characterization process. Why the other membranes did not exhibit similar properties is not known.

5.3.3 Morphology of Coated Layer: Laser Fluorescence Confocal Microscopy

The morphology of the coated membranes was examined by laser fluorescence confocal microscopy. As shown previously in **Chapter 3**, a laser fluorescence confocal micrograph of the base, polypropylene substrate is displayed again in **Figure 5.2** as a comparison to the fluorescence micrographs of the coated membranes displayed in **Figures 5.3-5.5**. The micrograph of the base membrane was obtained by fluorescence of an unknown intrinsic dye present in the polypropylene. All contrast is due to fluorescence of the dye because extraction of the base membrane, with trichloroethylene, removes the fluorophore and renders the polypropylene substrate invisible under identical imaging conditions.

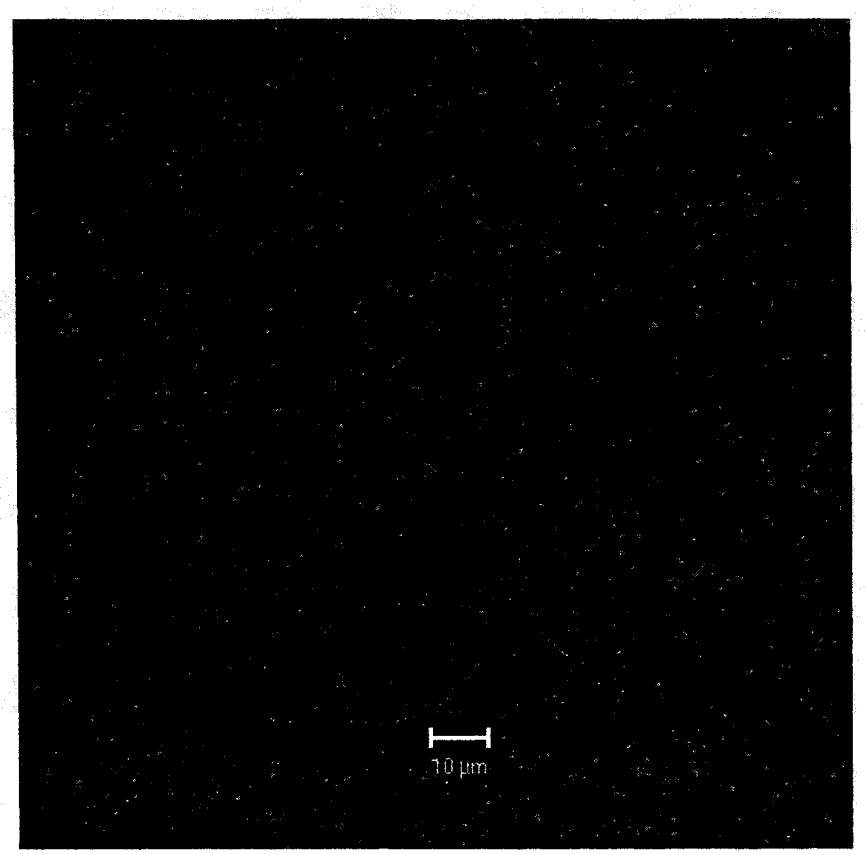

Figure 5.2 Laser fluorescence confocal micrograph of the base PP3 membrane

Figures 5.3 and **5.5** are fluorescence micrographs of the coated membranes imaged under identical conditions used for the base substrate. The coated membranes have, as expected, a similar morphological structure as the base substrate- except for a coated layer of polymer to which the anionic Direct Red dye binds. The confocal images of the coated membranes shown in **Figures 5.3, 5.4** and **5.6** have noticeable layers of the PEI gel coat, which is imaged in red due to the binding of the anionic fluorescence dye.

The importance of controlled solvent evaporation during the fabrication process is evident in **Figure 5.3**- the confocal image of membrane P1 made in the absence of controlled evaporation. The green signal from the base membrane can be seen where there is incomplete coverage of the BPEI gel coat. The red signal corresponding to the dye bound to the BPEI is sparse and scattered throughout the membrane. In membranes with a larger loading of BPEI, made under a methanol saturated atmosphere, such as P3 (77%) in **Figure 5.4** and E2 (71%) in **Figure 5.6**, the signal corresponding to the red dye is stronger and more uniformly distributed; although the green signal corresponding to the base membrane is still strongly evident in some areas. The signal is imaged as orange because the green and red signals from the base membrane and the Direct Red dye yields a composite orange signal.

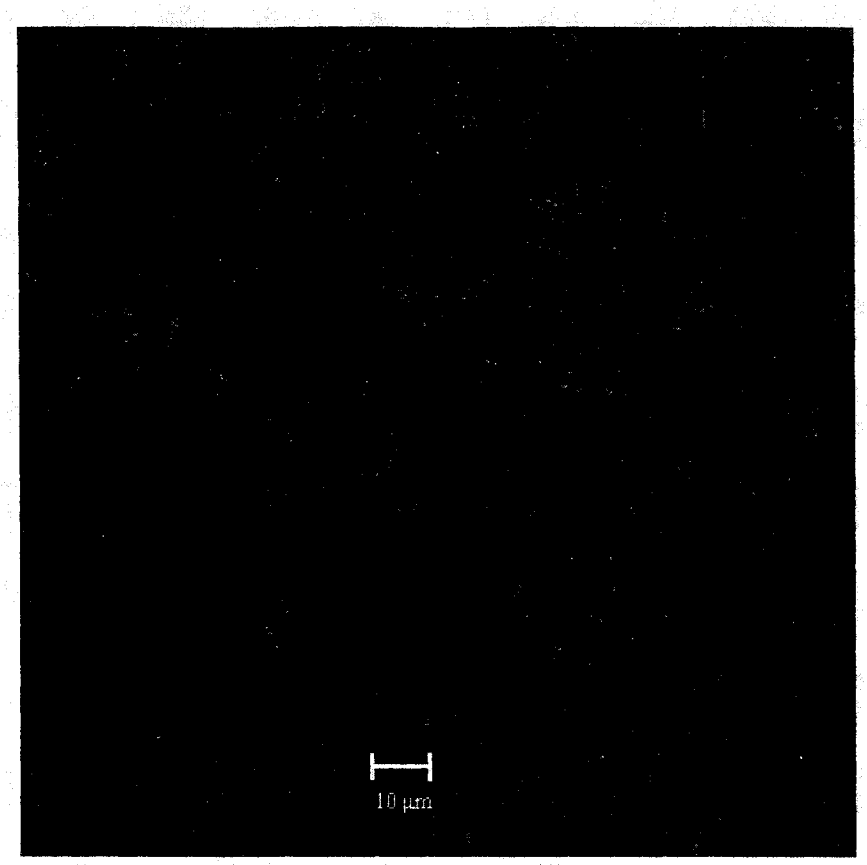

Figure 5.3 Confocal fluorescence micrograph of a hydrated sample of membrane P1

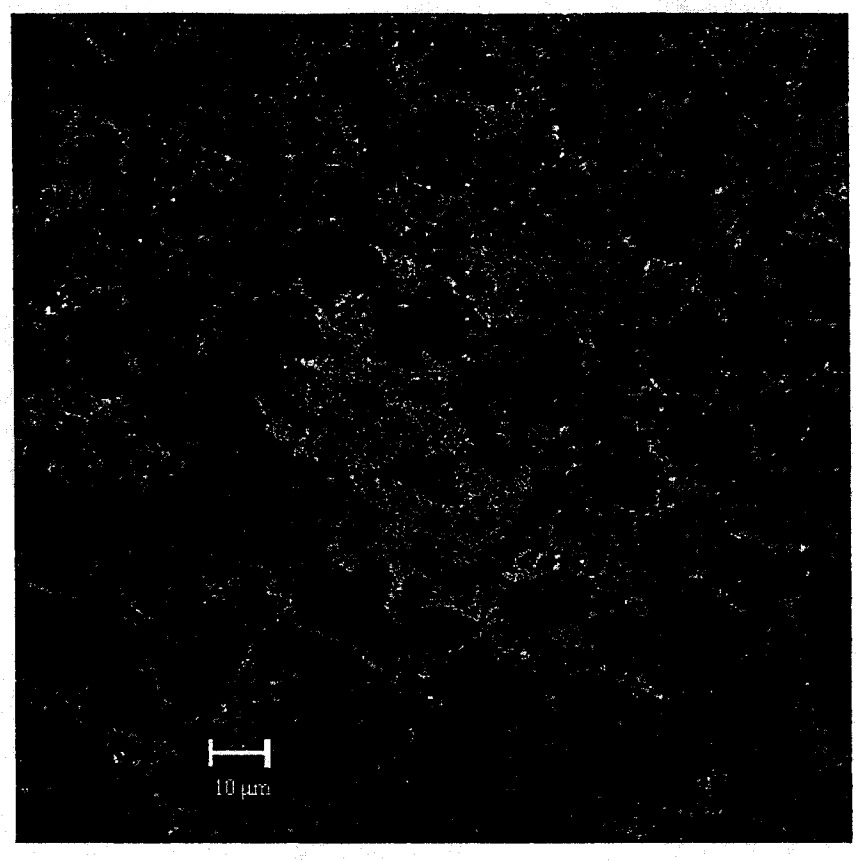

Figure 5.4 Confocal micrograph of a hydrated sample of membrane P3

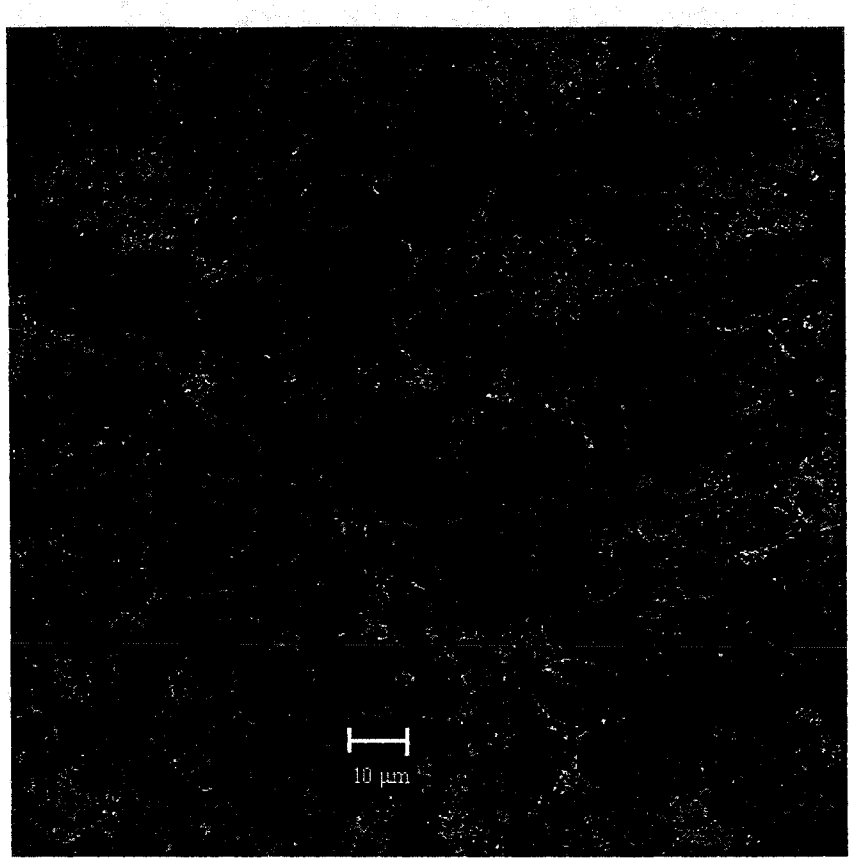

Figure 5.5 Confocal micrograph of a hydrated sample of membrane E2

5.3.4 Morphology of Coated Layer: STXM

The spectroscopic basis for distinguishing the polymer components by STXM is presented in **Figure 5.6**, where C 1s and N 1s NEXAFS spectra of polypropylene and polyethylenimine in linear mass absorption units are given. The calculated elemental absorption curves, used to convert the spectra into mass absorption units, for the C 1s transitions are also given. The C 1s→ $\sigma^*_{C\text{-}H}$ transitions for the polypropylene and

polyethylenimine are observed at 288 and 289 eV respectively. The broad peaks at 292 and 293 eV are associated with σ^*_{C-C} resonances. The N 1s spectrum is devoid of any polypropylene absorptions and the broad peak at 406.5 eV is associated with the N 1s→ σ^*_{N-H} transitions.

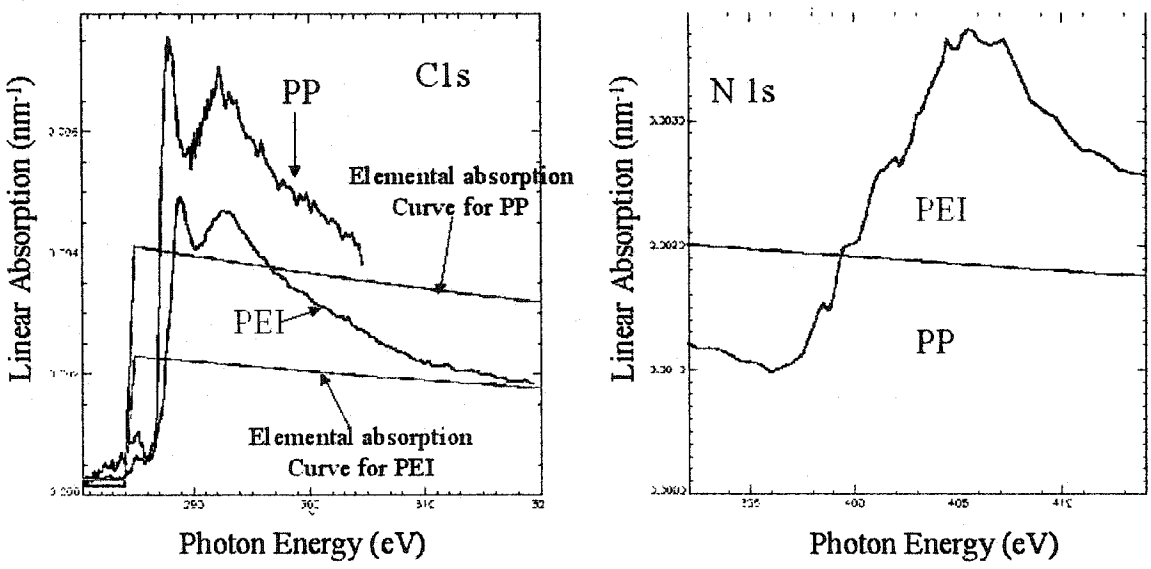

Figure 5.6 C 1s and N 1s NEXAFS spectra of PEI and polypropylene measured as linear absorption as a function of photon energy

Membrane samples P3 and E2 were analyzed by STXM. The STXM image of P3 was obscured by the presence of an impurity (acrylic adhesive used during sample preparation) that severely compromised the data set. The EDGE based membrane, however, was unaffected by the impurity. **Figure 5.7** are component maps derived from the SVD analysis of absorption spectra obtained from a stack analysis of a 400 μm^2 area

of a microtomed section of the hydrated E2 membrane sandwiched between two Si_3N_4 windows.

The images in **Figure 5.7**, obtained from STXM analysis of membrane E2, were measured at photon energies of 288 and 410 eV for the C 1s and N 1s respectively. The green phase represents the water swollen BPEI gel coated onto the polypropylene, represented by the red phase. Both the C 1s and N 1s images confirm the coating morphology observed through the fluorescence confocal microscope. In each case, the BPEI polymer is coated around the fibril structure of the host polypropylene membrane. As observed previously, the coating covers the majority of the host matrix but some of the nascent polypropylene is still visible.

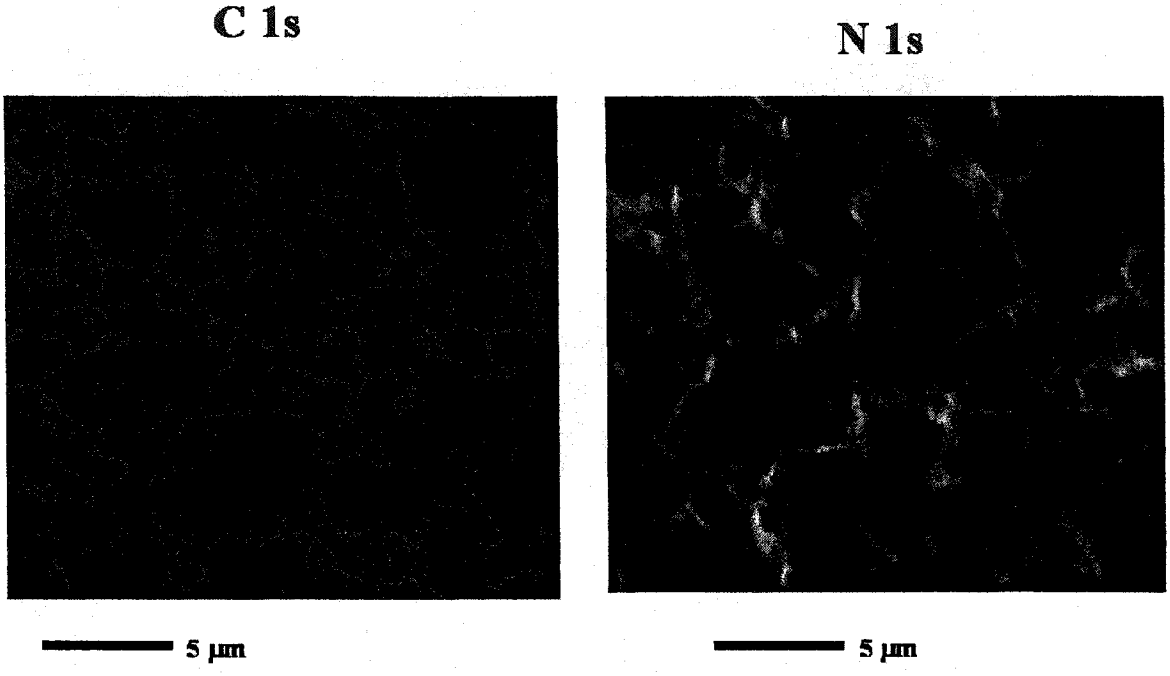

Figure 5.7 C 1s and N 1s images obtained from STXM analysis of membrane E2. Red color corresponds to polypropylene and green corresponds to the high mass gain BPEI coat

5.3.5 Permeability Results

Microscopy is an extremely useful tool for membrane characterization as it yields visual representations of morphology; however, it is limited in both resolution (limit of STXM is 50 nm and confocal ~0.2 μm) and depth of field (maximum 10 μm depth below surface for confocal). Furthermore, the conditions for samples prepared for microscopy may not accurately reflect the conditions inside a flow cell, thus microscopy alone is an insufficient method for determining the microstructure inside the membrane. Flux

measurements, however, can yield much information on the internal morphology of the membrane under flow conditions. Since Darcy's law governs flow through the membranes, as discussed in **Chapter 2**, the relative magnitude of the flux can give insights into the microstructure of the pores.

The measured pure water flux of the nascent PP3 membrane, used in this work, is 20,000 kg/m^2 h at 100kPa. The flux data of the coated membranes are presented in **Table 5.2** and are compared to two pore-filled membranes to illustrate how the different internal morphologies affect flux.

Table 5.2 Initial flux of BPEI coated membranes

Entry	Membrane	% PODGE cross-linker	% EDGE cross-linker	mass gain (%)	Flux (kg/m^{2}h)[a] at 100kPa
1	P2	10	/	53	13050
2	Pore filled PODGE (BP3)	10	/	56	8.3
3	P3	10	/	77	10021
4	P4	10	/	84	9483
5	P5	20	/	91	8521
6	E1	/	10	49	20080
7	Pore filled EDGE (BE1)	/	10	53	8.4
8	E2	/	10	71	3300

[a] Flux of base membrane 20,000 kg/m^{2}h at 100kPa. All flux data corrected to 25° C

Entries 1 & 2 and 6 & 7 compares coated membranes with pore-filled membranes of similar mass gain and composition. Even though the mass gains are virtually the same, the fluxes for the coated membranes are 4 orders of magnitude higher than the pore-filled membranes. The data in **Table 5.2** also shows that pure water flux, through

coated membranes, change as a function of both mass gain and type of cross-linker. As the mole % of the PODGE cross-linker is kept constant, and mass gain increased, the fluxes of the coated membranes decrease correspondingly as would be expected since an increase in gel polymer loading should increase the coated gel thickness. An increase in PODGE cross-linker concentration (membrane P5- 20% cross-linking) has no noticeable effect since the decrease in pure water flux is consistent with the trend in increased mass gain. It is interesting to note, however, that the BPEI-EDGE coated membranes have fluxes that are very different from the BPEI-PODGE membranes. For example, membrane E1 has a flux (20,080 kg/m^2h), similar to the flux measured for the nascent membrane, but a mass gain close to membrane P2 which has a much lower flux (13,050 kg/m^2h). Membrane E2, on the other hand, has a much lower flux than P3 despite their similar mass gains. The fluxes presented in **Table 5.2** are the initial values measured after the membranes were characterized, dried and rewetted, as specified in the experimental protocol. Care was taken to ensure all of the membranes went through identical characterization procedures prior to testing so that the flux values could be compared.

5.3.6 Soft Gel Coating- Effect on Flux

An interesting observation was made during the flux testing of the coated membranes. The fluxes of the membranes, at 100kPa, were observed to decrease continuously with time. Three membranes- P2, P3 and P5, after being conditioned as

indicated in the experimental protocol, were tested under pressure and the results are shown in **Figure 5.8.**

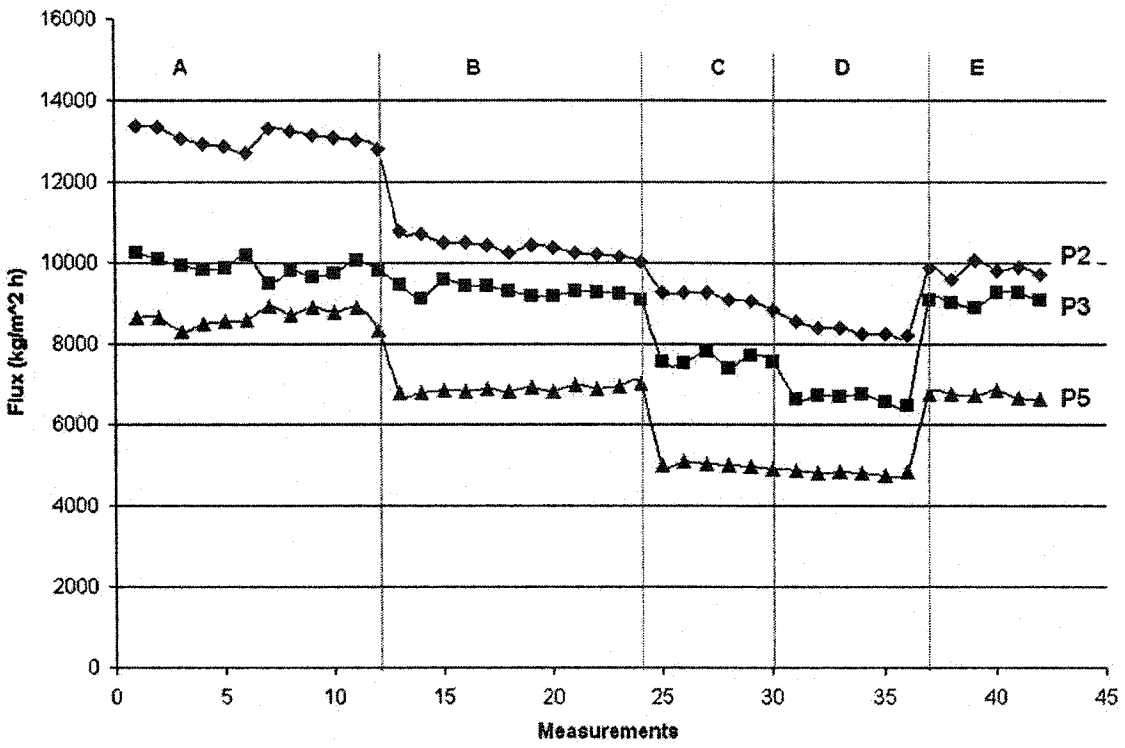

Figure 5.8 Change in flux, at 100kPa, as a function of membrane composition, feed composition and amount of material passed through the membrane. Each point refers to a single measurement. (A) deionized water. (B) deionized water after the membrane was treated with HCl (pH 2) and NaOH (pH 10). (C) HCl (pH 2). (D) deionized water immediately after passage of acid solution. (E) NaOH (pH 10)

Since the fluxes of the membranes are so high, the cells used to test the membranes drained very quickly; therefore each interval on the x-axis represents one measurement of flux from the passage of 300 ml of feed through the membrane. **Figure 5.8** is a plot of flux obtained at each interval. The plot is divided into 5 sections denoted

from A-E which represents different test conditions. Region A represents the membrane tested with the passage of deionized water (pH 6). Membrane P2 shows a gradual decrease in flux up to the 6^{th} interval. The increase in flux on the 7^{th} interval was due to the membrane taken out of the cell, flipped over and tested on the other side. This was done to ensure that the performance of these coated membranes were independent of which side was tested.

The membranes, while in the cell, were treated sequentially with HCl (pH 2) and NaOH (pH 10) for a few hours under no flow conditions. The fluxes of the membranes were then tested with deionized water as represented in Region B at 100kPa. There is a noticeable decrease in flux for membranes P2 and P5, but membrane P3 is relatively unaffected. The decrease in flux indicates expansion of the gel coat in P2 and P5 into the pores. A further decrease in flux is observed in Region C, for all the membranes, where the fluxes of an acid solution (HCl, pH 2) were measured. Region D represents the passage of deionized water after the test with acid. Membranes P2 and P3 have a continual flux decline whereas membrane P5 is essentially constant within experimental error. It is worthy to note that the flux through membrane P5 is relatively constant in each region indicating a relatively stable, non-swelling gel within the time frame tested. This is consistent with what is expected and observed in the swelling of gels at higher cross-linking.

All 3 membranes exhibit large increases in flux, in Region E, which represents the passage of NaOH (pH 10). The removal of charge eliminates the expansive forces of electrostatic repulsion and osmotic swelling resulting in a collapse of the gel, which has

been previously observed in the diminished swelling of the BPEI-PODGE gels in alkaline solution.

It is important to stress these membranes have a soft gel (fleece) coating that partially expands into the pores. This morphology is a new construct in ultrafiltration membrane technology as no previous reports of such membranes have been found. In effect, a partial valve is observed with the swelling of the coat; however, unlike poly(4-vinyl pyridine) grafted membranes discussed previously in **Chapter 2, section 2.2.3** [55], where the addition of an acidic feed converted an ultrafiltration membrane to one with reverse osmosis properties, the coated gel layer does not completely obstruct the pores nor is the valve effect instantaneous. Instead, the swelling of the gel is relatively slow and is restricted by the cross-linking.

The results of **Figure 5.8** demonstrated the dynamic gel properties of the BPEI coating. A more detailed and exhaustive experiment to demonstrate the swelling properties and dynamic nature of the BPEI gel coat was performed on membranes P4 and E1 over a period of 40 days and is shown below in **Figure 5.9**.

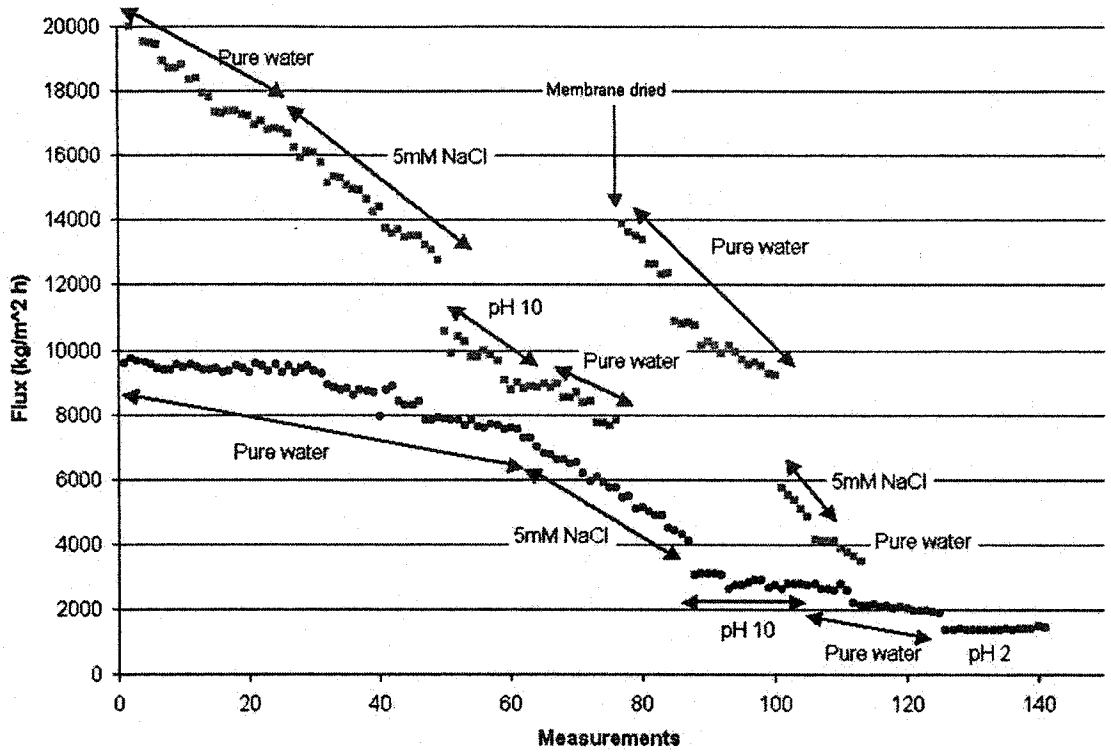

Figure 5.9 The change in flux of coated membranes P4 (black circles) and E1 (grey squares) over a period of 40 days. Data obtained by Erica Lee

Two membranes- one composed of 10% PODGE (P4) cross-linker and the other composed of 10% EDGE (E1) cross-linker were tested. The decrease in flux was particularly evident for the EDGE based membrane as shown in **Figure 5.9**. The steep slope of the flux decrease for E1 is the same for 5mM NaCl as for pure water, whereas the sharp decrease in flux for P4 became more apparent in the presence of salt. The sudden drop in flux observed in both membranes after the test in 5mM NaCl was due to the passage of one week during which time the membranes were stored in the cells under deionized water. During that time period, the gel coating swelled into the pores resulting

in a lower starting flux for the pH 10 solutions. The increase in flux observed with an alkaline feed (**Figure 5.8**) was not observed with P4 and E1. Instead there was a decrease in flux with E1 and a leveling off of P4.

After successive testing, membrane E1 was dried to collapse the gel onto the pore walls. The sharp increase in flux is a result of the collapse; however, the initial flux of 20,000 could not be obtained. It is interesting to note that the flux decrease, as evident in the slope, continued at the same rate until a final flux of 3,500 kg/m^2h (18% of initial flux) was obtained. The data in **Figure 5.9** suggests the swelling of the BPEI-EDGE coated gel is relatively unaffected by pH or salt concentration. The swelling of the BPEI-PODGE coated gel appears to be affected by salt concentration more than changes in pH. This is a surprising finding since the swelling data in **Chapter 4** shows diminished swelling in the presence of salt.

The rate of swelling is different for the EDGE and PODGE cross-linked gels. The flux for E1 drops to half the initial flux after 55 measurements, however membrane P4 experiences the same effect after 80 measurements. Furthermore, the slope of the flux decrease for E1 (rate of expansion of gel) is always more steep than the slope for P4. The differences in rate of swelling have been observed in the swelling behaviors of the gels in **Chapter 4**. Gels made with lower polymer concentration swelled to a much larger degree than gels made with higher polymer concentration; furthermore, gels with EDGE cross-linkers swelled to a much larger degree than gels cross-linked with PODGE. Since membrane E1 has a lower polymer concentration (lower mass gain) than P4 and is cross-linked with EDGE, both of these factors play a role in the faster flux decrease (gel

swelling) of membrane E1 over P4. And finally, the dynamic changes in gel swelling/flux decrease can be controlled or mitigated by increasing the degree of cross-linking as discussed previously in **Chapter 4, section 4.2.3** and shown for membrane P5 in **Figure 5.8**.

5.3.7 Thickness of the Gel Layer

Many methods have been proposed to calculate, or predict by a model, the hydrodynamic thickness of an absorbed polymer layer on a pore wall [33-38]. These methods are based on polymer layers with constant dimensions. In a recent paper published in the Journal of Membrane Science, Mika *et al.* [23] used a model of volume flow through brush lined pores, developed by Anderson *et al.* [33,35-38], to estimate the hydrodynamic thickness of grafted polymer chains. The Hagen-Poiseuille equation for pressure driven flow, Q, through a membrane of thickness d containing N_p right-cylindrical pores of radius R:

$$Q = N_p \frac{\pi R^4}{8\eta d} \Delta P \quad \textbf{(5.4)}$$

where η is the solution viscosity and ΔP is the pressure difference across the membrane was used to describe the flux. Based on the flux values reported for the nascent and coated membranes and **equation 5.4**, the ratio of nascent and coated pore radii is,

$$\frac{R_n}{R_c} = \left(\frac{Q_n}{Q_c}\right)^{\frac{1}{4}} \quad (5.5)$$

where the subscripts n and c refer to nascent and coated respectively. Determination of the radius of a coated membrane is trivial once the fluxes for the coated and nascent membranes are known with the pore size of the starting nascent membrane. The calculated pore radii and gel thickness of two coated membranes are presented in **Table 5.3**.

Table 5.3 Hydraulic pore radius, r_h, thickness of gel coating and permeability of nascent and coated membranes P4 & E1

Entry	Membrane	Permeability (kg/m^2 h)	Hydraulic pore radius r_h (nm)	Thickness of gel coating (nm)
1	PP3 Nascent	20000	410[a]	-
2	P4 initial	9504	340	70
3	P4 final	1476	214	196
4	E1 initial	19980	410	-
5	E1 final	3456	264	146

[a] Average pore radius determined from bubble point method

The calculated pore radii shown in **Table 5.3** shows that large decreases in permeability are not reflected in correspondingly large decreases in pore size due to their exponential relationship in **Equation 5.5**. The nascent membrane pore radius is an average value determined by a bubble point method. The calculated pore radii of the

coated membranes, therefore are also average values, with assumptions underlying the bubble point method, because of the use of the nascent pore size in the calculations.

In addition to the assumptions involved with the bubble point method, two more assumptions were made in calculations of the hydraulic pore radii. First, it was assumed that all flow occurred through the open pores and the amount of flow through the coated gel was negligible. Based on the hydrodynamic permeability model, discussed in **Chapter 2,** hydrodynamic flow through gels is 3-5 orders of magnitude less than convective flow through open channels. The bulk flow, therefore, is expected to occur through the open channels. The validity of this assumption is still expected to hold true for membranes such as P4 and E1 (entries 3 and 5 respectively) where the gel has swollen to reduce the pores by 48% for P4 and 36% for E1. However, as the gel expands to a greater extent into the pore the contribution of volume flow through the gel will become increasingly significant. This is an especially important point for applications of these membranes to ultrafiltration processes.

Second, the Hagen-Poiseuille equation, used to calculate pore radii from flux, describes flow through straight channel pores. The TIPS membranes, however, have a dendritic morphology with high pore tortuosity, as described by the relationship $\tau = K_s/K^* = 2.5$ derived by Anderson *et al.* [56], where tortuosity (τ) is dependent on the ratio of the Kozeny constants (K_s) for porosity ≈2/3 and parallel capillary pores of circular cross section (K^*). Justification for using the Hagen-Poiseuille equation was based on the

assumption that the tortuosity in the coated membrane did not differ much from that of the nascent membrane and, thus, could be cancelled out in the ratio of **Equation 5.5**.

5.4 Conclusions

As shown in this work, gel coated membranes could be made from a modification of the pore filling fabrication procedure. Membranes made by this process are robust and change the surface properties of the base polyolefinic substrate from hydrophobic to hydrophilic. The gel coating is permanent, as no mass loss was observed after extraction in boiling methanol. Comparison of the coated membranes with pore filled membranes of similar mass loadings of cross-linked polyethylenimine showed dramatic differences in flux demonstrating the effect of different pore morphologies on membrane performance. The coated gel has a high affinity for water and swells to reduce the effective pore size and thus the resulting flux. The gels are responsive to changes in pH and salt concentration. The expanded coated gels can also be collapsed onto the pore walls by drying.

The coated membranes discussed in this chapter can be considered *soft-coated* or *fleece-coated* membranes. These membranes are significantly different from coated membranes reported in the literature and studied previously at McMaster. These soft-coated membranes can be fabricated in a single step and the gel properties of the coating have been well characterized.

Soft-coated membranes have many potential applications; particularly within biomolecule separations in membrane chromatography. The high flux at low pressures, coupled with a potentially very high absorption capacity (surface area of the gel) makes the membranes highly attractive for such applications. Furthermore, these membranes can be fabricated in water (with appropriate surfactants for hydrophobic host substrates) thus eliminating the need for volatile organic solvents making them industrially attractive.

5.5 References

1. J.E. Cadotte, Evolution of composite reverse osmosis membranes, in: D.R. Lloyd, (Ed.), Material Science of Synthetic membranes, ACS Symp. Ser. 269, Chap. 12, Washington, D.C., 1985
2. W. Ho, K.K. Sirkar (Eds.), Membrane Handbook, Van Nostrand Reinhold, New York, 1992
3. Akhtar, S.; Hawes, C.; Dudley, L.; Reed, I.; Stratford, P *J. Memb. Sci.* **1995**, *107*, 209
4. Dudley, L. Y.; Stratford, P.; Aktar, S.; Hawes, C.; Reuben, B.; Perl, O.; Reed, I. M. *Chem. Eng. Res. Des.* **1993**, *71*, 327
5. Gershoni, J. M. US Patent 4,601,828, **1986**
6. Ostreicher, E. A.; Knight, R. A.; Fiore, J. V.; Emond, G. T.; Hou, K. C. US Patent 4,473,474, **1984**

7. Gagnon, D.R.; Grosh, S.K.; Brizuela, C.C.; Krinke, H.L.; Strobel, J.M. WO 9207899, **1992**

8. Lee, J.M.; Yeom, C.K; Kim, C.U; Kim, B.S.; Kim, K.J. WO 9920378, **1999**

9. Merril,E.W.; Allgor, S.S.; Leung, G.C. WO 9718904, **1997**

10. Wang, D. US Patent 5,137,633, **1992**

11. Hvid, K. B.; Nielsen, P. S.; Stengaard, F. F. *J. Memb. Sci.* **1990**, *53*, 189

12. Steuck, M.J. US Patent 4,944,879, **1990**

13. Otani, S; Sasaki, J; Naruo, K Japanese Patent 62,014,903, **1987**

14. Murashige, Y; Fukahori, N; Yanagase, A; Kawachi, Y JP 62,039,636, **1987**

15. Vaillancourt, V.L. US Patent 4,525,374, **1985**

16. Gregor, H.P.; Burshteyn, A.; Hodgins, L.T.; Kassotis, J.; Samuelson, E. US Patent 5,059,659, **1991**

17. Childs, R.F.; Mika, A.M.; Pandey, A.; McCrory, C.; Mouton, S.; Dickson, J.M. *Separation and Purification Technology* **2000**, *22-23*, 507

18. Pandey, A.; Childs, R.F.; West, M.; Lott, J.; McCarry, B.E.; Dickson, J.M. *J.Pol.Sci.: Part A: Pol.Chem.* **2001**, *39,* 807

19. Mika, A. M.; Childs, R.F.; Dickson, J.M.; McCarry, B.E.; Gagnon, D.R. *J.Memb.Sci.* **1995**, *108*, 37

20. Mika, A. M.; Childs, R.F.; West, M.; Lott, J. *J.Memb.Sci.* **1997**, *136*, 221

21. Mika, A.M.; Childs, R.F.; Dickson, J.M,; McCarry, B.E.; Gagnon, D.R. *J.Memb.Sci.* **1997**, *135*, 81

22. Mika, A.M. & Childs, R.F. *J.Memb.Sci* **1998**, *152,* 129

23. Mika, A.M.; Childs, R.F.; Dickson, J.M. *J.Memb.Sci* **1999**, *153*, 45

24. Mika, A.M.; Childs, R.F.; Dickson, J.M. *Desalination* **1999**, *121*, 149

25. Stachera, D.; Childs, R.F.; Mika, A.M.; Dickson, J.M. *J.Memb.Sci* **1998**, *148*, 119

26. Shipman, G. EP 105629, **1984**

27. Mika, A. M. & Childs, R.F. *Ind.Eng.Chem.Res.* **2001**, *40,* 1694

28. Dickson, J.M.; Childs, R.F.; McCarry, B.E.; Gagnon, D.R. *J.Memb.Sci* 148 (1998) 25

29. L. Wang, Internal surface coating and photochemical modification of polypropylene microfiltration membranes, Ph.D. Thesis, McMaster University, Hamilton, Ont., Canada, 1997

30. Childs, R.F.; Weng, J.F.; Kim, M.Y.; Dickson, J.M. *J. Polym. Sci. Part A: Polym. Chem.* **2002**, *40*, 242

31. Kawai, T; Sugita, K; Saito, K; Sugo, T. *Macromolecules* **2000**, *33*, 1306

32. Saito, K. *Sep. Sci. Tech.* **2002**, *37,* 535

33. Idol, W.K. & Anderson, J.L. *J. Memb. Sci.* **1986**, *28*, 269

34. Kontturi, K.; Mafe, S.; Manzanares, J.A.; Svarfvar, B.L.; Viinika, P. *Macromolecules* **1996**, *29*, 5740

35. Anderson, J.L.; McKenzie, P.F.; Webber, R.M. *Langmuir* **1991**, *7*, 162

36. Webber, R.M.; Anderson, J.L.; Jhon, M.S. *Macromolecules* **1990**, *23*, 1026

37. Kim, J.T. & Anderson, J.L. *Ind. Eng. Chem. Res.* **1991**, *30*, 1008

38. Kim, J.T. & Anderson, J.L. *J. Memb. Sci.* **1989**, *47*, 163

39. F.J. Green. The Sigma-Aldrich Handbook of Stains, Dyes and Indicators. Aldrich Chemical Co. Milwaukee, Wi (1990). P. 270

40. Warwick, T.; Padmore, H; Ade, H; Hitchcock, A.P.; Rightor, E.G.; Tonner, B.P. *J. Electron Spectrosc.,* **1997**, *84*, 85

41. Warwick, T.; Franck, K.; Kortwight, J.B.; Meigs, G.; Moronne, M.; Myneni, S.; Rotenberg, E.; Seal S.; Steele, W.F.; Ade, H.; Garcia, A.; Cerasari, S.; Denlinger, J.; Hayakawa, S.; Hitchcock, A.P.; Tyliszczak, T.; Rightor, E.G.; Shin, H.; Tonner, B. *Rev. Sci. Inst.* **1998**, *69*, 2964

42. Jacobsen, C.; Wirick, S.; Flynn, G.; Zimba, C. *J. Microscopy.* **2000**, *197*, 173

43. Claesson, P.M.; Blomberg, E.; Paulson, O.E.; Malmsten, M. *Coll.Surf.* **1996**, *112*, 131

44. Alpert, A.J. & Regnier, F.E. *J.Chrom.* **1979**, *185*, 375

45. Erim, F.B.; Cifuentes, A.; Poppe, H.; Kraak, J.C. *J.Chromatography.* **1995**, *708*, 356

46. Erim, F.B. *Microchemical.J.* **1997**, *57*, 283

47. Claesson, P.M.; Paulson, O.E.; Blomberg, E.; Burns, N. *Coll.Surf.* **1997**, *123*, 341

48. McNeff, C.; Zhao, Q.; Carr, P.W. *J.Chrom.A* **1994**, *684*, 201

49. Rounds, M.A.; Rounds, W.D.; Regnier, F.E. *J.Chrom.* **1987**, *397*, 25

50. Chanda, M.; Rempel, G.L. *Ind. Eng. Chem. Res.* **2001**, *40*, 1624

51. Cabasso, I.; Tamvakis, A.P. *J.Appl.Pol.Sci.* **1979**, *23*, 1509

52. Sata, T. & Izuo, R. *Coll.Sci.* **1978**, *256*, 757

53. Petsch, D; Rantze, E; Anspach, F.B. *J. Mol. Recog.* **1998**, *11*, 222

54. Wu, X.; Hou, C.J.; Dharia, J.; Konstantin, P.; Yang, Y. WP 050161, **2000**

55. Mika, A.M.; Childs, R.F.; Dickson, J.M.; McCarry, B.E.; Gagnon, D.R. *J. Memb. Sci.* **1995**, *108*, 37

56. Kapur, V.; Charkoudian, J.C.; Kessler, S.B.; Anderson, J.L. *Ind. Eng. Chem. Res.* **1996**, *35*, 3179

CHAPTER SIX

CONCLUSION AND RECOMMENDATIONS

The concept of a hydrogel stabilized within the matrix of an inert, porous support is a fascinating idea. Beyond the obvious practical applications in pressure driven separation processes, the pore filled construct also serves as a basis for fundamental research into gel properties. The pore filled architecture has allowed for developments such as the hydrodynamic permeability model, to describe flow through gel filled membranes [1], and models of neutral [2] and electrolytes [3] separations, still being developed, that describes solute interactions within a polyelectrolyte matrix. These models are significant breakthroughs in both the membrane and gel sciences and would not have been possible without the pore-filled paradigm. The skeletal host, therefore, acts as a containment vessel for the gel much like an NMR tube would for a solution of interest.

In this work, the gel properties of polyethylenimine have been studied both in the bulk, unsupported state and enmeshed within the protective confines of a polypropylene host. The major conclusions that can be drawn from this work are as follows:

1) Polyethylenimine can be incorporated into a porous host substrate by an *in situ* cross-linking process. This technique is indeed applicable to any polymer with functional groups by reaction with an appropriate bi-functional cross-linker and has been applied within the membrane group to gels based on poly(benzyl

ammonium) and poly(4-vinyl pyrdinium) chemistry. The advantages of this technique over the photochemically or thermally initiated *in situ* polymerization methods are many. First, the conditions under which the gellation process occurs are mild; therefore, no thermal degradation of the host substrate is possible. The *in situ* polymerization process, however, could affect the structural properties of the host substrate because of possible heat generated from the polymerization reaction and/or heat added to thermally initiate the polymerization. Furthermore, there are unresolved issues regarding the possible interpenetration of monomer into the bulk polypropylene and the effects such a breach would have on the stability of the membrane if polymerization occurred within the bulk polymer of the host- especially when the polyelectrolyte gel undergoes dimensional changes from ionization. No such possibility of interpenetration of the polyelectrolyte into the host is possible with the *in situ* cross-linking process.

The *in situ* cross-linking technique can make membranes with excellent and reproducible properties. Knowledge of the porosity and volume of a host substrate allows for the ability to fabricate membranes with predictable properties by using the appropriate concentration of polymer and cross-linker. Furthermore, this technique can be completely water based (with the appropriate choice of surfactants for hydrophobic hosts) thus making the process industrially attractive.

2) Membranes made from gels of polyethylenimine cross-linked with ethylene glycol diglycidyl ether perform exceptionally well in the nanofiltration

of ionic solutes. No prior acidification of the feed or *N*-alkylation of the nitrogens are required to achieve the separation. Instead, the polymer is sufficiently charged from an acid/base reaction with the solvent (water) to separate electrolytes by a Donnan exclusion mechanism. The membranes exhibit high rejections towards multivalent co-ions, diminished rejections towards multivalent counter-ions and no rejections of neutral solutes. The acid/base properties of the incorporated polyethylenimine gel, determined by titration, differs substantially from that of the polymer in solution; that is, incorporation of the gel into the hydrophobic host reduces the basicity of the polymer ($pK_{\alpha=0.5}$) typically by three orders of magnitude. Despite the substantial reduction in charge, relative to the unconfined-uncross-linked polymer, the polyethylenimine gel is still sufficiently charged to effect separation of 5mM NaCl over a wide range of pH (2-10). The separation vs. pH profile of the BPEI-EDGE membranes show a relative constant rejection with diminished rejections at the pH extremes (2&12). The BPEI-EDGE membranes, furthermore, do not exhibit any changes in flux as a function of pH indicating a relative insensitivity to pH induced conformational changes.

3) The influence of the cross-linker properties on BPEI gel properties is substantial. BPEI cross-linked with ethylene glycol diglycidyl ether produce clear, space filling gels with large swelling capabilities. EDGE based gels incorporated in membranes have permeabilities that are consistent with those

predicted from the hydrodynamic permeability model and exhibit high rejection towards 5mM NaCl. A large, rigid and hydrophobic cross-linker such as bis-phenol-A-diglycidyl ether can cause substantial heterogeneity within the gel manifested in changes in the index of refraction, gel syneresis and diminished swelling in the bulk state and enhanced permeability with reduced separation of 5mM NaCl when incorporated into a membrane.

Cross-linking with a large flexible molecule such as polypropylene glycol diglycidyl ether results in space filling gels with coloration and moderate swelling capabilities. The most surprising discovery, however, is the effect the PODGE cross-linker has on membrane morphology. Membranes made from the PODGE cross-linker show evidence of coating despite the absence of possible factors that would result in such a morphology (i.e., solvent evaporation during fabrication). STXM analysis of PODGE gels showed the presence of microholes with a concentration of the cross-linker around their periphery. Furthermore, coating experiments of PODGE on polypropylene showed a non-linear concentration/mass gain relationship suggestive of a possible interaction between the cross-linker and the polypropylene. Possible phase separation of the PODGE from BPEI, coupled with an affinity between PODGE and polypropylene could have resulted in the observed coating morphologies. The enhanced permeabilities through the PODGE based membranes are due to the thin gel plug and the reduced 5mM NaCl rejections are attributable to concentration polarization.

4) The versatility of the *in situ* cross-linking method of fabrication was demonstrated in the manufacture of coated membranes. By cross-linking the polyethylenimine gel in the pores under controlled solvent evaporation conditions, a soft gel coat was deposited on the walls of the pores. These membranes exhibit very large fluxes characteristic of ultrafiltration membranes; furthermore, the gel coating undergo a slow and gradual swelling into the pores resulting in a steady decrease in flux. These membranes exhibit a slight valve effect; however the swollen gels did not completely occlude the pores due to the cross-linking. The swollen gels could be collapsed onto the pore walls by drying the membrane and continued flow tests re-expanded the gels.

The importance of the contributions made in this thesis can only be assessed from the impact this current work has in future developments. Despite the many answers that have been provided, or attempted, in this work, many more questions have arisen. These questions can be addressed as recommendations for future study. Because of the fundamental and practical natures of the gel filled membrane research, the recommendations for future study will be discussed in that context.

Fundamental Research

I) As mentioned earlier, a new model developed by Mika and Childs has been successfully applied to predict the rejection capabilities of poly(acrylic

acid) filled membranes [4]. A more rigorous study of the salt rejection capabilities of PEI filled membranes is suggested to test the effectiveness of the new model.

II) The results on polyethylenimine gel properties obtained with various cross-linkers were intriguing. A more detailed study is proposed separately for PODGE and BADGE gel systems. For example, the PODGE molecule used in this work had a number average molecular weight of ~ 640 corresponding to 8 to 10 propyleneoxide monomeric units. What are the effects of using both smaller PODGE molecules (2-3 repeat units) and larger PODGE molecules (>10 repeat units) on both gel and gel filled membrane properties? Can the same coated/filled membrane morphology be obtained with a polyethyleneoxide diglycidyl ether cross-linker? And what is the source of coloration in the BPEI-PODGE gels?

The heterogeneity observed in the BADGE system could not be experimentally verified through STXM analysis of the membranes because of an error made during the sample preparation that destroyed the membranes. A re-examination of the membranes with varying BADGE concentration by STXM is suggested. If evidence of heterogeneity cannot be determined by STXM, small angle neutron scattering experiments are suggested.

III) The coated membranes studied were based on the EDGE and PODGE cross-linkers. BADGE cross-linked gels, based on the low swelling properties would be an interesting choice as a cross-linker for coated membrane studies. A

higher degree of cross-linking was demonstrated to stabilize the swelling of the coated gel. How would the choice of cross-linker affect the swelling properties of a coated gel? Could the properties of the coated gel be adjustable between *hard* and *soft* based on the cross-linker used?

IV) The pore radii and gel thickness calculations reported for the coated membranes were based on a few simplifying assumptions- for example, tortuosity was not considered. A more rigorous study of permeability through open pores is suggested. Furthermore, calculated pore radii can be verified by tapping mode atomic force microscopy measurements.

Practical applications

V) As reported in **Chapter 5**, polyethylenimine coated membranes have been used for recovery of proteins. A negatively charged protein will bind to the positively charged polymer and can be recovered by extracting with salt. Preliminary work on static/diffusion protein binding (bovine serum albumin) experiments with polyethylenimine pore filled membranes has shown exceptionally high absorption capacities. The soft-coated membranes, with properties in between an ultrafiltration and nanofiltration membrane, provide an intriguing platform to study protein absorption. Work is currently being pursued in this direction.

VI) The coating of a polyolefinic host with a polyethylenimine coat provides a chemically rich surface upon which further chemistry can be performed. For example, ligand molecules with specificity for metals or proteins can be grafted onto a PEI surface. A polyolefinic host, such as the TIPS substrates reported in this thesis, has an extremely high surface area for the polyethylenimine coated/activated layer thus representing the potential for high absorption capacities.

VII) As mentioned in **Chapter 2** [5], the use of a thermally degradable molecule (4,4'-azobis(4-cyanovaleryl chloride)) was reported. This molecule, or variants of it, could be used as a degradable cross-linker for PEI gel filled substrates. A photochemically or thermally degradable gel could be one of great usefulness in controlled release applications in the agricultural or fragrance industries.

VIII) The hydrodynamic permeability model allows for the determination of a gel's mesh size. Confirmation of the modeled predictions can be verified by diffusion studies with biomolecules. Based on this data, gel filled substrates can be considered for encapsulation of cells for applications as artificial organs and tissues or encapsulation of proteins/drugs for controlled release applications. The suitability of polyethylenimine, or derivatized polyethylenimine (for example, *N*-acetylated PEI, PEO grafted etc...) as the gel filling will be contingent upon its toxicity to the host organism or the encapsulated cell.

References:

1. Mika, A.M.; Childs, R.F. *Ind. Eng. Chem. Res.* **2001,** *40*, 1694
2. Mika, A.M.; Childs, R.F. *Ultrafiltration with gel-filled membranes: Predictability and control of molecular weight cut-off* presented at NAMS 2002, Long Beach, California
3. Mika, A.M.; Childs, R.F. *Transport of charged and neutral solutes through gel-filled microporous membranes* presented at ICOM 2002, Toulouse, France
4. McCrory, C.T.M. Ph.D. Thesis: Impact of gel morphology on pore filled membranes. 2001. McMaster University
5. Childs, R.F.; Weng, J.F.; Kim, M.Y.; Dickson, J.M. *J. Pol. Sci. Part A: Polym. Chem.* **2002**, *40*, 242